P517610.PDF [Page: 3 of 123]

DEFENCE R&D DÉFENSE

Naval Radar Performance Under Ducting Conditions

S.M. Gauthier, E.S. Riseborough and A.D. Thomson

Defence R&D Canada

TECHNICAL REPORT
DREO TR 2001-148
December 2001

National Defence / Defense nationale

Canada

REPRODUCTION QUALITY NOTICE

This document is the best quality available. The copy furnished to DRDCIM contained pages that may have the following quality problems:

: Pages smaller or Larger than normal

: Pages with background colour or light coloured printing

: Pages with small type or poor printing; and or

: Pages with continuous tone material or colour photographs

Due to various output media available these conditions may or may not cause poor legibility in the hardcopy output you receive.

☒ If this block is checked, the copy furnished to DRDCIM contained pages with colour printing, that when reproduced in Black and White, may change detail of the original copy.

P517610.PDF [Page: 5 of 123]

105-03240/

Naval Radar Performance Under Ducting Conditions

Gauthier, S.M.
DREO, Ottawa

Riseborough, E.S.
DREO, Ottawa

Thomson, A.D.
DREO, Ottawa

Defence Research Establishment Ottawa

Technical Report

DREO TR 2001-148

December 2001

© Her Majesty the Queen as represented by the Minister of National Defence, 2001

© Sa majesté la reine, représentée par le ministre de la Défense nationale, 2001

Abstract

This report evaluates the detection capabilities of three naval radars against current antiship missile (ASM) threats under various ducting conditions. The parameters of three naval radars and ASMs are first defined for this study. The subject radars are the SPS-49, the Sea Giraffe and an active multifunction radar (MFR). The ASMs of concern in this study are the Exocet, the SS-N-22, and the Novator sea skimming missiles. The defined radars are then evaluated against the ASMs under four atmospheric conditions: standard atmosphere, and with evaporation ducts at heights of 10 m, 20 m and 30 m. The results show that ducting conditions can have a strong impact on the detection capability of naval radars. The maximum detection range is often increased by the presence of ducts but can also be significantly decreased which puts the survivability of the ship at higher risk. The volume search radar has the best detection capability against the missiles flying 15 m and higher for any atmospheric conditions. The MFR of this report, using a 3-out-of-4 binary detector, has its performance seriously degraded in the presence of evaporation ducts.

Résumé

Ce rapport évalue les performances de détection de trois radars navals contre des missiles anti-navires sous différentes conditions atmosphériques. Le rapport débute en définissant les paramètres de trois radars navals et missile antinavires utilisées pour cette étude. Les trois radars en question sont le SPS-49, le Sea Giraffe et un radar de surveillance d'horizon, et un radar multifonctions à réseaux d'antenne active. Les missiles anti-navires définis dans cette étude sont le Exocet, le SS-N-22 et un nouveau missile produit par Novator. La performance des radars est évaluée pour quatre conditions atmosphériques différentes: une atmosphère standard, des canaux d'évaporation de 10 m, 20 m, et 30 m. Ce rapport démontre que les canaux d'évaporation peuvent avoir un très grand impact sur la performance des radars navales. La portée maximum de détection est souvent augmentée en présence de canaux d'évaporation mais cependant peut aussi être réduite considérablement mettant la survivabilité du navire à plus grand risque Dans ce rapport, le radar de surveillance de volume obtient les meilleures performances de détection contre les missiles anti-navires qui volent à une hauteur 15 m et plus, et cela pour toutes les conditions atmosphériques Le radar multifonctions de ce rapport qui utilise un détecteur binaire avec un critère de 3 sur 4 voit sa performance dégradée sévèrement en présence de canaux d'évaporation.

P517610.PDF [Page: 8 of 123]

This page intentionally left blank.

Executive summary

This report evaluates the detection capabilities of three naval radars against current antiship missile (ASM) threats under various ducting conditions. The parameters of three naval radars and ASMs are first defined for this study. The subject radars are the SPS-49, the Sea Giraffe and an active multifunction radar (MFR). The ASMs of concern in this study are the Exocet, the SS-N-22, and the Novator sea skimming missiles. The defined radars are then evaluated against the ASMs under four atmospheric conditions: standard atmosphere, and with evaporation ducts at heights of 10 m, 20 m and 30 m.

Under standard atmospheric conditions, the radars defined in this report are unable to detect existing ASM threats at the radar horizon. The ASM missiles must fly several kilometers inbound from the radar horizon before they are detected.

This report shows that ducting conditions can have a strong impact on the detection capability of naval radars. The maximum detection range is often increased by the presence of ducts but can also be significantly decreased, which puts the survivability of the ship at higher risk. The volume search radar has the best detection capability against the missiles flying 15 m and higher for any atmospheric conditions. A 3-out-of-4 binary detector, as defined in this report, has its performance seriously degraded in the presence of evaporation ducts. The result shows that under ducting conditions the integration of the volume search radar with the MFR would improve overall detection capability.

More resources should be allocated for the study of atmospheric conditions in maritime environments to evaluate the real threat to the Canadian Navy. Wideband radars such as the MFR defined in this study, have the capability of taking advantage of ducting conditions. Such a radar can change its transmitted frequency within a large bandwidth of operation, which makes it possible to optimise the frequency with respect to radio frequency propagation. However, equipment will be needed to measure the refractivity structure of the atmosphere in real time to exploit that capability.

Gauthier, S.M., Riseborough, E S , Thomson, A.D., 2001 Naval Radar Performance Under Ducting Conditions DREO TR 2001-148, Defence Research Establishment Ottawa.

Sommaire

Ce rapport évalue les performances de détection de trois radars navals contre des missiles anti-navires sous différentes conditions atmosphériques. Le rapport débute en définissant les paramètres de trois radars navals et missile antinavires utilisées pour cette étude. Les trois radars en question sont le SPS-49, le Sea Giraffe et un radar multifonctions à réseaux d'antenne active. Les missiles anti-navires définis dans cette étude sont le Exocet, le SS-N-22 et un nouveau missile produit par Novator. La performance des radars est évaluée pour quatre conditions atmosphériques différentes: une atmosphère standard, des canaux d'évaporation de 10 m, 20 m, et 30 m.

Pour une atmosphère standard, les radars examinés dans ce rapport sont tous incapables de détecter les missiles anti-navires directement sur l'horizon. Les missiles anti-navires peuvent voler plusieurs kilomètres après avoir croisé l'horizon avant d'être détecter.

Ce rapport démontre que les canaux d'évaporation peuvent avoir un très grand impact sur la performance des radars navals. La portée maximum de détection est souvent augmentée en présence de canaux d'évaporation mais cependant peut aussi être réduite considérablement mettant la survivabilité du navire à plus grand risque. Dans ce rapport, le radar de surveillance de volume obtient les meilleures performances de détection contre les missiles anti-navires qui volent à une hauteur 15 m et plus, et cela pour toutes les conditions atmosphériques. Le radar multifonctions de ce rapport qui utilise un détecteur binaire avec un critère de 3 sur 4 voit sa performance dégradée sévèrement en présence de canaux d'évaporation.

Des ressources additionnelles devraient être allouées pour étudier les conditions atmosphériques en milieu maritime afin d'obtenir une évaluation plus complète de leur impact potentiel sur la marine canadienne. Des radars à large bande, comme le radar multifonction définis dans ce rapport, ont la capacité de prendre avantage du canal d'évaporation. Ce type de radar peut changer sa fréquence d'opérations à l'interieur de plusieurs GHz ce qui rend possible l'optimisation de la forme d'onde pour la propagation des ondes radars. Cependant, un équipement spécial est nécessaire pour mesurée le profile vertical de réfraction en temps réelle en vue de pouvoir exploiter cette capacité.

Gauthier, S.M., Riseborough, E.S., Thomson, A.D., 2001, Naval Radar Performance Under Ducting Conditions. DREO TR 2001-148, Centre de recherches pour la défense Ottawa.

P517610.PDF [Page: 11 of 123]

Table of contents

Abstract i

Executive summary iii

Sommaire iv

Table of contents v

List of figures vii

1. Introduction 1

2. Low – Altitude RF Propagation 2
   - 2.1 Horizon 2
     - 2.1.1 Optical 2
     - 2.1.2 Non-homogeneous Atmosphere 3
       - 2.1.2.1 Standard Atmosphere 3
       - 2.1.2.2 Atmospheric Ducts 4
   - 2.2 Multipath 4
     - 2.2.1 Point Source 4
     - 2.2.2 Finite size antenna 7
   - 2.3 TERPEM 8

3. Sea Skimming Threats 10
   - 3.1 AM39 Exocet 10
   - 3.2 SS-N-22 Sunburn 10
   - 3.3 Novator 3M-54E 11
   - 3.4 Overall Threat 12

4. Detection Performance Criteria 13
   - 4.1 Evaluation Criteria 13
   - 4.2 Maximum Detection Range 13
     - 4.2.1 Incoherent Integration 13
       - 4.2.1.1 Average Signal to Noise Ratio 14

P517610.PDF [Page: 12 of 123]

4.2.2 Binary integration 15

5. Radar Systems 17

5.1 Volume Search Radar 17

5.2 Sea Giraffe 22

5.3 MFR 27

5.4 Comparison Of Radars Performance 36

6. Conclusion 38

7. References 40

Annex A: SPS-49 Performance 42

Annex B: SEA GIRAFFE Performance 52

Annex C: MFR Performance 64

List of symbols/abbreviations/acronyms/initialisms 100

P517610.PDF [Page: 13 of 123]

List of figures

Figure 1. Optical Horizon and LOS Optical Range 3

Figure 2. Multipath Interference 5

Figure 3. Multipath Pattern 6

Figure 4. Multipath Pattern for extended antenna 8

Figure 5. TERPEM Output 9

Figure 6. Exocet Flight Profile 10

Figure 7. SS-N-22 Flight Profile 11

Figure 8. NOVATOR 3M-54E Missile Flight Profile 11

Figure 9. Propagation factor for the SPS-49 at 850 MHz 19

Figure 10. Propagation factor for the SPS-49 at 942 MHz 20

Figure 11. Propagation factor for the Sea Giraffe at 5.4 GHz 24

Figure 12. Propagation factor for the Sea Giraffe at 5.9 GHz 25

Figure 13. Example of discontinuity in the 0.9 P_d detection range coverage. The figure gives the probability of Detection for Sea Giraffe, standard atmosphere, SS-N-22 at 30 m 26

Figure 14. Propagation factor for the MFR at 8.0 GHz 29

Figure 15. Propagation factor for MFR at 9.5 GHz 30

Figure 16. Propagation factor for MFR at 10.5 GHZ 31

Figure 17. Propagation factor for MFR at 12 0 GHz 32

Figure 18. Propagation factor for SPS-49, standard atmosphere, Exocet at 9 m 42

Figure 19. Propagation factor for SPS-49, standard atmosphere, Exocet at 15 m 42

Figure 20. Propagation factor for SPS-49, standard atmosphere, Exocet at 3 m 42

Figure 21. Propagation factor for SPS-49, standard atmosphere, SS-N-22 at 20 m 43

Figure 22. Propagation factor for SPS-49, standard atmosphere, SS-N-22 at 30 m 43

P517610.PDF [Page: 14 of 123]

Figure 23. Propagation factor for SPS-49, standard atmosphere, SS-N-22 at 7 m 43
Figure 24. Propagation factor for SPS-49, standard atmosphere, NOVATOR at 15 m 43
Figure 25. Propagation factor for SPS-49, standard atmosphere, NOVATOR at 50 m 44
Figure 26. Propagation factor for SPS-49, standard atmosphere, NOVATOR at 3 m 44
Figure 27. Propagation factor for SPS-49, 10m duct, Exocet at 9 m 44
Figure 28. Propagation factor for SPS-49, 10m duct, Exocet at 15 m 44
Figure 29. Propagation factor for SPS-49, 10m duct, Exocet at 3 m 45
Figure 30. Propagation factor for SPS-49, 10m duct, SS-N-22 at 20 m 45
Figure 31. Propagation factor for SPS-49, 10m duct, SS-N-22 at 30 m 45
Figure 32. Propagation factor for SPS-49, 10m duct, SS-N-22 at 7 m 45
Figure 33. Propagation factor for SPS-49, 10m duct, NOVATOR at 15 m 46
Figure 34. Propagation factor for SPS-49, 10m duct, NOVATOR at 50 m 46
Figure 35. Propagation factor for SPS-49, 10m duct, NOVATOR at 3 m 46
Figure 36. Propagation factor for SPS-49, 20m duct, Exocet at 9 m 46
Figure 37. Propagation factor for SPS-49, 20m duct, Exocet at 15 m 47
Figure 38. Propagation factor for SPS-49, 20m duct, Exocet at 3 m 47
Figure 39. Propagation factor for SPS-49, 20m duct, SS-N-22 at 20 m 47
Figure 40. Propagation factor for SPS-49, 20m duct, SS-N-22 at 30 m 47
Figure 41. Propagation factor for SPS-49, 20m duct, SS-N-22 at 7 m 48
Figure 42. Propagation factor for SPS-49, 20m duct, NOVATOR at 15 m 48
Figure 43. Propagation factor for SPS-49, 20m duct, NOVATOR at 50 m 48
Figure 44. Propagation factor for SPS-49, 20m duct, NOVATOR at 3 m 48
Figure 45. Propagation factor for SPS-49, 30m duct, Exocet at 9 m 49
Figure 46. Propagation factor for SPS-49, 30m duct, Exocet at 15 m 49
Figure 48. Propagation factor for SPS-49, 30m duct, SS-N-22 at 20 m 49

P517610.PDF [Page: 15 of 123]

Figure 49. Propagation factor for SPS-49, 30m duct, SS-N-22 at 30 m 50
Figure 50. Propagation factor for SPS-49, 30m duct, SS-N-22 at 7 m 50
Figure 51. Propagation factor for SPS-49, 30m duct, NOVATOR at 15 m..... 50
Figure 52. Propagation factor for SPS-49, 30m duct, NOVATOR at 50 m..... 50
Figure 53. Propagation factor for SPS-49, 30m duct, NOVATOR at 3 m..... 51
Figure 54. Propagation factor for Sea Giraffe, standard atmosphere, Exocet at 9 m..... 52
Figure 55. Propagation factor for Sea Giraffe, standard atmosphere, Exocet at 15 m..... 52
Figure 56. Probability of Detection for Sea Giraffe, standard atmosphere, Exocet at 15 m 52
Figure 57. Propagation factor for Sea Giraffe, standard atmosphere, Exocet at 3 m..... 53
Figure 58. Propagation factor for Sea Giraffe, standard atmosphere, SS-N-22 at 20 m..... 53
Figure 59. Propagation factor for Sea Giraffe, standard atmosphere, SS-N-22 at 30 m..... . 53
Figure 60. Probability of Detection for Sea Giraffe, standard atmosphere, SS-N-22 at 30 m . 53
Figure 61. Propagation factor for Sea Giraffe, standard atmosphere, SS-N-22 at 7 m..... 54
Figure 62. Propagation factor for Sea Giraffe, standard atmosphere, NOVATOR at 15 m..... 54
Figure 63. Propagation factor for Sea Giraffe, standard atmosphere, NOVATOR at 50 m..... 54
Figure 64. Probability of Detection for Sea Giraffe, standard atmosphere, NOVATOR at 50 m54
Figure 65. Propagation factor for Sea Giraffe, standard atmosphere, NOVATOR at 3 m..... 55
Figure 66. Propagation factor for Sea Giraffe, 10 duct, Exocet at 9 m..... 55
Figure 67. Propagation factor for Sea Giraffe, 10 duct, Exocet at 15 m..... 55
Figure 68. Probability of Detection for Sea Giraffe, 10 duct, Exocet at 15 m..... 55
Figure 69. Propagation factor for Sea Giraffe, 10 duct, Exocet at 3 m 56
Figure 70. Propagation factor for Sea Giraffe, 10 duct, SS-N-22 at 20 m 56
Figure 71. Probability of Detection for Sea Giraffe, 10 duct, SS-N-22 at 20 m..... 56
Figure 72. Propagation factor for Sea Giraffe, 10 duct, SS-N-22 at 30 m 56
Figure 73. Probability of Detection for Sea Giraffe, 10 duct, SS-N-22 at 30 m..... 57

P517610.PDF [Page: 16 of 123]

Figure 74. Propagation factor for Sea Giraffe, 10 duct, SS-N-22 at 7 m 57
Figure 75. Propagation factor for Sea Giraffe, 10 duct, NOVATOR at 15 m 57
Figure 76. Propagation factor for Sea Giraffe, 10 duct, NOVATOR at 50 m 57
Figure 77. Probability of Detection for Sea Giraffe, 10 duct, NOVATOR at 50 m 58
Figure 78. Propagation factor for Sea Giraffe, 10 duct, NOVATOR at 3 m 58
Figure 79. Propagation factor for Sea Giraffe, 20 duct, Exocet at 9 m 58
Figure 80. Propagation factor for Sea Giraffe, 20 duct, Exocet at 15 m 58
Figure 81. Propagation factor for Sea Giraffe, 20 duct, Exocet at 3 m 59
Figure 82. Propagation factor for Sea Giraffe, 20 duct, SS-N-22 at 20 m 59
Figure 83. Propagation factor for Sea Giraffe, 20 duct, SS-N-22 at 30 m 59
Figure 84. Propagation factor for Sea Giraffe, 20 duct, SS-N-22 at 7 m 59
Figure 85. Propagation factor for Sea Giraffe, 20 duct, NOVATOR at 15 m 60
Figure 86. Probability of Detection for Sea Giraffe, 20 duct, NOVATOR at 15 m 60
Figure 87. Propagation factor for Sea Giraffe, 20 duct, NOVATOR at 50 m 60
Figure 88. Probability of Detection for Sea Giraffe, 20 duct, NOVATOR at 50 m 60
Figure 89. Propagation factor for Sea Giraffe, 20 duct, NOVATOR at 3 m 61
Figure 90. Propagation factor for Sea Giraffe, 30 duct, Exocet at 9 m 61
Figure 91. Probability of Detection for Sea Giraffe, 30 duct, Exocet at 9 m 61
Figure 92. Propagation factor for Sea Giraffe, 30 duct, Exocet at 15 m 61
Figure 93. Propagation factor for Sea Giraffe, 30 duct, Exocet at 3 m 62
Figure 94. Propagation factor for Sea Giraffe, 30 duct, SS-N-22 at 20 m 62
Figure 95. Propagation factor for Sea Giraffe, 30 duct, SS-N-22 at 30 m 62
Figure 96. Propagation factor for Sea Giraffe, 30 duct, SS-N-22 at 7 m 62
Figure 97. Propagation factor for Sea Giraffe, 30 duct, NOVATOR at 15 m 63
Figure 98. Propagation factor for Sea Giraffe, 30 duct, NOVATOR at 50 m 63

P517610.PDF [Page: 17 of 123]

Figure 99. Probability of Detection for Sea Giraffe, 30 duct, NOVATOR at 50 m 63

Figure 100. Propagation factor for Sea Giraffe, 30 duct, NOVATOR at 3 m 63

Figure 101. MFR results, Standard atmosphere, Exocet at 9 m 64

Figure 102. MFR results, duct 10m, Exocet at 9 m 65

Figure 103. MFR results, duct 20m, Exocet at 9 m 66

Figure 104. MFR results, duct 30m, Exocet at 9 m 67

Figure 105. MFR results, Standard atmosphere, Exocet at 15 m 68

Figure 106 MFR results, 10m duct, Exocet at 15 m 69

Figure 107. MFR results, 20m duct, Exocet at 15 m 70

Figure 108. MFR results, 30m duct, Exocet at 15 m 71

Figure 109. MFR results, Standard atmosphere, Exocet at 3 m 72

Figure 110. MFR results, 10m duct, Exocet at 3 m 73

Figure 111. MFR results, 20m duct, Exocet at 3 m 74

Figure 112. MFR results, 30m duct, Exocet at 3 m 75

Figure 113. MFR results, Standard atmosphere, SS-N-22 at 20 m 76

Figure 114. MFR results, 10m duct, SS-N-22 at 20 m 77

Figure 115. MFR results, 20m duct, SS-N-22 at 20 m 78

Figure 116. MFR results, 30m duct, SS-N-22 at 20 m 79

Figure 117 MFR results, Standard atmosphere, SS-N-22 at 30 m 80

Figure 118. MFR results, 10m duct, SS-N-22 at 30 m 81

Figure 119. MFR results, 20m duct, SS-N-22 at 30 m 82

Figure 120. MFR results, 30m duct, SS-N-22 at 30 m 83

Figure 121. MFR results, Standard atmosphere, SS-N-22 at 7 m 84

Figure 122. MFR results, 10m duct, SS-N-22 at 7 m 85

Figure 123. MFR results, 20m duct, SS-N-22 at 7 m 86

P517610.PDF [Page: 18 of 123]

Figure 124. MFR results, 30m duct, SS-N-22 at 7 m 87
Figure 125. MFR results, standard atmosphere, NOVATOR at 15 m 88
Figure 126. MFR results, 10m duct, NOVATOR at 15 m 89
Figure 127. MFR results, 20m duct, NOVATOR at 15 m 90
Figure 128. MFR results, 30m duct, NOVATOR at 15 m 91
Figure 129. MFR results, Standard atmosphere, NOVATOR at 50 m 92
Figure 130. MFR results, 10m duct, NOVATOR at 50 m 93
Figure 131. MFR results, 20m duct, NOVATOR at 50 m 94
Figure 132. MFR results, 30m duct, NOVATOR at 50 m 95
Figure 133. MFR results, standard atmosphere, NOVATOR at 3 m 96
Figure 134. MFR results, 10m duct, NOVATOR at 3 m 97
Figure 135. MFR results, 20m duct, NOVATOR at 3 m 98
Figure 136. MFR results, 30m duct, NOVATOR at 3 m 99

List of tables

Table 1 LOS Radar Range in km for Standard Propagation 4

Table 2. Approximation error on arcsin θ 6

Table 3. Height of lowest two maxima for APAR-like radar 7

Table 4. ASM Threat Parameters 12

Table 5. List of α and β Values 14

Table 7. Volume Search Radar parameters 17

Table 8. Volume Search Radar Waveform Selected Parameters 18

Table 9 SPS-49 Maximum detection range for incoherent integration of four bursts 21

Table 10. Sea Giraffe 150HC 22

Table 11 Sea Giraffe Maximum Detection Range for incoherent integration of four bursts .. 26

Table 12. MFR Parameters 27

Table 14 MFR maximum detection range for 3-out-of-4 binary integration of four bursts 33

Table 15 MFR maximum detection range for incoherent integration of four bursts 34

Table 16 MFR maximum detection range: binary via incoherent integration 35

1. Introduction

The sea-skimming missile is one of the more stressing threats for naval air defence radars. These missiles fly at low-altitude with high velocity, and have low radar cross-section (RCS). This makes them extremely difficult to detect and track early enough for successful engagement as will be seen in this report. Certain ducting conditions can make their detection even more difficult.

This study evaluates the detection capabilities of three naval radars against current antiship missile (ASM) threats under various ducting conditions. Propagation of radio frequency (RF) energy at low-altitude is first examined to demonstrate the limitations and problems associated with detection of low flying targets. Then, the parameters of three naval radars and ASMs are defined for this study. The subject radars are the SPS-49, the Sea Giraffe and an active multifunction radar (MFR). The ASMs of concern in this study are the Exocet, the SS-N-22, and the Novator sea skimmer. The defined radars are evaluated against the ASMs under four atmospheric conditions: standard atmosphere, and with evaporation ducts at heights of 10 m, 20 m and 30 m.

2. Low –Altitude RF Propagation

Detection of low-level targets is strongly affected by the RF propagation conditions between the targets and the radar. The amount of RF energy that illuminates a given target is a function of the atmospheric and surface conditions.

2.1 Horizon

2.1.1 Optical

At low elevation angles, the horizon limits what the radar can illuminate. The optical horizon is defined as the distance from the observer to the surface of the earth, along a line that is tangent to the earth's surface (Figure 1). The area below the horizon is called the shadow region. The radar RF energy is rapidly attenuated in this region. The distance between a radar, at height h_{radar} above the surface, and the horizon is given by:

$$R^2_{optical\ horizon} = (r_{earth} + h_{radar})^2 - r^2_{earth} = 2\, r_{earth}\, h_{radar} + h^2_{radar} \quad (1)$$

If h_{radar} is much smaller than r_{earth} then

$$R_{optical\ horizon} \approx \sqrt{2\, r_{earth}\, h_{radar}} \quad (2)$$

This distance is called the optical horizon. The range at which a missile crosses the line-of-sight (LOS) optical horizon is called the LOS optical range and is given by:

$$R_{LOS\ optical\ range} \approx \sqrt{2\, r_{earth}} \left(\sqrt{h_{radar}} + \sqrt{h_{missile}} \right) \quad (3)$$

The accepted value of earth radius is 6371 km. The LOS optical range represents a good reference range for evaluating the detection capability of naval radars. A good naval defence radar should detect targets as soon as they cross this point.

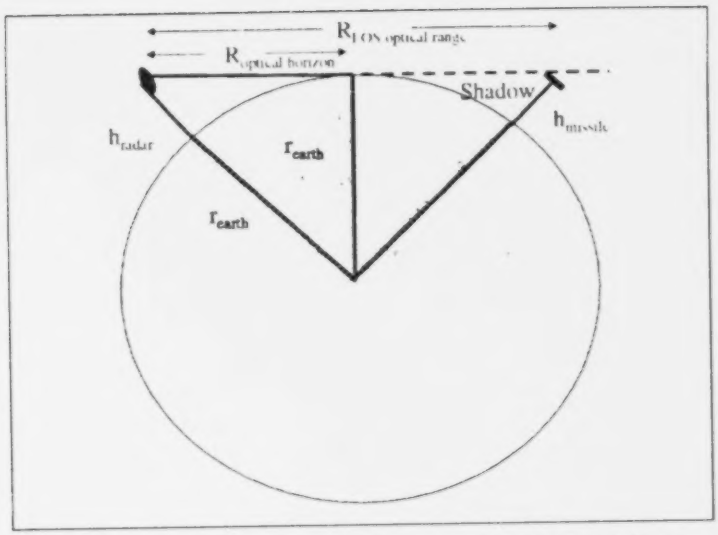

Figure 1. *Optical Horizon and LOS Optical Range*

For radars 20 m above mean sea level, a fast boat and a missile flying 7.5 m above mean sea level the LOS optical range are at 16 and 26 km respectively. The only way to increase the LOS optical range is by increasing the antenna height above the sea.
Although the electromagnetic energy is rapidly attenuated beyond the optical horizon, there is still energy propagating beyond the horizon through diffraction [1]. The amount of energy diffracted into the shadow region increases with the wavelength. Only meter and centimeter wavelengths produce enough diffraction to be useful for the detection of targets beyond the horizon. At optical frequencies, the geometrical horizon represents the boundary between the regions of propagation and non-propagation.

2.1.2 Non-homogeneous Atmosphere

2.1.2.1 Standard Atmosphere

Radar energy propagates in straight lines for homogenous atmospheres. However, most of the time, the atmosphere is inhomogeneous and refracts the radar's electromagnetic beam. A standard (or average) atmosphere is defined as an atmosphere having a vertical refractivity gradient that decreases by 39 N-units per kilometer [1, 2]. This refractivity gradient bends the radar antenna beam downwards and extends the radar horizon. It is common practice to assume standard atmosphere conditions to account for the atmosphere's effects on radar propagation. In this case, the actual earth radius is simply replaced by an effective earth radius of 4/3 over that of the actual earth radius. Hence, the LOS radar range in kilometers is given by

$$R_{LOS\ radar\ range} \approx 4.12\left(\sqrt{h_{radar}} + \sqrt{h_{missile}}\right) \tag{4}$$

where h_{radar} and $h_{missile}$ are in meters. Table 1 shows the LOS radar range for standard propagation conditions. Frequently, especially in maritime environments, the conditions for standard atmosphere seldom occur. Depending on the atmospheric conditions, the LOS radar range can either be extended or reduced.

***Table 1 LOS** Radar Range in km for Standard Propagation*

LOS Radar Range in km		Radar Height in meters				
		10	15	20	25	30
Target Height in meter	0	13 03	15 95	18 42	20 60	22 56
	3	20 16	23 09	25 56	27 73	29 70
	5	22 24	25 17	27 63	29 81	31 77
	7 5	24 31	27 24	29 70	31 88	33 84
	10	26 05	28 98	31 45	33 62	35 59
	20	31 45	34 38	36 85	39 02	40 99
	30	35 59	38 52	40 99	43 16	45 13
	50	42 16	45 08	47.55	49 73	51 69
	100	54 22	57 15	59 62	61 79	63 76

2.1.2.2 Atmospheric Ducts

At the ocean's surface there is often a surface evaporation duct, which can trap part of the incident RF energy [1, 3]. These ducts can either increase or decrease detection range depending on the frequency used and the height of the duct. Reducing detection range would make a warship more vulnerable to sea skimmers.

2.2 Multipath

Multipath is caused by the interference between the direct ray and the ray reflected by the surface. Multipath caused by a flat surface does not broaden the antenna beam but creates nulls and maximas in it

2.2.1 Point Source

Let us consider, for simplicity, a point source antenna radiating above a flat surface that is perfectly reflecting (Figure 2).

Figure 2. *Multipath Interference*

The reflected ray is equivalent to a ray transmitted from a mirror point source radiating 180 degrees out of phase. The path difference between each source in the far field is given by

$$2h_{radar} \sin\theta = \Delta x \tag{5}$$

Where h_{radar} is the antenna height and θ is the elevation angle, shown in Figure 2. The summation of the direct and indirect ray is a maximum value when the path difference is equal to an odd number of half wavelengths.

$$2h_{radar} \sin\theta_{n\max} = \left(n - \frac{1}{2}\right)\lambda; \qquad \text{where n = 1,2, ...} \tag{6}$$

By reorganizing the equation we get,

$$\theta_{n\max} = \arcsin\left[(n - \frac{1}{2})\frac{\lambda}{2h_{radar}}\right]; \qquad \text{where n = 1,2, ...} \tag{7}$$

The interference is a minimum when the path difference is an even number of wavelengths. Hence,

$$\theta_{n\min} = \arcsin\left[(n)\frac{\lambda}{2h_{radar}}\right]; \qquad \text{where n = 1,2, ...} \tag{8}$$

For small angles, the arcsin is approximately equal to the angle in radians (see Table 2). Hence, the angular position of the first interference maximum is given by

$$\theta_{1\max} \approx \left[\frac{\lambda}{4h_{radar}}\right]; \qquad \text{where n} = 1.2, \ldots. \tag{9}$$

Table 2. Approximation error on arcsin θ

θ degree	θ radian	Arcsin (θ rad) in degree	Error in % on
5	0.0873	5.0064	0.13
10	0.1745	10.0515	0.51
15	0.2618	15.1769	1.2

The null to null angle separation is equal to:

$$\phi_{null-to-null} \approx \frac{\lambda}{2h_{radar}} = \frac{\lambda}{L} \tag{10}$$

where L is equal to $2h_{radar}$ and represents the length of the equivalent antenna array. In summary, the radiation pattern including the multipath is the same as an antenna array having two point sources 180 degrees out of phase and separated by $2h_{radar}$ (Figure 3).

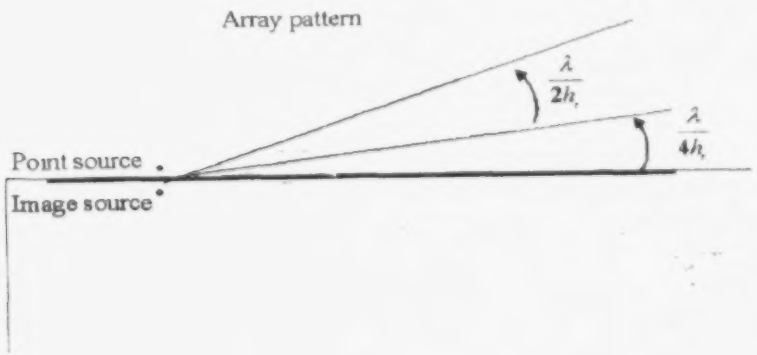

***Figure 3.** Multipath Pattern*

The detection range is twice that of free space at the maxima of the pattern [1]. The peaks of the maxima are given by:

$$h_{lobe} = R \arcsin\left[(n-\frac{1}{2})\frac{\lambda}{2h_{radar}}\right] \tag{11}$$

We have used the exact expression of lobe angle since an error of 1 percent at a one-km range means an error of ten meters. For radars like APAR (Active Phased Array Radar [24, 25]) transmitting at a wavelength of 3 cm and an antenna height of 20 m, the height of the first two lobes are shown in Table 3.

Table 3. Height of lowest two maxima for APAR-like radar

Range (km)	Height of first lobe (m)	Height of second lobe (m)
30	11.3	33.7
25	9.4	28.1
20	7.5	22.5

This situation is advantageous for the detection of low flying missiles since the height of the first peak is very low at the range of interest, i.e., when cruise missiles cross the horizon. Below the first lobe, the propagation factor is still superior to that of free space until the missile reaches the angle

$$\theta_{freespace} \approx \frac{\lambda}{12h_{radar}} \tag{12}$$

at approximately 1/3 of the first lobe height.

2.2.2 Finite size antenna

For an antenna with a physical extent, the resultant pattern can be calculated by multiplying the element pattern by the array pattern as shown in antenna theory [6].

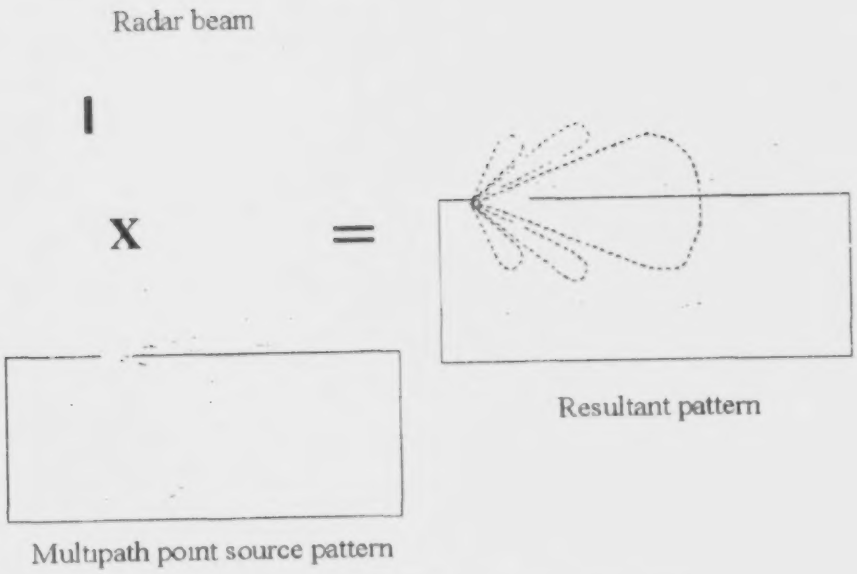

Figure 4. Multipath Pattern for extended antenna

From Figure 4, we see that multipath caused by a flat surface does not broaden the antenna beam but creates nulls and maximas in it. The array pattern suppress the multipath outside of the beam. Basically, multipath creates nulls and peaks in the radar antenna beam. If required, the gaps within the main beam have to be filled by other radars or by switching frequency. The lobe structure is frequency dependent as shown in equations (8), (9) and (10). Although the use of a reflecting flat surface is simplistic, it allows one to see the impact of multipath on antenna beam coverage. For a curved earth the nulls and peaks are not as pronounced.

2.3 TERPEM

In this report, the propagation factor F is calculated by the commercial program TERPEM, developed by Signal Sciences Limited, U.K. [7]. The TERPEM models and calculations include the propagation effects from both multipath and inhomogeneous atmospheric conditions (reflection, refraction, and diffraction). These factors are very important for low level propagation. TERPEM is based on the parabolic equation

$$\frac{\partial^2 u}{\partial z^2} + 2ik\frac{\partial^2 u}{\partial x^2} + k^2(m^2(x,y)-1)\,u = 0 \qquad (13)$$

where u is the electric or magnetic field component, k is the wave number, and m is the modified refractive index.

The parabolic equation is a very popular and powerful tool for solving radiowave propagation problems. It is a very good approximation to the full electromagnetic wave equation [8, 9].

This equation is solved numerically through iterative techniques. The user specifies the initial values of the electric field at the antenna. A solution is found for the first iterative range cell by satisfying the boundary conditions at the bottom and the top of the range cell. This solution is then "passed" to the next range cell and so on. An advantage of the marching technique is that it can handle changing conditions along the range coordinates. The solution u(x,z) represents the electric field that would be measured. The electric field that would exist in free space can be calculated using the radar range equation. The propagation factor F can then be calculated from these two values of electric field. The propagation factor is the ratio of the electric field strength that is actually present at a point in space to that which would have been present if free-space propagation had occurred [18]. The propagation factor accounts for the beam pattern and all the propagation effects resulting from reflection, refraction, and diffraction. In free space, the propagation factor is equal to one.

In Figure 5, we have an example of the output produced by TERPEM. We can recognize the usual lobed structure caused by interference. We can also see that electromagnetic energy propagates beyond the horizon, mainly due to ducting effects and to a lesser extent by diffraction. The parabolic equation includes all the propagation effects due to reflection, refraction, and diffraction in a single model.

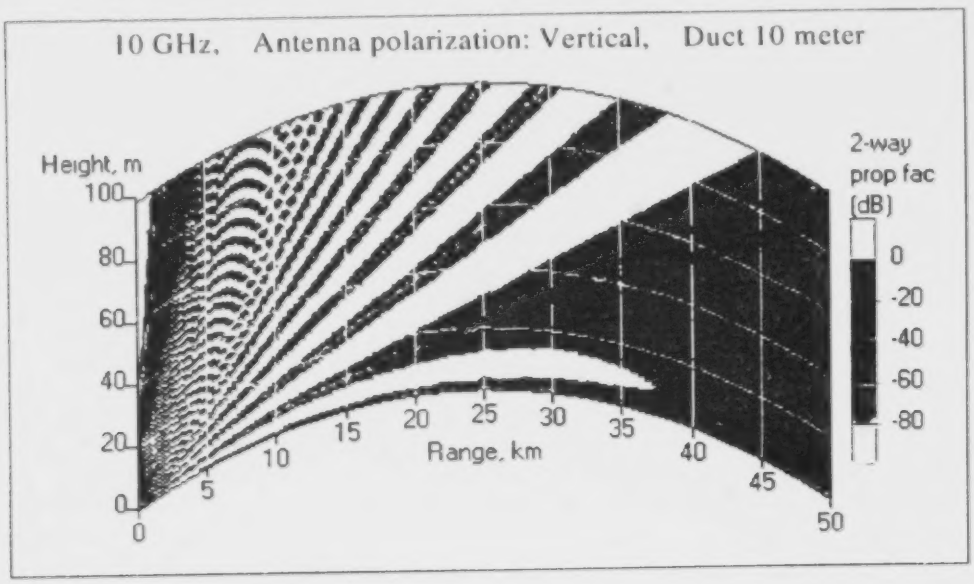

Figure 5. TERPEM Output

3. Sea Skimming Threats

The sea skimming missiles of concern for these studies are the Exocet MM-39, the SS-N-22 Sunburn, the Novator 3M-54E. These missiles are representative of the threats to be encountered by the Canadian Navy in future conflicts. The values of the parameters used in this section have been taken from open literature or estimated when not available. This approach is sufficient for one to evaluate radar performance [11 to 15].

3.1 AM39 Exocet

The Exocet missile is a sea-skimming missile that has a reported range of 50 km [11, 12]. It has a nose-on RCS of 0.1 m^2 and cruises at a speed of mach 0.93. Its initial height is between 9-15 m (Figure 6). The Exocet's radar seeker acquires its target at between 12 and 15 km in range. Then, the Exocet drops to about 3-8 m for its second cruise phase depending on the sea conditions.

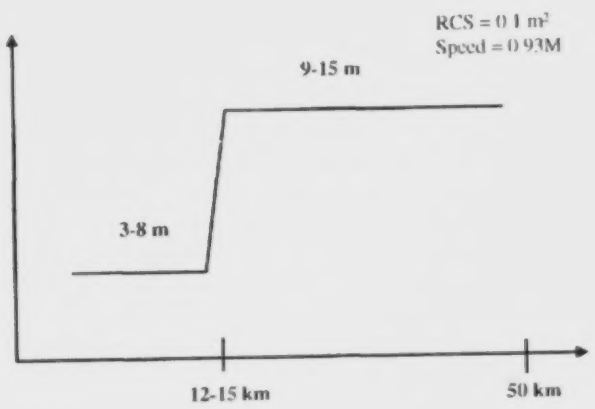

Figure 6. Exocet Flight Profile

The RCS value of 0.1 m^2 is valid only for a nose aspect and represents the worst case scenario for the targeted ship. At other aspects the RCS will increase. Therefore, for this study, we use a nominal value of 0.1 m^2.

3.2 SS-N-22 Sunburn

The SS-N-22 is a supersonic (mach 2) sea skimmer, believed to have been designed to defeat the Aegis Cruiser [13, 14]. It has impressive maneuvering capability. It has a maximum range of 120 km but would need targeting support for ranges greater than 55 km. Its initial cruising height is between 20 to 30 m (Figure 7). At about 20 km it will acquire the targeted ship and lower its flight to its second cruising height of 7 m. The SS-N-22 is a large missile with a nose-on RCS of 1 m^2.

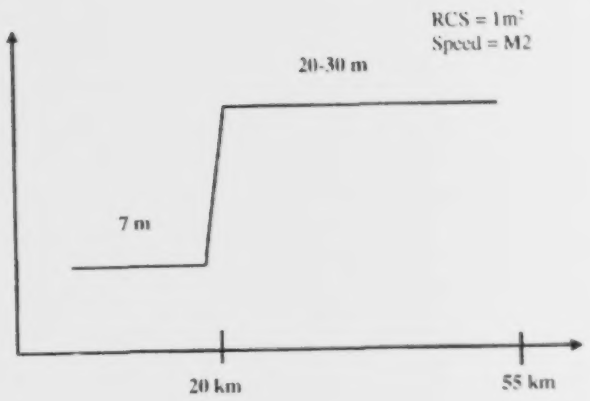

Figure 7. SS-N-22 Flight Profile

3.3 Novator 3M-54E

The Novator 3M-54E is a new Russian ASM. A version of this missile is now being offered for export [15]. These missiles first cruise at an altitude of 10-15 m above mean sea level (Figure 8). At a range of 30-40 km to the target, the missile climbs to a higher altitude and activates its homing radar. Once the seeker has detected the target and locks-onto it, the missile flies at supersonic speed (1100 m/s) and at about 20 km range descends to 3-5 meters above water. For simplicity, the RCS value, which is in Table 4 is kept constant for the whole duration of the flight.

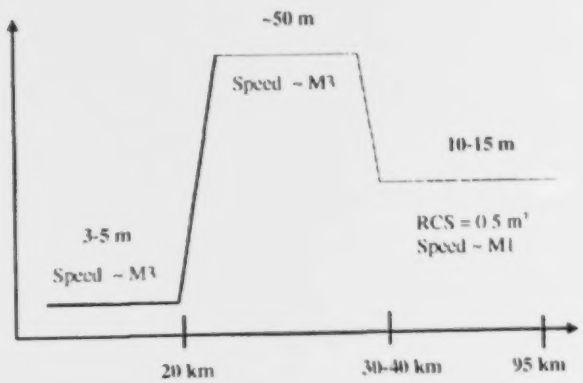

Figure 8. NOVATOR 3M-54E Missile Flight Profile

3.4 Overall Threat

The parameters in Table 4 summarize properties of each ASM threat. As shown, the ASMs cruise initially at, between 9 to 50 m. The terminal phase starts between 10 to 20 km with a cruising height from 3 to 8 meters. For simplicity, the variation of RCS with frequency has not been considered in this initial study.

Table 4. ASM Threat Parameters

	RCS m^2	Max R km	Initial height m	Cruising Speed (m/s)	Terminal height
AM39 Exocet	0.1	50	9-15	308 (M0.93)	3-8 m (start ~ at 12-15 km)
SS-N-22 Sunburn	1	90	20-30	662	7 m (start ~ 20 km)
Novator 3M-54E	0.5	100	10-15 (50 m middle)	333 initial 1100 final	3-5 m (start ~ at 20 km)

In this study, the detection range is defined as the maximum range where the probability of detection, P_d, is greater than or equal to 0.9. This range is calculated at 3 different heights for each missile, i.e.,

AM39 Exocet	9, 15, and 3 m
SS-N-22 Sunburn	20, 30, and 7 m
Novator 3M-54E	15, 50, and 3 m.

4. Detection Performance Criteria

4.1 Evaluation Criteria

This study evaluates the detection capability of the SPS-49, the Sea Giraffe, and a multifunction radar (MFR) against low-level ASM threats. The detection capability of these radars will be evaluated in terms of the maximum range at which the target gives the required P_d. For this study, the required probability of detection P_d and the probability of false alarm P_{fa} are set to 0.9 and 10^{-6} respectively.

The radar horizon limits the maximum range at which the sea skimmer can be detected. For optimal defence against sea skimmers, the radars should be able to detect targets and initiate tracking as soon as they cross the LOS radar range. As an initial study, we assume clutter has been suppressed to 10dB below noise level. This means the target power is only limited by thermal noise.

4.2 Maximum Detection Range

The maximum detection range at which a target produces the desired P_d is calculated in two steps. The probability of detection is first calculated and then the range at which the P_d first exceeds the given value is identified. The Sea Giraffe and the SPS-49 radar integrate the coherent bursts incoherently before applying a threshold. The MFR of this study uses binary integration of the bursts to detect targets. Each integration type requires different steps to calculate the probability of detection of the dwell.

4.2.1 Incoherent Integration

The probability of detection P_d, when n_{bursts} bursts are incoherently integrated is calculated using the equation of Neuvy [16, 17].

$$P_d = 10^{-u}; \qquad where\ u = \left[\frac{\alpha \log\left(\frac{\ln(2)}{P_{fa}} \right)}{n_{bursts}^{\frac{2}{3}}\, \overline{SNR}_{bursts}} \right]^{\frac{1}{\beta}} \tag{14}$$

The value of the parameters α and β are given in Table 5 and are functions of the Swerling models, which define different target RCS statistics [1], [2].

Table 5. List of α and β Values		
Swerling Model	α Value	β Value
0	$1+2e^{-\frac{n_{bursts}}{3}}$	**0.167**
1	$0.67\ (1+0.67\,e^{-\frac{n_{bursts}}{3}})$	**1**
2	**1**	$0.167+e^{-\frac{n_{bursts}}{3}}$
3	$0.75\ (1+0.67\,e^{-\frac{n_{bursts}}{3}})$	**0.67**
4	**1**	$0.167+0.67\,e^{-\frac{n_{bursts}}{3}}$

The equations of Neuvy are based on the well-known theory of Swerling and Marcum.

4.2.1.1 Average Signal to Noise Ratio

The equations of Neuvy have been developed for a signal-to-noise-ratio (SNR) that has a constant mean and standard deviation from burst to-burst. For the cases investigated here, the frequency can change from burst-to-burst, which then causes the mean and standard deviation of the SNR to change with each burst. For example, the effects of multipath and ducting are very dependent on frequency. Consequently, an average value of SNR for all bursts is first determined. This average value is then used in the Neuvy equations.

For a radar system that is limited by thermal noise, the SNR of a single burst is given by:

$$SNR = \frac{n_c P_t G A_e \sigma F^4}{(4\pi)^2 R^4 fKTB} \tag{15}$$

where P_t is the peak power of the transmitted signal, G is the antenna gain, σ is the radar cross section of the target in m^2, A_e is the effective antenna aperture in m^2, R is the range of the target in m, K is the Boltzmann's constant (1.38 x 10-23 Joules per degree), T is the system reference noise temperature, B is the receiver bandwidth, f is the receiver noise figure, F is the propagation factor at range R. As stated in section 2.3, the propagation factor is calculated using TERPEM.

The average value of SNR for the bursts is calculated as follows.

$$\begin{aligned} \overline{SNR}_{burst} &= \sum_{i}^{n_{bursts}} \frac{SNR_i}{n_{bursts}} \\ &= \sum_{i}^{n_{bursts}} \left(\frac{n_c P_t G A_e \sigma}{(4\pi)^2 R^4 fKTB} \right)_i \left(\frac{F_i^4}{n_{bursts}} \right) \end{aligned} \tag{16}$$

This is the value of SNR that is used in Equation (14).

The Neuvy equation can also be used to determine the minimum value of the burst SNR for a given required P_d and P_{fa}.

$$\overline{SNR}_{burst} = \frac{\alpha \log\left(\frac{\ln(2)}{P_{fa}}\right)}{n_{bursts}^{\beta}\left[\log\left(\frac{1}{P_d}\right)\right]^{\beta}} \qquad (17)$$

The SNR requirement changes significantly as a function of the statistics associated with the RCS of the target. *Table 6* shows the required SNR per burst for a P_d of 0.9 and a P_{fa} of 10^{-6} for each type of Swerling target.

Table 6 SNR Requirements for $P_d = 0.9$ and $P_{fa} = 10^{-6}$

SNR PER BURST		NUMBER OF BURSTS				
		1	2	4	50	100
SWERLING TYPE	0	23 79	12 48	5 93	0 72	0 45
	1	126 58	72 41	39 93	6 30	3 97
	2	89 12	30 01	8 75	0 72	0 45
	3	51 20	29 2	16 15	2 55	1 61
	4	42 98	17 79	6 69	0 72	0 45

4.2.2 Binary integration

An M-out-of-N detector uses two thresholds to decide if a target is present or not. A first threshold is applied to each of the N pulse bursts to be integrated. A counter that determines the number of times the first threshold is exceeded follows this. Detection is reported when the second counter reaches or exceeds a certain value M. The M-of-N detectors are easy to implement and are more resistant to noise and sea spikes.

Usually, the probability that the signal exceeds the first threshold is the same for all events. In this case, the probability that the first threshold will be exceeded at least M times in N events is,

$$P_{d_dwell} = \sum_{i=M}^{N} C_{iN} \, (p_{d_burst})^{i} \, (1 - p_{d_burst})^{N-i}; \qquad C_{iN} = \frac{N!}{i!(N-i)!} \tag{18}$$

P_{d_dwell} is the probability of detection of the dwell and p_{d_burst} is the probability of detection of an individual burst [17]. If the frequency is changed from burst to burst, the SNR and P_d may also change for each burst. In this case, the probability that the first threshold will be exceeded at least M times in N events is given by

$$P_{d_dwell} = \sum_{i=M}^{N} \left(\sum_{(M \text{ hits, } "(N-M) \text{ misses}")}^{All\ Combinations} \prod_{j=1}^{N} probability\ of\ burst\ j \right) \tag{19}$$

where the probability of the burst j is its probability of detection or non-detection depending on whether it is a hit or a miss [17]. The burst j is considered a hit if the threshold is exceeded, otherwise it is a miss. The summation within the bracket represents the sums of all combinations having M hits, and (N-M) misses. In this report, we only consider a 3-out-of-4 binary detector.

Considering the case where M=3 and N=4 we have.

$$\begin{aligned} P_{d_dwell(3out4)} = {} & p_{d_b1}p_{d_b2}p_{d_b3} + p_{d_b1}p_{d_b2}p_{d_b4} + p_{d_b1}p_{d_b3}p_{d_b4} \\ & + p_{d_b2}p_{d_b3}p_{d_b4} - 3p_{d_b1}p_{d_b2}p_{d_b3}p_{d_b4} \end{aligned} \tag{20}$$

On the other hand, the P_{fa} is constant from burst to burst, hence:

$$P_{fa_dwell(3out4)} = 4p_{fa_burst}^{3} - 3p_{fa_burst}^{4} \tag{21}$$

The P_d of the dwell is calculated as follows. First, the SNR for each burst is calculated as a function of range using equation (15). Second, the p_d for each burst is calculated as a function of range using the Neuvy equation (14) for a single burst (n_{bursts}=1). Third, the P_d of the dwell is calculated using (21). We can then determine the range at which the P_d of the dwell will first exceed the required 0.9 probability of detection. This will give the maximum detection range of the radar corresponding to a P_d of 0.9 and a 3-out- of-4 binary detector.

5. Radar Systems

The radars under consideration for this study are the SPS-49, the Sea Giraffe and an MFR. The parameters of these radars are based on open literature and not on those radar installed on the Canadian patrol frigates. In particular, the height of the Sea Giraffe radar as defined in this report is only 15 m as opposed to 26m for the one installed on the Canadian Patrol Frigates. Hence, results and conclusions obtained in this study are not directly applicable to the CPF radar components.

5.1 Volume Search Radar

An example of a volume search radar is the AN/SPS-49, which is a 2D long-range air search radar [10, 19, 20]. Associated parameters are given in Table 7.

Table 7. Volume Search Radar parameters

Peak and average Power	360 Kw / 12-13 Kw
Pulsewidth	2 µs, 65 µs (Chirped), and 125 µs (Chirped)
Compressed pulse	~2 µs
Bandwidth	0 5 MHz
Frequency range	850 to 942 MHz
Frequency mode	Fixed, or agile
PRF mode	Fixed, and staggered
PRF range	280-1000 Hz
Antenna Height	20 4 m
Antenna RPM	6 or 12 RPM
Antenna dimensions	7 3 m (wide) by 4 3 m (height)
Antenna beam	3 3° in azimuth and 11° in elevation Cosec square to 20 degree
Antenna Gain	28 5 dB
Antenna polarisation	Vertical
Noise Figure	4 5 dB
System temperature	290 Kelvin
Signal Processing	Doppler and MTI

For this study, we are interested in the earliest possible detection of a sea skimmer. The selected waveform for this study consists of four bursts at different frequencies and PRFs.

Table 8. *Volume Search Radar Waveform Selected Parameters*

Burst	Number of pulses	PRF in Hz	Frequency in MHz
1	5	288	850
2	5	300	875
3	5	313	915
4	5	248	942

Each coherent burst consists of 5 pulses. The center of the antenna is 20.4 m above sea level. The required P_d and P_{fa} are respectively set to 0.9 and 10^{-6}. The ASMs are assumed to be targets of Swerling type 3.

The maximum detection range where a target produces a P_d of 0.9 is calculated in two steps. The probability of detection as a function of range is first calculated using Equations (16) and (14). Then, the range where the P_d first exceeds 0.9 is extracted from these P_d curves. The TERPEM software is used to calculate the propagation factors in the presence of the sea for the SPS-49 bursts. These values of the propagation factor are given in Annex A. Figure 9 and 10 give the value of the propagation factor along the range and height co-ordinates for 850 MHz and 942 MHz respectively. In each figure, four different atmospheric conditions are considered: standard atmosphere, and evaporation ducts at 10, 20, and 30 meters height. From these figures, we note that the propagation factor increases at low-altitudes as the duct height increases. We also note that there is little difference between the propagation plots for the 850 MHz and 942 MHz frequencies. This shows that changing the frequency of the SPS-49 within its frequency band will have little impact on its detection capability whatever the atmospheric conditions.

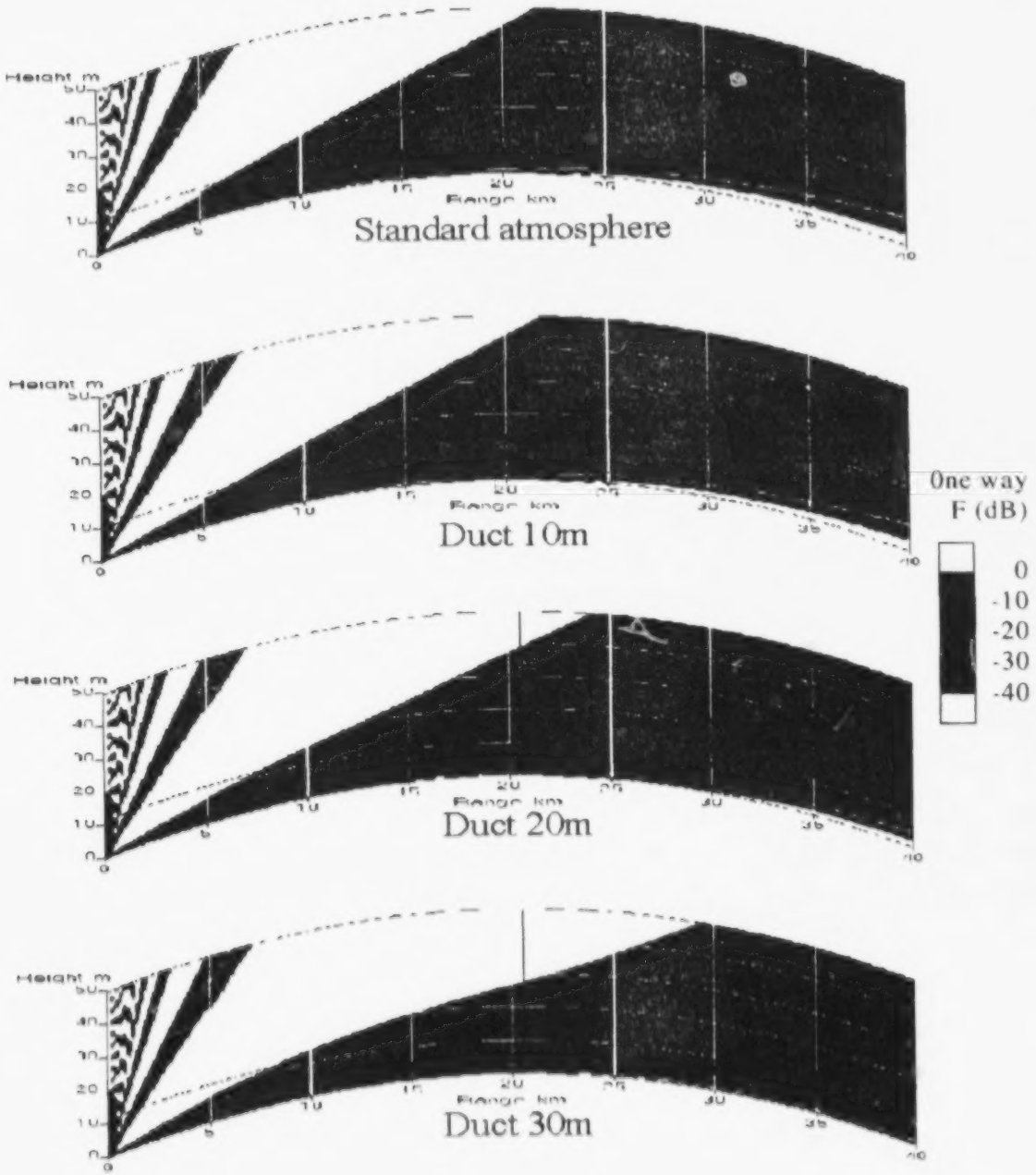

Figure 9. Propagation factor for the SPS-49 at 850 MHz

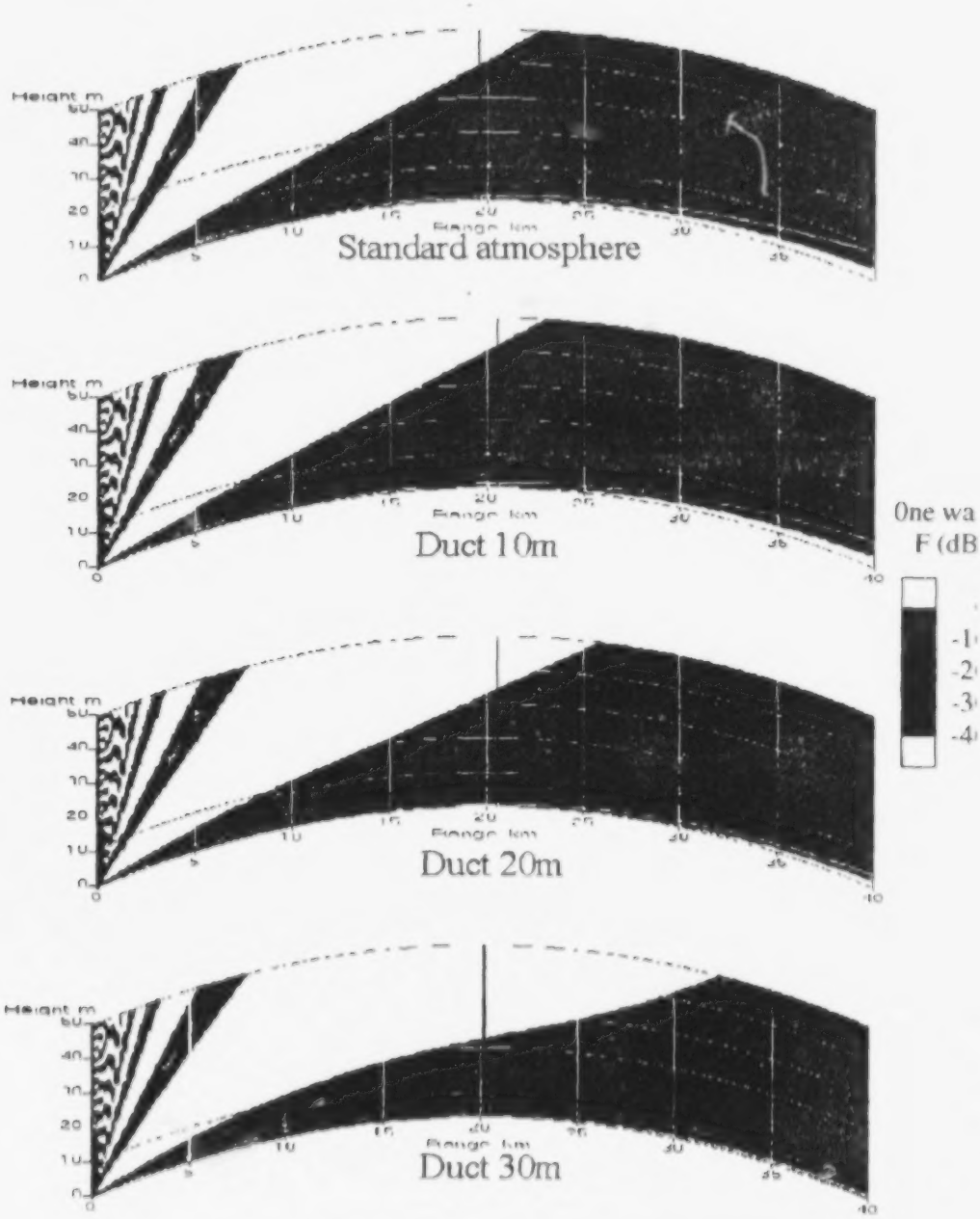

Figure 10. Propagation factor for the SPS-49 at 942 MHz

The ranges of the missiles where the 0.9 P_d condition is first met are shown in Table 9. In this table, the missiles fly at constant height for each case.

***Table 9** SPS-49 Maximum detection range for incoherent integration of four bursts*

	VSR ANTENNA HEIGHT 20 4M) 4 Burst (850, 875, 915, 942 MHz)			MAXIMUM DETECTION RANGE (KM) (WHERE $P_D \geq 0.9$)			
	ASM Height (m)	LOS optical range (km)	LOS radar range (km)	Standard atmosphere	Duct 10 m	Duct 20 m	Duct 30 m
EXOCET RCS = 0 1m²	9	26 8	31 0	18 8	19 0	22 0	48 0
	15	30 0	34 6	22 6	22 8	26 2	34 4
	3	22 3	25 8	11 8	12 0	13 6	15 0
SS-N-22 RCS = 1m²	20	32 1	37 0	29 6	28 4	32 4	44 0
	30	35 7	41 2	33 6	33 8	36 2	48 4
	7	22 3	29 5	21 0	21 2	23 4	30 2
3M-54E RCS=0 5 m²	15	30 0	34 6	25 6	26 0	30 0	40 6
	50	41 4	47 8	37 8	38 2	>40	53 0
	3	22 3	25 8	14 0	14 2	16 4	19 0

The LOS radar ranges have been calculated using Equation (4), and represent the earliest range at which the missile can be detected in the standard atmosphere. From Table 9, we see that for the standard atmosphere the missiles are always detected from 7.4 to 14.0 km after they have crossed the LOS radar range. These targets must be detected earlier to increase the probability of a successful engagement.

Ducts always enhance the detection range of the SPS-49 radar against the ASMs described in this report except for one case. Ten-meter ducts have little impact on detection range increasing it by only 0.2 km in certain cases and 0.4 km in others. In one case, however, the maximum detection range is reduced by 1.2 km. A twenty-meter duct increases the detection range by about 2 to 5 km, which is not negligible. A thirty-meter duct increases detection range between 3 to 29 km

The SPS-49 radar has the worst detection performance against the missiles flying at 3 m above sea. This would be particularly troublesome for the case of an ASM having a constant cruise height at 3 m, and with the RCS and speed capability of the Novator (1100 m/s). In this case detection would only occur at a range of 14 km.

It should be noted that a target could be detected even if the target is within a duct and the antenna outside it. Similarly, a target can be detected if the antenna is within the duct and the target outside.

By calculating the maximum detection range using incoherent integration of four bursts but with the same frequency, we can compare the performance of multiple frequencies against that of a single frequency. It is found that higher frequencies always produce longer-range performance. The reason being that the first multipath lobe is lower at higher frequencies. We also note that the use of multiple frequencies produces a detection range between those that would be obtained for single frequency using the minimum and maximum frequency. There is little performance gain to win in terms of maximum detection range by changing the frequency of operation of the SPS-49 (when clutter is not considered).

5.2 Sea Giraffe

The Sea Giraffe 150HC radar is a medium range air and surface surveillance radar [10, 21, 22, 23]. Its parameters are given in Table 10.

Table 10. *Sea Giraffe 150HC*

Peak and average Power	60 Kw and 1 2 KW
Uncompressed Pulsewidth	4 microseconds
Compression Ratio	12
Bandwidth	3 MHz
Frequency range	5 4 to 5 9 GHz (AMB version)
Frequency mode	Fixed, agile (scan, sector, or burst)
PRF mode	Fixed, scan agility, or Staggered
PRF range	1 to 7 KHz
Antenna height	15 m
Antenna RPM	30 or 60 RPM
Antenna dimensions	2 4 m by 0 8 m
Antenna beams	3 or 4 sequential beam in elevation
Antenna first beam	1 80 in azimuth and 80 in elevation Cosec square to 40 degree
Antenna Gain first beam	30 dB
Antenna Polarisation	Vertical
Noise Figure	5 dB
System noise	290 Kelvin
Signal Processing	MTI

The waveform selected for this study consists of four bursts of different frequencies (5.40, 5.55, 5.75, and 5.90 GHz). Each burst consists of 5 coherently integrated pulses. Although not used in our calculation, the PRF is staggered from burst to burst with a mean of 5 kHz.

The antenna height of this radar is taken as 15 meters above sea level as on a small craft [10]. This is different than the antenna height of the Sea Giraffe radar installed on the CPF, which is about 26 m. The required P_d and P_{fa} are respectively set to 0.9 and 10^{-6}. The ASMs are assumed to have a Swerling type 3 fluctuating RCS.

The maximum detection range at which a target produces a P_d of 0.9 is calculated in two steps. The probability of detection as a function of range is first calculated using Equations (16) and (14). Then the range where the P_d first exceeds the given value is extracted from these P_d curves.

The commercial software TERPEM is used to calculate the propagation factors for each Sea Giraffe burst and missile height. These values of propagation factor are given in Annex B. Figure 11 and Figure 12 show that ducting has a strong impact on the propagation factor at low-altitude for the Sea Giraffe. We note that the propagation factor plots at 5.4 GHz and 5.9 GHz look similar. Thus changing the frequency of operation within the Sea Giraffe band will not significantly change its detection range.

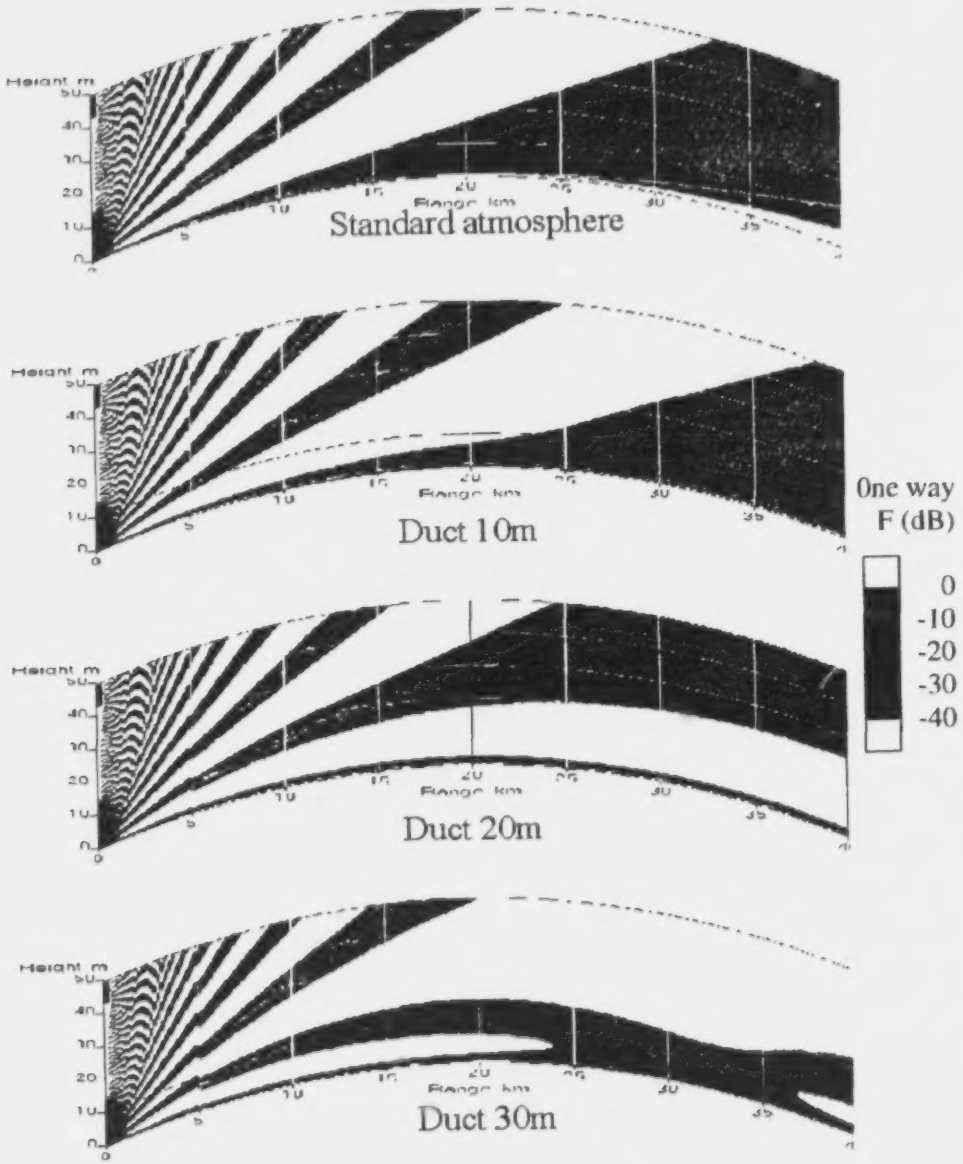

Figure 11. Propagation factor for the Sea Giraffe at 5.4 GHz

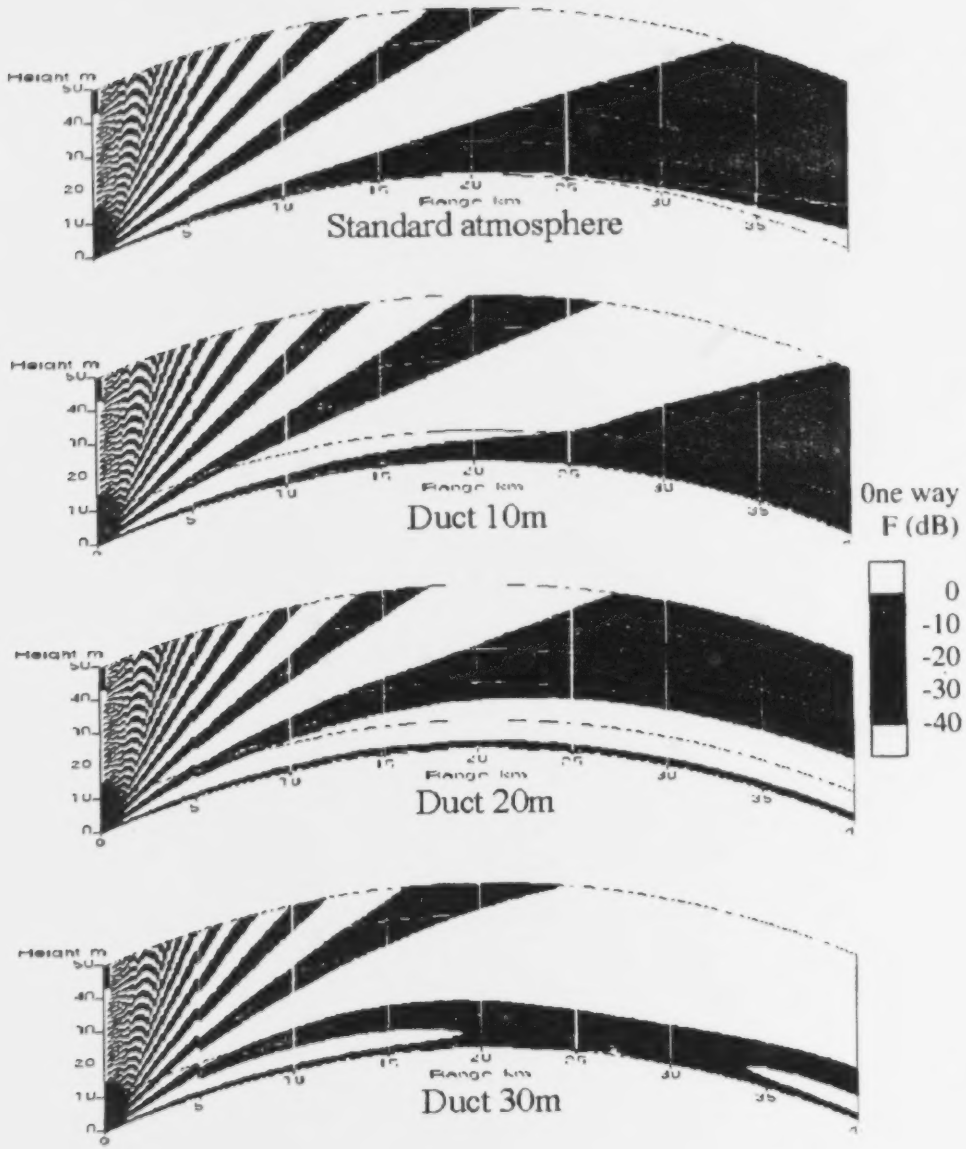

Figure 12. Propagation factor for the Sea Giraffe at 5.9 GHz

The ranges of the missiles where the 0.9 P_d condition is first met are shown in Table 11.

Table 11 *Sea Giraffe Maximum Detection Range for incoherent integration of four bursts*

	Sea Giraffe (Antenna 15 m) (5 4, 5 55, 5 75, and 5 9 GHZ)		**Maximum Detection Range (km)** (Where Pd is greater than 0 9)			
	ASM Height (m)	LOS optical and radar range (km)	Standard atmosphere	Duct 10 m	Duct 20 m	Duct 30 m
Exocet RCS = 0 1 m²	9	24 5 28 3	15.4	19 6	29 0	11 5 ***(10.5)*** 6 5
	15	27 7 31 9	18 4	21 4 ***(9.4)*** 8 0	9 5	14 0
	3	20 0 23 1	10 4	13 2	19 0	18 0
SS-N-22 RCS = 1 m²	20	29 8 34 4	23 8	28 8 ***(11.8)*** 10 6	14 0	34 5
	30	33 4 38 5	27 2 ***(14.0)*** 12 8	31 2 ***(16.6)*** 14 2	20 0	36 5
	7	23 3 26 9	17 0	24 0	55 5	23 5
3M-54E RCS=0 5 m²	15	27 7 31 9	20 6	25 6	33 5 ***(13.0)*** 10 0	26 5
	50	39 1 45 1	31 2 ***(21.0)*** 18 0	31 8 ***(26.4)*** 19 8 ***(13.0)*** 12 6	25 5 ***(15.0)*** 14 0	31 5 ***(20.5)*** 16 0
	3	20 0 23 1	12.2	16 2	30 0	21 0

Numbers in Bold and italic means that the Pd falls under 0 9 at that range

For the standard atmosphere. the ASMs are all detected from 9.9 to 13.9 kilometers after they have passed the LOS radar range. The Sea Giraffe has several discontinuities in the 0.9 P_d detection range coverage (see Figure 13).

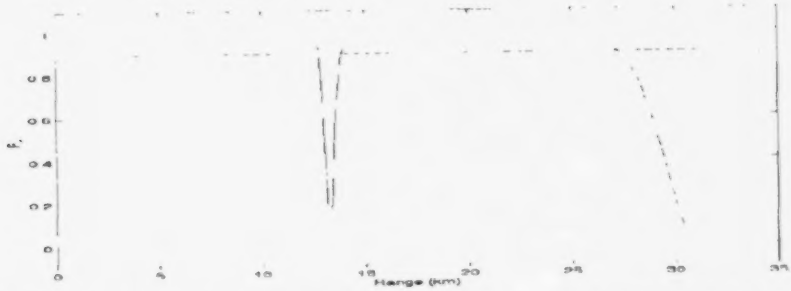

Figure 13. Example of discontinuity in the 0.9 P_d detection range coverage. The figure gives the probability of Detection for Sea Giraffe, standard atmosphere, SS-N-22 at 30 m

The worst case in terms of the 0.9 detection range discontinuity coverage is for the SS-N-22 flying at 50 m. which has detection coverage discontinuities under all atmospheric conditions.

Ducts have a strong impact on the detection capability of the Sea Giraffe, which can be significantly increased or decreased. Most of the time, however, the detection range will be increased over that corresponding to standard atmospheric conditions.

A 10-meter duct height can increase the detection range by as much as 7 km compared to that corresponding to a standard atmosphere. The impact of a twenty-meter duct height is stronger than that of the 10 meters duct height. In this case, the detection range can be increased by 9 to 38 km over the detection range in a standard atmosphere. Unfortunately, the 20 m duct height can also significantly reduce detection range thus putting the survivability of the ship at risk. For example, the Exocet missile, flying 15 m above sea level is only detected at 9.5 km. Therefore, ducting conditions cannot be ignored for the Sea Giraffe radar. A thirty-meter duct height has less impact on detection range but still can increase it by as much as 10 km as in one case, or decrease it by 4 km as in two cases.

5.3 MFR

The parameters of the MFR for this study are given in Table 12 and are similar to APAR, which is currently being developed by the Netherlands, Germany, and Canada [10, 24, 25]. However, the MFR defined in this report use a three-out-of-four binary detector rather than a two-out-of-four detector as APAR does. APAR is a very capable radar and is responsible for horizon search, track, fire control, and so on.

Table 12. *MFR Parameters*

Peak power	13 kw
Pulsewidth (unc/comp)	50 µs
Compressed pulse	0 2 µs
Bandwidth	5 MHZ
Frequency range	8 to 12 GHz
Frequency mode	agile
PRF mode	Agile
PRF range	4100 – 4900 Hz
Antenna Height	20 4 m
Antenna RPM	Electronic scan
Antenna dimensions	1 by 1 m
Antenna beam	Taylor 2 by 2 degree
Antenna Gain	38 0 dBi
Antenna Polarisation	Vertical
Noise Figure	7 5 dB
System temperature	290 Kelvin
Signal Processing	Doppler and MTI

MFRs can operate in different modes. The selected waveform for this study consists of four bursts with 32 coherent pulses per burst. Each burst has a different frequency and PRF (Table 13).

Table 13. MFR Selected Waveform Parameters

Burst	# of pulses per burst	PRF	Frequency
1	32	4800	8.0
2	32	4900	9.5
3	32	4200	10.5
4	32	4100	12.0

The ASMs are assumed to be Swerling type 3. The required P_d and P_{fa} are set respectively to 0.9 and 10^{-6}. The binary detector uses an M of N criteria of 3 out of 4. The P_{fa} for the dwell is given by

$$P_{fa_dwell(3out4)} = 4p^{3}_{fa_burst} - 3p^{4}_{fa_burst} \tag{22}$$

Solving for the P_{fa} per burst we get 6.31×10^{-4}. The SNR of each burst is calculated as a function of range using (15) and the required propagation factors are given in Annex C. Once the SNR per burst is known we can calculate its P_d using the Neuvy equation with $n_{burst}=1$.

$$P_d = 10^{-u}; \qquad where\ u = \left[\frac{\alpha \log\left(\frac{\ln(2)}{P_{fa}} \right)}{n^{2\beta}_{bursts}\, SNR} \right]^{1/\beta} \tag{23}$$

Once the P_d of each burst is known we can calculate the P_d of the dwell for a binary detector with 3-out-of-4 criteria as follows

$$\begin{aligned} P_{d_dwell(3out4)} = {} & p_{d_b1}p_{d_b2}p_{d_b3} + p_{d_b1}p_{d_b2}p_{d_b4} + p_{d_b1}p_{d_b3}p_{d_b4} \\ & + p_{d_b2}p_{d_b3}p_{d_b4} - 3p_{d_b1}p_{d_b2}p_{d_b3}p_{d_b4} \end{aligned} \tag{24}$$

The range at which the P_d first exceeds 0.9 is extracted from these calculated P_d curves. The results are shown in Table 14. The propagation factor plots for each burst of the MFR waveform are shown in Figure 14, 15, 16 and 17. They show that ducts have a very strong impact on the propagation factors at any frequency. Furthermore, there is a large difference in the propagation plots at 8.0 GHz and 12.0 GHz. Hence, the choice of the burst frequencies can make quite a difference for a given duct condition.

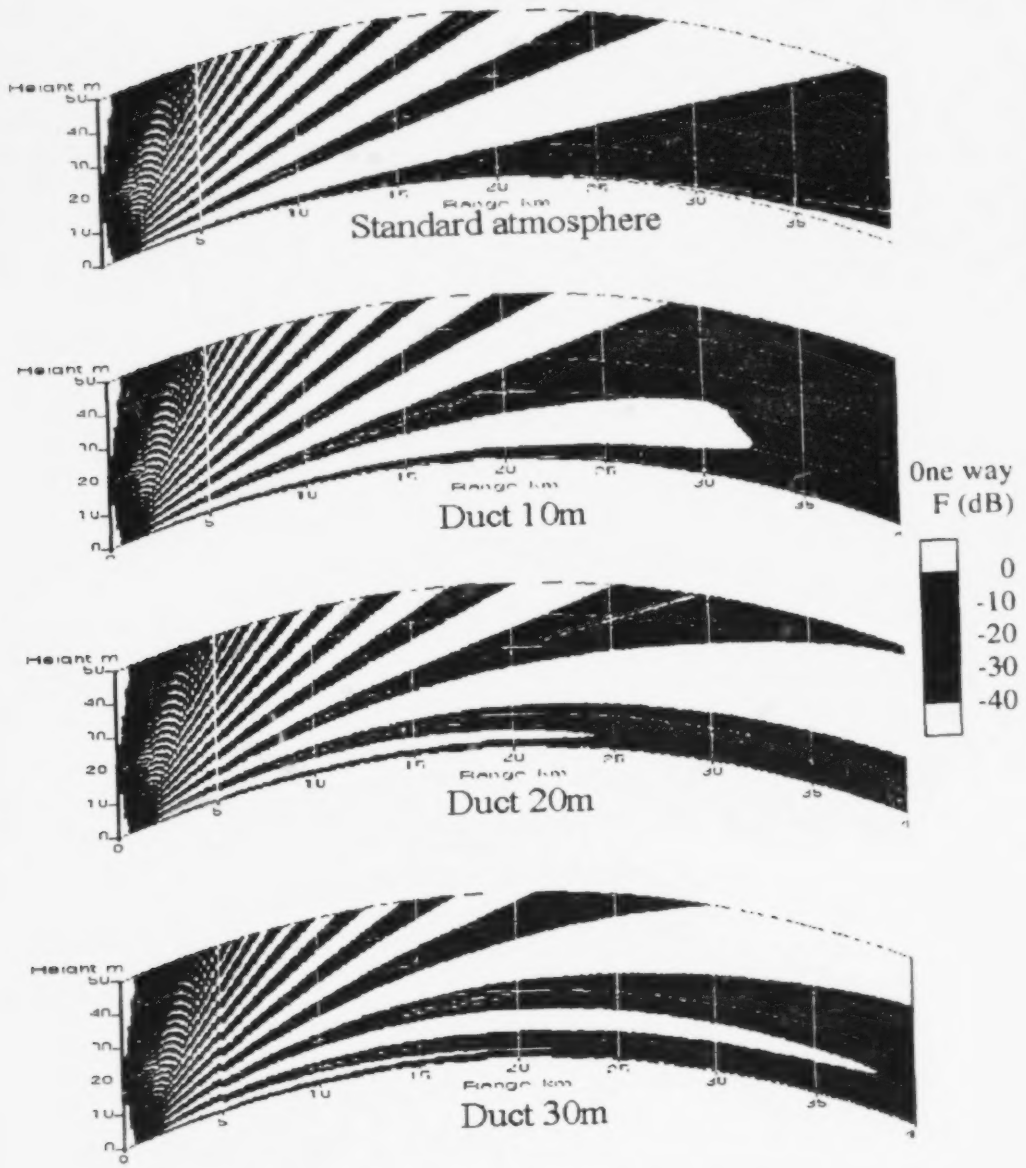

Figure 14. Propagation factor for the MFR at 8.0 GHz

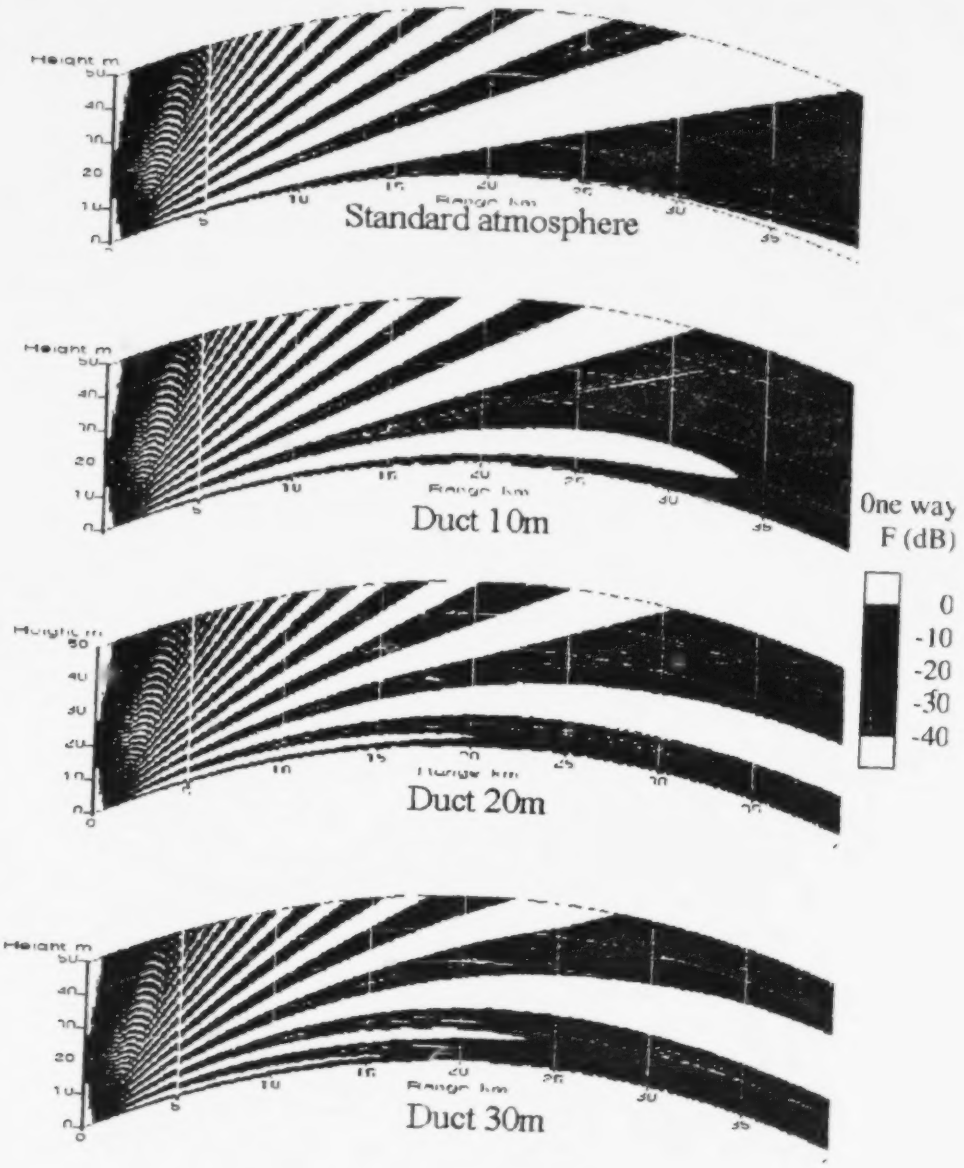

Figure 15. Propagation factor for MFR at 9.5 GHz

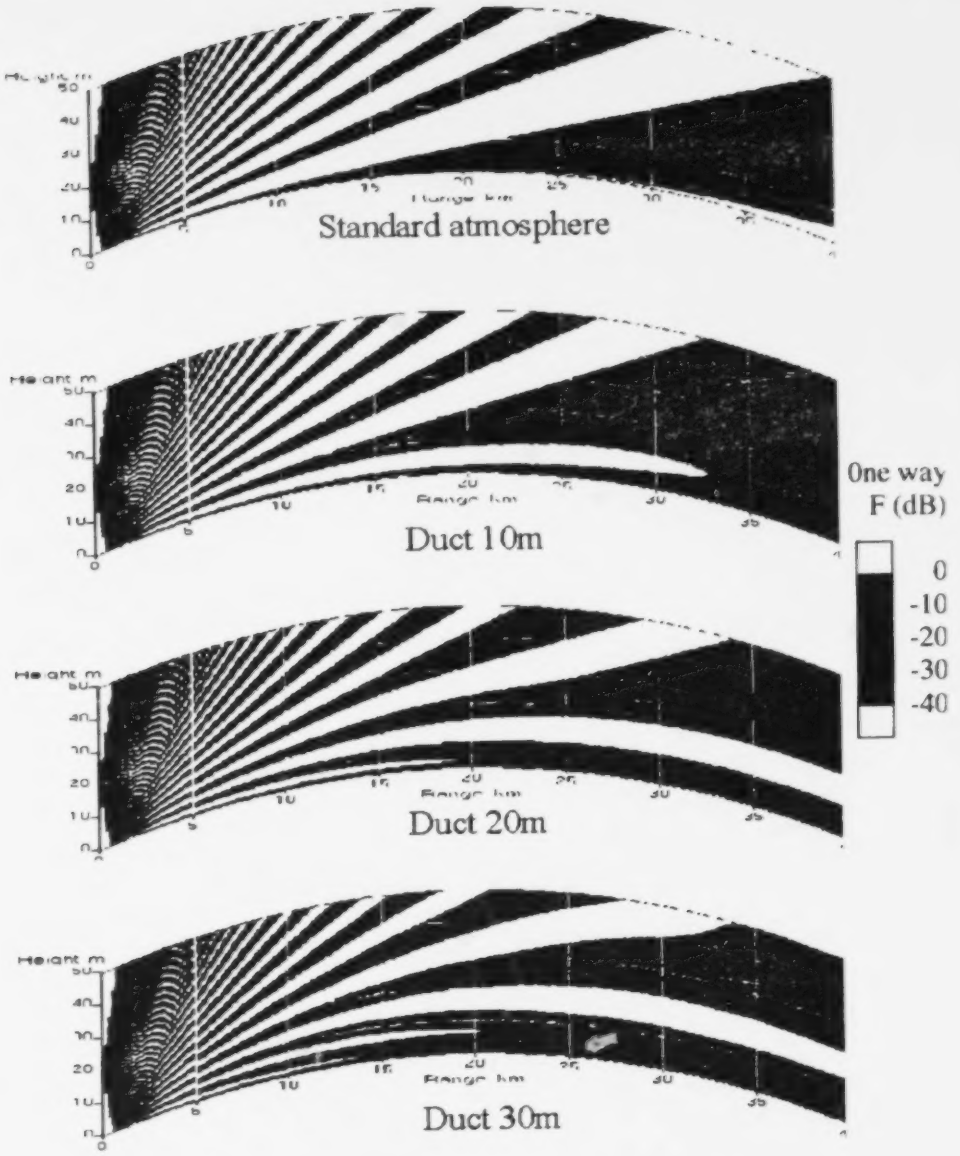

Figure 16. Propagation factor for MFR at 10.5 GHZ

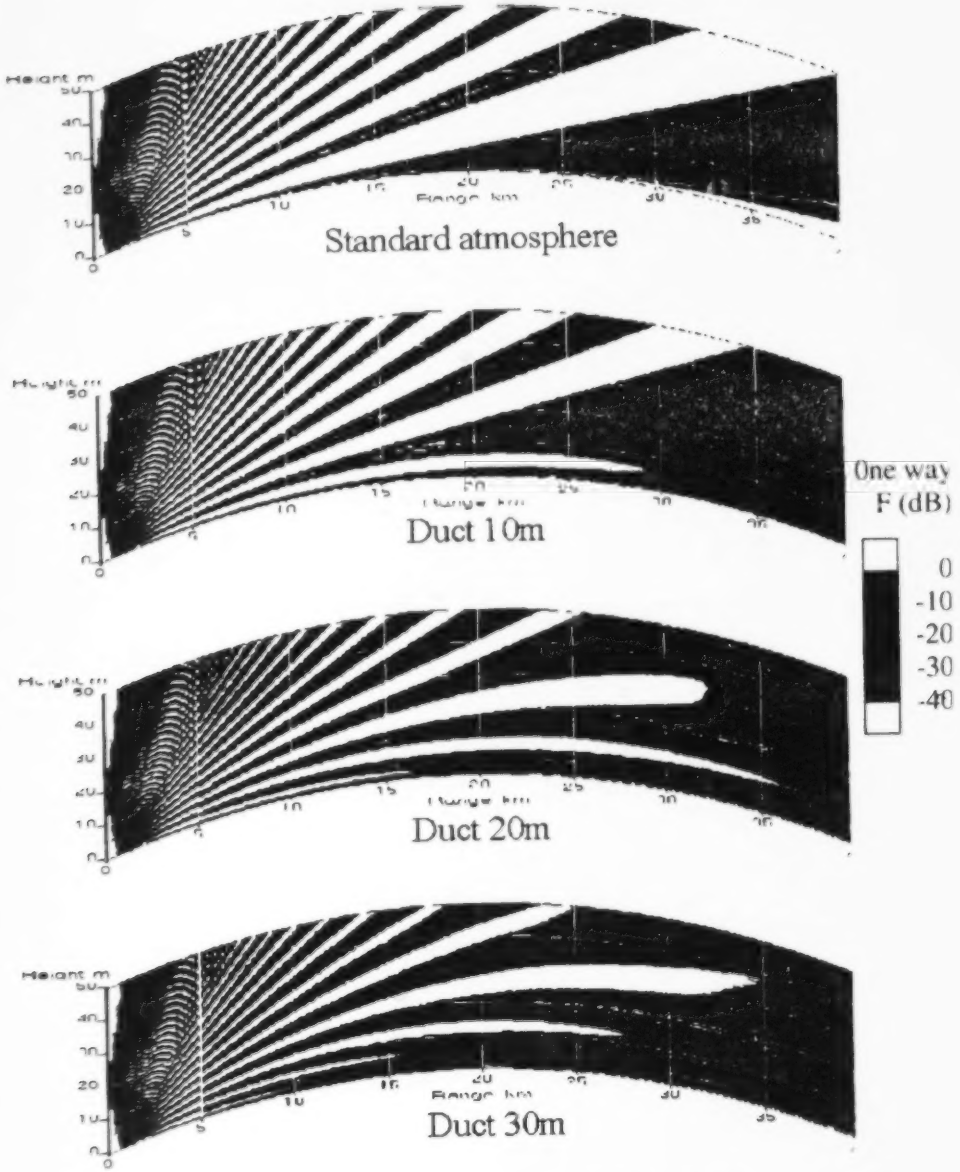

Figure 17. Propagation factor for MFR at 12.0 GHz

Table 14 *MFR maximum detection range for 3-out-of-4 binary integration of four bursts*

Binary Integration	MFR (antenna 20.4 m) (8.0, 9.5, 10.5, 12.0 GHz)			Maximum Detection Range (km) (Where Pd is above 0.9)			
	ASM Height (m)	LOS optical and radar range (km)		Standard Atmosphere	Duct 10 m	Duct 20 m	Duct 30 m
Exocet RCS = 0.1 m²	9	26.8	31.0	19.6 ***(11.2)*** 9.2	10.6	15.6	11.4
	15	30.0	34.6	22.6 ***(16.6)*** 12.6	15.2	12.6 ***(10.0)*** 9.2	11.2
	3	22.3	25.8	14.2	18.2	16.4	10.0
SS-N-22 RCS = 1 m²	20	32.1	37.0	28.2 ***(18.4)*** 16.2	19.6	23.0 ***(21.2)*** 18.6 ***(13.6)*** 13.0	19.0
	30	35.7	41.2	31.8 ***(23.6)*** 20.0 ***(13.2)*** 13.0	24.0 ***(14.6)*** 14.2	24.0 ***(22.8)*** 18.8	21.8 ***(20.2)*** 18.2
	7	25.6	29.5	21.2	29.6 ***(12.4)*** 11.6 ***(10.6)*** 10.2	15.6	21.6
3M-54E RCS=0.5 m²	15	30.0	34.6	25.0 ***(15.6)*** 13.6	16.4	25.8	21.6 ***(14.6)*** 11.8
	50	41.4	47.8	35.6 ***(32.8)*** 25.8 ***(23.4)*** 21.2 ***(19.8)*** 18.6 ***(etc)***	23.2 ***(21.8)*** 20.2 ***(17.6)*** 17.2 ***(etc)***	20.6 ***(19.2)*** 17.6 ***(17.0)*** 16.0	19.0 ***(16.0)*** 15.4
	3	22.3	25.8	16.0	22.8	21.6	14.4

Numbers in bold and italics means that the Pd falls under 0.9 at that range

For the standard atmosphere, the ASMs are always detected 8.3 to 12.2 km after they are unmasked. A MFR using a 3 out of 4 scheme performs poorly against current ASM cruise missiles. There are also several discontinuities in the 0.9 detection coverage. It would be interesting to examine the performance of the AN/SPY-1F radar to compare with an X-band MFR.

Ducting can also not be ignored for MFR too. The ten-meter duct has a strong impact on detection capability. So that targets flying at 3 and 7 m have their detection range increase to between 4 to 8 km. Those flying above 7 m see their detection range reduced by up to 12 km. For 20 m ducts, targets flying at 3 m have their detection range increased by 2.2 and 5 km. All others missiles flying above 3 m see their detection range decreased or changed slightly compared to the standard atmospheric condition case. The 30 m duct decreases the maximum

detection range by as much as 10 km in comparison to the standard atmosphere case, except for one case. Overall, detection ranges are not enhanced but decreased in comparison to the standard atmosphere case, which is not acceptable. In fact, a 3-out-of-4 binary detector is not an optimum choice for an MFR, especially in the presence of ducting. Indeed, a low SNR for one of the bursts significantly reduces the probability of detecting the target, and a small SNR for two bursts makes it extremely difficult to detect the target. The maximum detection ranges of the MFR have also been calculated for incoherent integration rather than binary integration. The results are shown in Table 15.

Table 15 *MFR maximum detection range for incoherent integration of four bursts*

Incoherent Integration	**MFR** (antenna 20.4 m) (8.0, 9.5, 10.5, 12.0 GHz)			**Maximum Detection Range (km)** (Where Pd is above 0.9)			
	ASM Height (m)	LOS optical range (km)	LOS radar range (km)	Standard atmosphere	Duct 10 m	Duct 20 m	Duct 30 m
Exocet RCS = 0.1 m^2	9	26.8	31.0	19.4	19.0 ***(13.6)*** 12.8	17.4	18.2
	15	30.0	34.6	22.2 ***(14.2)*** 13.8	16.2	21.4	16.6
	3	22.3	25.8	14.0	18.0	17.8	14.6
SS-N-22 RCS = 1 m^2	20	32.1	37.0	28.0	21.6	34.0	32.2
	30	35.7	41.2	31.4	25.4	30.0	29.4
	7	25.6	29.5	21.0	29.4	20.0	23.0
3M-54E RCS=0.5 m^2	15	30.0	34.6	24.8	18.4	29.8	24.8
	50	41.4	47.8	26.8	28.8	24.4	21.0
	3	22.3	25.8	16.0	22.4	22.4	19.6

Numbers in bold and italic means that the Pd fall under 0.9 at that range

Incoherent integration of the bursts performs better in thermal noise than binary 3 out of 4 integration. There are fewer discontinuities in the detection coverage for incoherent integration as opposed to binary integration.

The 10 m ducts increase detection range between 4 to 8 km for the missiles flying at 3 and 7 m. However, the detection range of the ASMs flying above 7 m all decrease by about 6 km except for one case. The 20 m duct increases and decreases detection range of ASMs depending on their flying height. Those flying at 3 m still see their detection range increase by up to 6 km. Those flying at 50 m see their detection range decrease by as much as 10.8 km. Those flying between 9 and 30 m see their detection range increase or decrease. The 30 m duct produces similar results, either increasing or decreasing the detection range according to the flying height.

Table 16 compares the maximum detection range of the MFR obtained by using incoherent integration or by using binary 3 out of 4 scheme.

***Table 16** MFR maximum detection range binary via incoherent integration*

		INTEGRATION	MAXIMUM DETECTION RANGE (km) (Where Pd > 0 9)			
Missile	ASM height (m)		Standard atmosphere	Duct 10 m	Duct 20 m	Duct 30 m
Exocet (RCS = 0 1 m²)	9	binary	19 6*	10 6	15 6	11 4
		incoherent	19 4*	19 0*	17 4	18 2
	15	binary	22 6	15 2	12 6*	11 2
		incoherent	22 2*	16 2	21 4	16 6
	3	binary	14 2	18 2	16 4	10 0
		incoherent	14 0	18 0	17 8	14 6
SS-N-22 (RCS = 1 m²)	20	binary	28 2*	19 6	23 0*	19 0
		incoherent	28 0	21 6	34 0	32 2
	30	binary	31 8*	24 0*	24 0*	21 8*
		incoherent	31 4	25 4	30 0	29 4
	7	binary	21 2	29 6*	15 6	21 6
		incoherent	21 0	29 4	20 0	23 0
3M-54E (RCS = 0 5 m²)	15	binary	25 0*	16 4	25 8	21 6*
		incoherent	24 8	18 4	29 8	24 8
	50	binary	35 6*	23.2*	20 6*	19 0*
		incoherent	26 8	28 8	24 4	21 0
	3	binary	16 0	22 8	21 6	14 4
		incoherent	16 0	22 4	22 0	19 6

* means the Pd falls under 0.9 at some point after that range

For a standard atmosphere the performances are similar. For 10 m ducts, incoherent integration is a better choice since detection performances are mostly increased (up to 9 km).

The situation is similar for 20 m ducts, however, the increase in detection range is much larger. For 30 m ducts, the incoherent integration always produces better performance (up to 11 km).

Ducts can have a dramatic impact on MFR using either a 3-out-of-4 binary detector or an incoherent detector. However, a priori knowledge of the atmospheric conditions, if favorable, could be used to select the optimum frequencies to significantly enhance detection performance.

5.4 Comparison Of Radars Performance

In this section we compare the performance of the SPS-49, the Sea Giraffe and the MFR radar. Only MFR using incoherent integration is used here since it performs better than the binary detector used in this study.

From Table 17, it is clear that in general the SPS-49 radar has the best detection capability against the missiles flying 15 m and above under various atmospheric conditions. For missiles flying at 7 and 9 m, the detection capabilities of the SPS-49 radar are comparable, in most cases, to those obtained with the others radars. Missiles flying at 3 m are the most difficult targets to detect for the SPS-49 radar.

Against the targets flying at 3 m above sea level, the MFR radar performs better in the standard atmosphere and 10 m duct case, whereas the Sea Giraffe performs better for the 20 and 30 m duct cases. The MFR defined here will see a benefit to be integrated with the SPS-49 and to a less extent with the Sea Giraffe especially in the presence of ducts. All of these radars, however, detect missiles several km after they have crossed the horizon, significantly decreasing the time to react and intercept the incoming missile.

Table 17 MFR/Sea Giraffe maximum detection range for incoherent integration of four bursts

		RADAR SYSTEM	MAXIMUM DETECTION RANGE (km) (Where Pd > 0 9)			
Missile	ASM height (m)		Standard atmosphere	Duct 10 m	Duct 20 m	Duct 30 m
Exocet (RCS = 0 1 m²)	9	SPS-49	18 8	19 0	22 0	48 0
		SEA GIRAFFE	15 4	19 6	29 0	11 5
		MFR incoherent	19 4	19 0	17 4	18 2
	15	SPS-49	22 6	22 8	26 2	34 4
		SEA GIRAFFE	18 4	21 4	9 5	14 0
		MFR incoherent	22 2	16 2	21 4	16 6
	3	SPS-49	11 8	12 0	13 6	15 0
		SEA GIRAFFE	10 4	13 2	19 0	18 0
		MFR incoherent	14 0	18 0	17 8	14 6
SS-N-22 (RCS = 1 m²)	20	SPS-49	29 6	28 4	32 4	44 0
		SEA GIRAFFE	23 8	28 8	14 0	34 5
		MFR incoherent	28 0	21 6	34 0	32 2
	30	SPS-49	33 6	33 8	36 2	48 4
		SEA GIRAFFE	27 2	31 2	20 0	36 5
		MFR incoherent	31 4	25 4	30 0	29 4
	7	SPS-49	21 0	21 2	23 4	30 2
		SEA GIRAFFE	17 0	24 0	55 5	23 5
		MFR incoherent	21 0	29 4	20 0	23 0
3M-54E (RCS = 0 5 m²)	15	SPS-49	25 6	26 0	30 0	40 6
		SEA GIRAFFE	20 6	25, 6	33 5	26 5
		MFR incoherent	24 8	18 4	29 8	24 8
	50	SPS-49	37 8	38 2	>40	53 0
		SEA GIRAFFE	31 2	31 8	25 5	31 5
		MFR incoherent	26 8	28 8	24 4	21 0
	3	SPS-49	14 0	14 2	16 4	19 0
		SEA GIRAFFE	12 2	16 2	30 0	21 0
		MFR incoherent	16 0	22 4	22 0	19 6

6. Conclusion

The Sea Giraffe 150HC, the SPS-49 and the MFR have been evaluated under four different atmospheric conditions: standard atmosphere and 3 ducting conditions with evaporation ducts at 10 m, 20 m and 30 m. The results clearly show that ducting conditions can have a strong impact on the detection capability of these radars. The SPS-49 sees its detection range increased with increasing duct height. The impact of ducts on the MFR and the Sea Giraffe are much more difficult to predict. Their detection ranges are not only increased by ducts but can also be significantly reduced. Such decreases in detection range definitely put ship survivability at higher risk. More resources should be allocated to the study of atmospheric conditions in the maritime environment to evaluate the real threat to the Canadian Navy.

For the Sea Giraffe, changing the transmitted frequency within its agile bandwidth has little effect on the radio frequency (RF) propagation and radar performance for the given ducting conditions. If the detection range is reduced for one frequency then it will be reduced at all frequencies. APAR-like radars, on the other hand, have the capability of exploiting ducting conditions to their advantage. This radar can change its frequency anywhere within the range 8.5 to 11.5 GHz, which makes it possible to optimize the waveform with respect to RF propagation. However, meteorological equipment would be needed to measure the refractivity structure of the atmosphere in real time to fully exploit this capability.

Under standard atmospheric conditions, the Sea Giraffe 150HC, the SPS-49 and the MFR are all unable to detect existing ASM threats at the LOS radar range. The ASM missiles fly several kilometers in from the LOS radar range on before they can be detected.

The SPS-49 has the best detection capability of all the given radar against the missiles flying 15 m and higher for any atmospheric conditions. For missiles flying at 7 and 9 m, the detection capability of the SPS-49 radar is comparable to that obtained with the others radars. Missiles flying at 3 m are the most difficult targets to detect for the SPS-49 radar. Overall, the integration of the SPS-49 radar with the MFR would improve air defence capability. However, the SPS-49 radar will have to cue the MFR immediately after detection to take advantage of this earlier detection. Indeed, the SPS-49 radar needs a few antenna rotations to confirm the initial detection, which can be done faster by the MFR. In a standard atmosphere, the Sea Giraffe radar has the worst detection capability against current ASM threats. In the presence of 20 and 30 m ducts, the Sea Giraffe has a better capability against ASMs flying 3 m above sea level. For ASMs flying above 3 m, however, the SPS-49 and the MFR give better maximum detection ranges.

A 3–out-of-4 binary detector is considered in this report for the MFR. The results clearly show that this binary detector performs very poorly especially under ducting conditions. In this study, incoherent integration produces better detection ranges.

As stated previously, this study has not used the actual antenna heights of the radar systems as they are used on the Canadian patrol Frigates. Furthermore, the effects of sea clutter on detection range have been ignored. Thus, it is recommended that a further study be performed to consider these factors. This proposed study would generate results that are directly

P517610.PDF [Page: 59 of 123]

applicable to the Canadian Patrol Frigates. The capability to perform this study exists at the Defence research Establishment Ottawa in the form of a radar simulator called MFRSIM [10, 16, 17].

7. References

1. Skolnik, M., (1980), Introduction to Radar Systems, McGraw-Hill Inc.

2. Mahafza, R., (1998), Introduction to Radar Analysis, CRC Press,

3. Patterson, W.L., and al., (May 1994), Engineer's Refractive Effects Prediction System (EREPS), Technical Document 2648

4. Brooker, E., (July 1998), Radar Performance During Propagation Fades in the Mid-Atlantic Region. IEEE Transactions on Antennas and Propagations, Vol. 46, No. 7

5. (01 Nov. 1996), Naval Radars Form New Tracks, Jane's Navy International, Vol. 101, Issue 009.

6. Jordan, E.C., Balmain, K.G., (1968), Electromagnetic Waves and Radiating Systems, Prentice-Hall, Inc.

7. (June 1998), TERPEM User Guide Signal Science Limited. U.K.

8. A.E. Barrios, "A Terrain Parabolic Equation Model For Propagation In The Troposphere", IEEE Transactions on Antennas And Propagation, Vol. 42, No. 1, January 1994

9. K.H. Craig, M.F. Levy, "Parabolic Equation Modelling Of The Effects Of Multipath And Ducting On Radar Systems", IEE Proceedings-F, Vol. 138, No. 2, April 1991.

10. Jones, G., and al., (Sep. 2000), Optimization of Multifunction Radars Through Simulation, Contractor Report (038SV.W7714-8-0220)

11. (Oct. 1995), AM-39 Exocet, Jane's Air Launch Weapons, Issue 22

12. (Sep. 1997), "MM38/40, AM39 and SM39 Exocet", Jane's Strategic Weapons Systems, Issue 25

13. (15 Apr. 1995), "SS-N-22 SUNBURN (P270 Moskit)", Jane's Naval Weapons Systems, Vol. 15

14. (Sep 1997), "SS-N-22 Sunburn (P-80/3M-80 Zubr)", Jane's Strategic Weapons Systems, Issue 25

15. (Aug. 1999), Novator Missile Variants Offer Subsonic and Supersonic Attack, Jane's Missile & Rocket, Vol 3, No 8

16. Lightstone, L., Vrzic, S., (Nov 1992). Simulation Studies for the Horizon Search Performance of a Multi-Function Array Radar, Atlantis Scientific Systems Group Inc. Contract Number: W7714-2-0043)

17. Gauthier, S. (Oct. 1998). Simulation of a Multifunction Radar Operating in Horizon Search Mode. Proceeding NATO-IRIS. Vol. 43. No 2

18. Barton, D.K., Leonov, S.A., (1997). Radar Technology Encyclopedia. Artech House, Inc.

19. (1999-2000). AN/SPS-49 Air Surveillance Radar. Jane's Radar and Electronic Warfare Systems

20. (Nov 1990). Radar Set AN/SPS-49A(V)5. Technical Manual

21. (May 1993). Sea Giraffe. Operator's Manual

22. (2001-2002). Sea Giraffe Naval Radar. Jane's Radar and Electronic Warfare Systems

23. (1998-1999). Sea Giraffe AMB Multimode Naval Radar. Jane's Radar and Electronic Warfare Systems

24. (10 Jan 1996). International APAR Radar Aims for 2000. Jane's Defence Weekly

25. (11 Nov 1995). Interest Grows in APAR Radar. Jane's Defence Weekly

Annex A: SPS-49 Performance

This annex gives the value of propagation factors calculated by TERPEM for the SPS-49 radar.

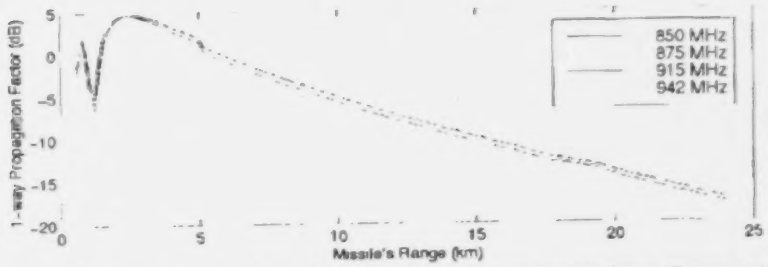

Figure 18. Propagation factor for SPS-49, standard atmosphere, Exocet at 9 m

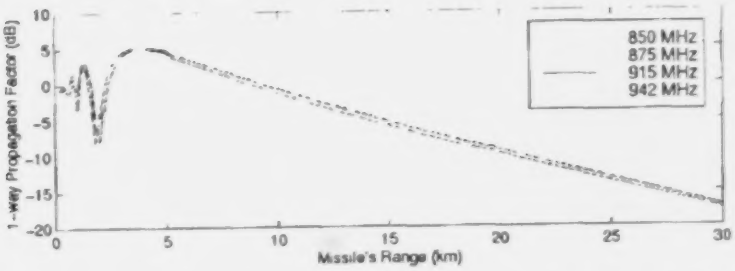

Figure 19. Propagation factor for SPS-49, standard atmosphere, Exocet at 15 m

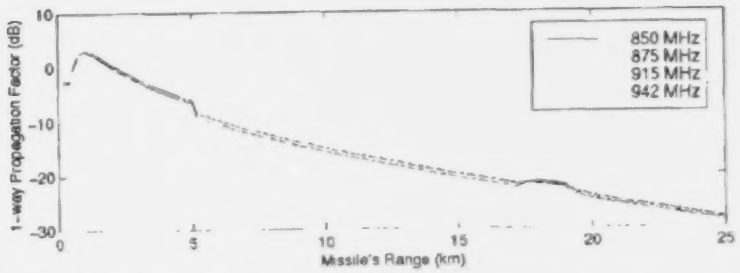

Figure 20. Propagation factor for SPS-49, standard atmosphere, Exocet at 3 m

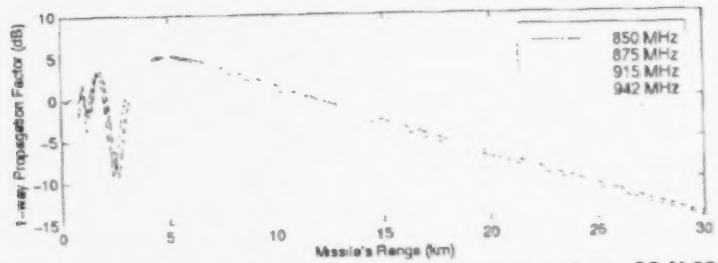

Figure 21. Propagation factor for SPS-49, standard atmosphere, SS-N-22 at 20 m

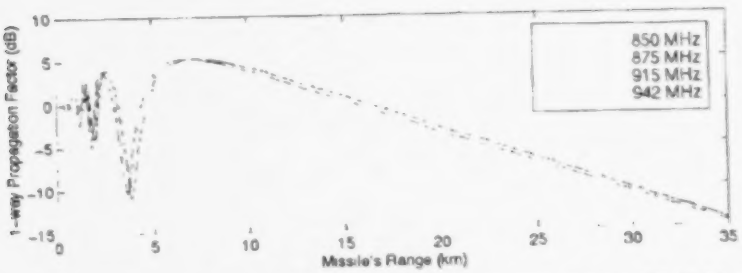

Figure 22. Propagation factor for SPS-49, standard atmosphere, SS-N-22 at 30 m

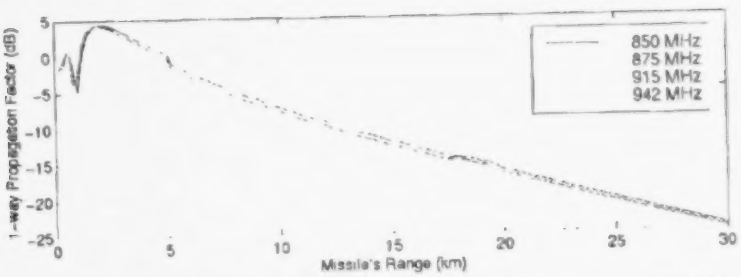

Figure 23. Propagation factor for SPS-49, standard atmosphere, SS-N-22 at 7 m

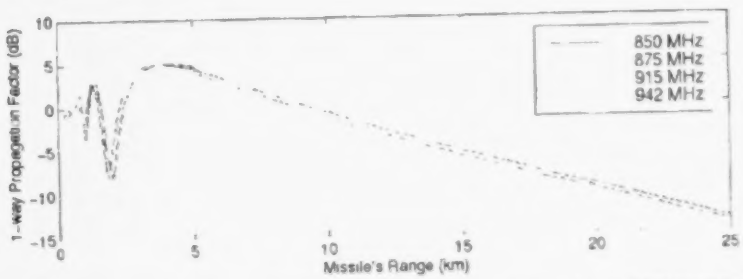

Figure 24. Propagation factor for SPS-49, standard atmosphere, NOVATOR at 15 m

P517610.PDF [Page: 64 of 123]

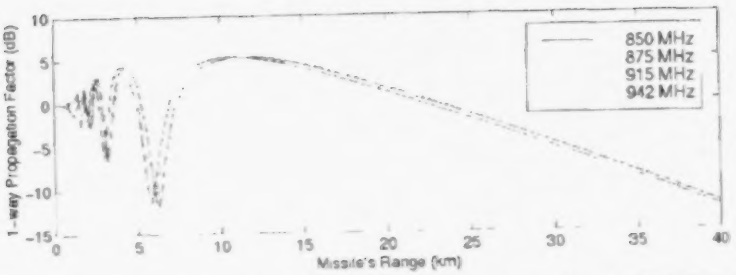

Figure 25. Propagation factor for SPS-49, standard atmosphere, NOVATOR at 50 m

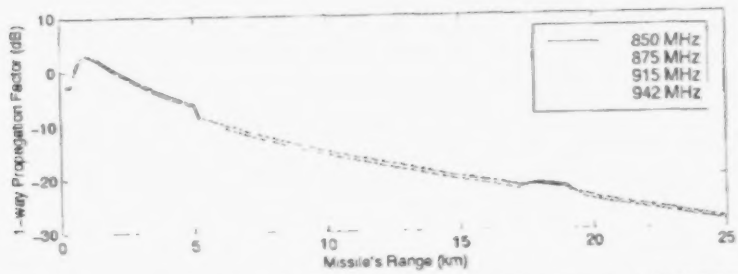

Figure 26. Propagation factor for SPS-49, standard atmosphere, NOVATOR at 3 m

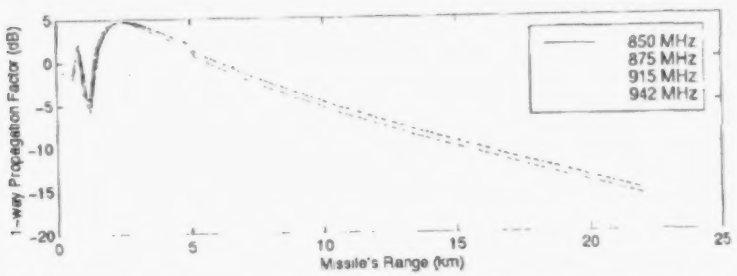

Figure 27. Propagation factor for SPS-49, 10m duct, Exocet at 9 m

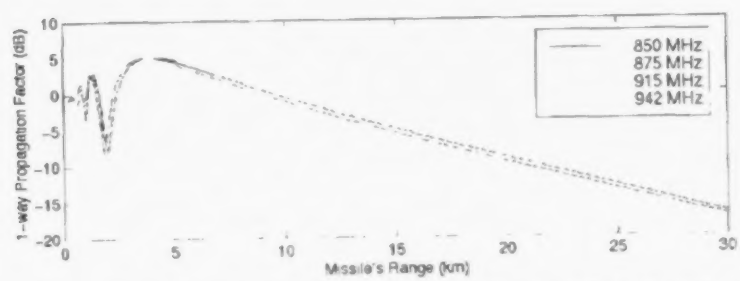

Figure 28. Propagation factor for SPS-49, 10m duct, Exocet at 15 m

Figure 29. Propagation factor for SPS-49, 10m duct, Exocet at 3 m

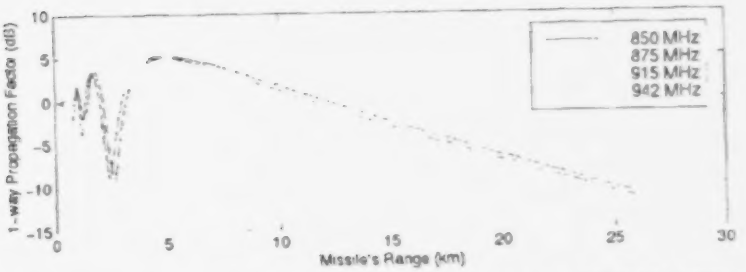

Figure 30. Propagation factor for SPS-49, 10m duct, SS-N-22 at 20 m

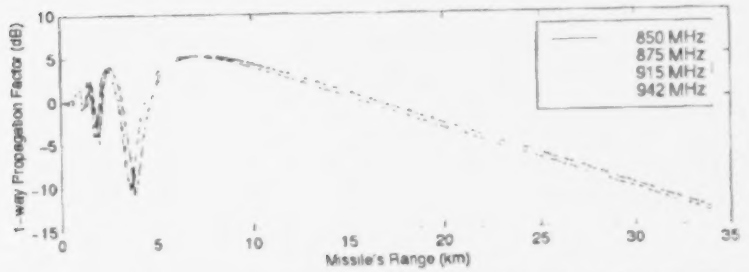

Figure 31. Propagation factor for SPS-49, 10m duct, SS-N-22 at 30 m

Figure 32. Propagation factor for SPS-49, 10m duct, SS-N-22 at 7 m

P517610.PDF [Page: 66 of 123]

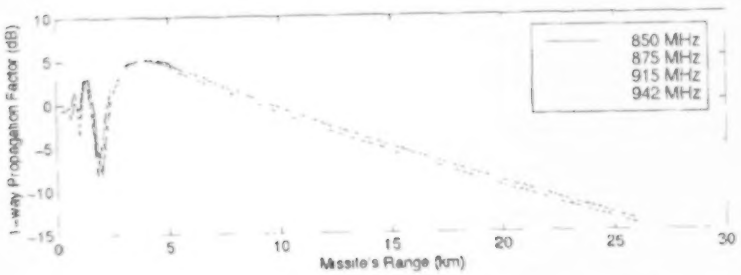

Figure 33. Propagation factor for SPS-49, 10m duct, NOVATOR at 15 m

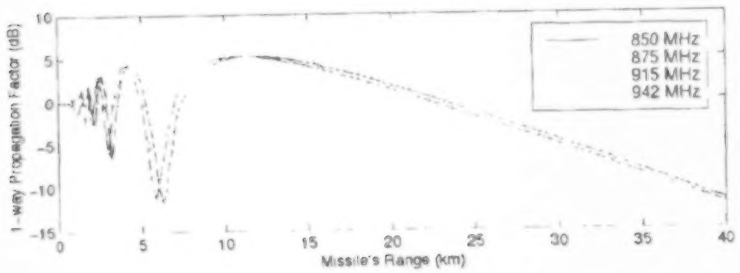

Figure 34. Propagation factor for SPS-49, 10m duct, NOVATOR at 50 m

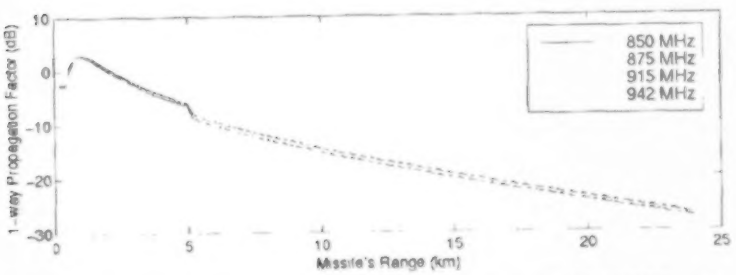

Figure 35. Propagation factor for SPS-49, 10m duct, NOVATOR at 3 m

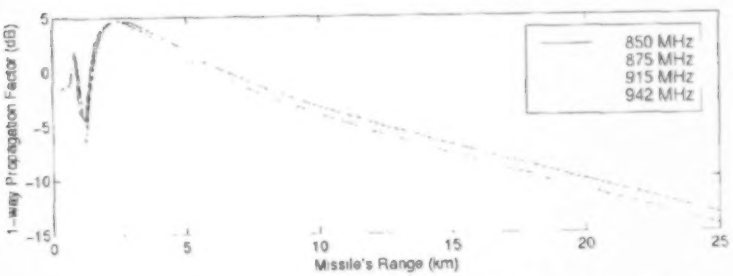

Figure 36. Propagation factor for SPS-49, 20m duct, Exocet at 9 m

P517610.PDF [Page: 67 of 123]

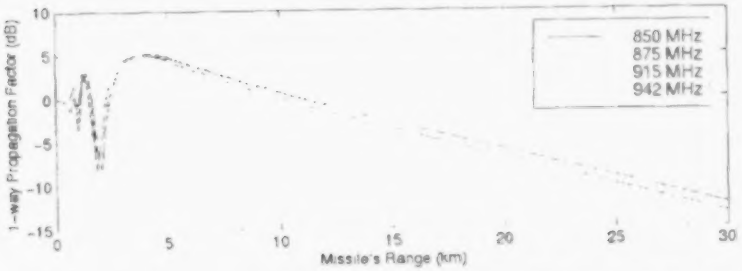

Figure 37. Propagation factor for SPS-49, 20m duct, Exocet at 15 m

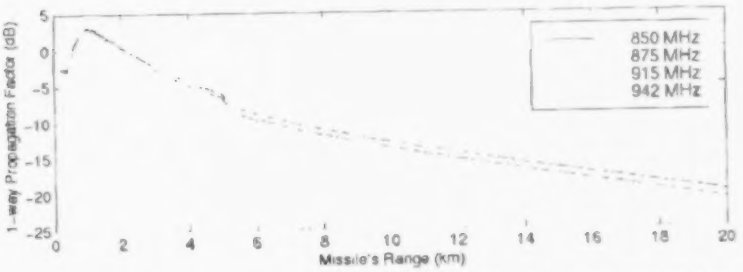

Figure 38. Propagation factor for SPS-49, 20m duct, Exocet at 3 m

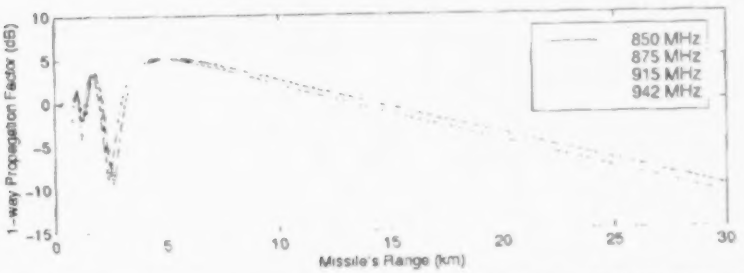

Figure 39. Propagation factor for SPS-49, 20m duct, SS-N-22 at 20 m

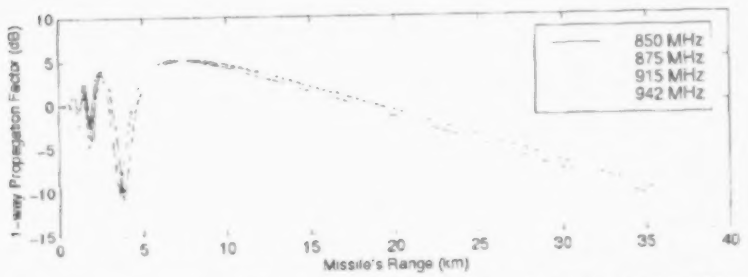

Figure 40. Propagation factor for SPS-49, 20m duct, SS-N-22 at 30 m

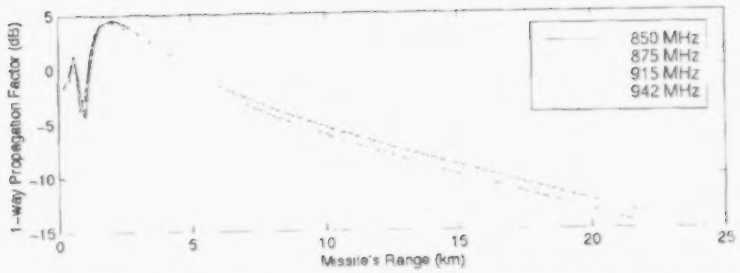

Figure 41. Propagation factor for SPS-49, 20m duct, SS-N-22 at 7 m

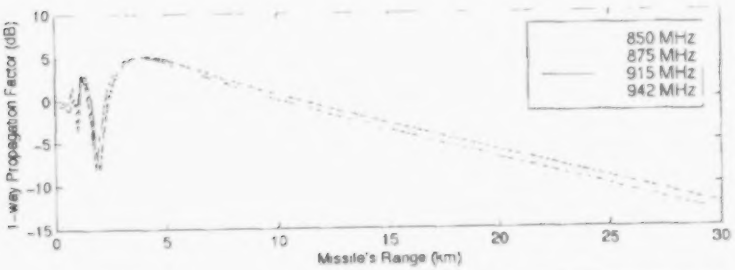

Figure 42. Propagation factor for SPS-49, 20m duct, NOVATOR at 15 m

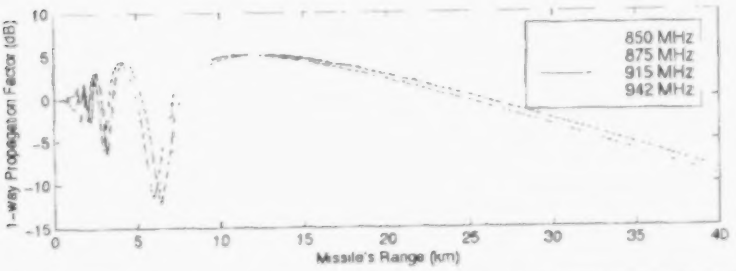

Figure 43. Propagation factor for SPS-49, 20m duct, NOVATOR at 50 m

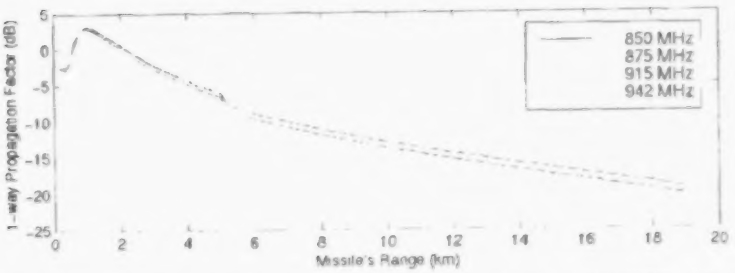

Figure 44. Propagation factor for SPS-49, 20m duct, NOVATOR at 3 m

Figure 45. Propagation factor for SPS-49, 30m duct, Exocet at 9 m

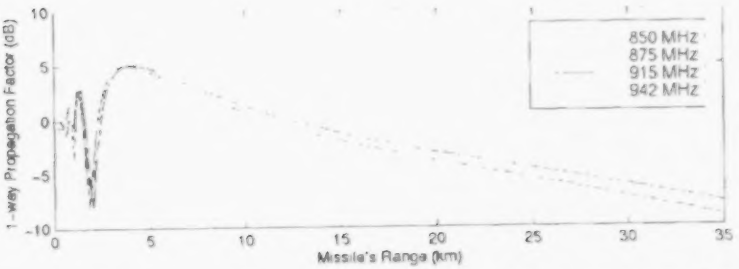

Figure 46. Propagation factor for SPS-49, 30m duct, Exocet at 15 m

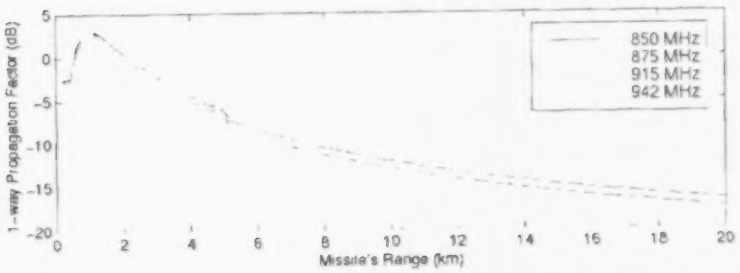

Figure 47 Propagation factor for SPS-49, 30m duct, Exocet at 3 m

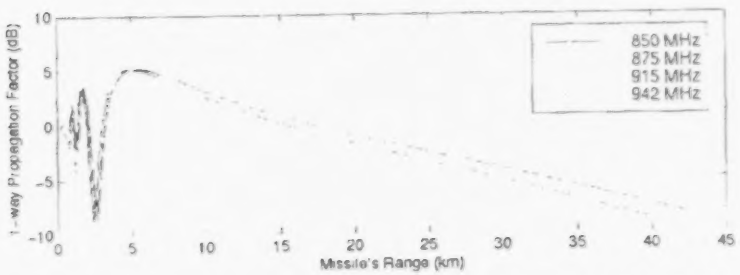

Figure 48. Propagation factor for SPS-49, 30m duct, SS-N-22 at 20 m

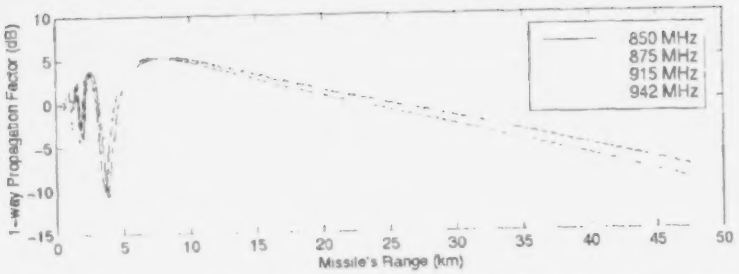

Figure 49. Propagation factor for SPS-49, 30m duct, SS-N-22 at 30 m

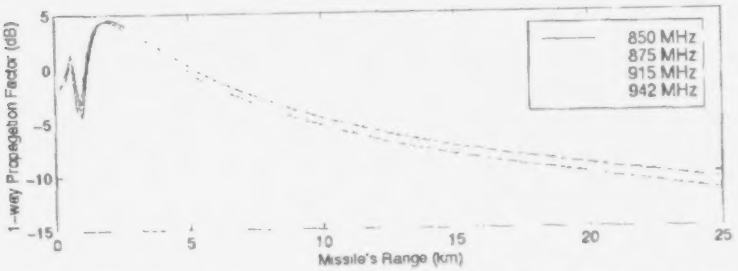

Figure 50. Propagation factor for SPS-49, 30m duct, SS-N-22 at 7 m

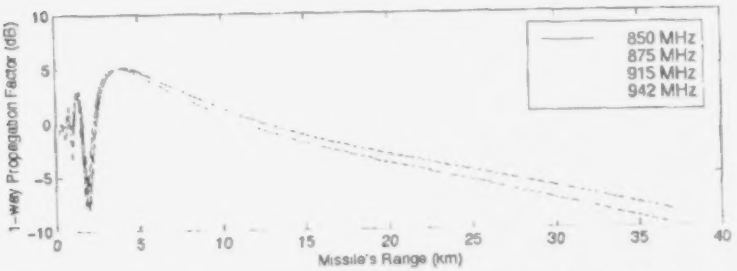

Figure 51. Propagation factor for SPS-49, 30m duct, NOVATOR at 15 m

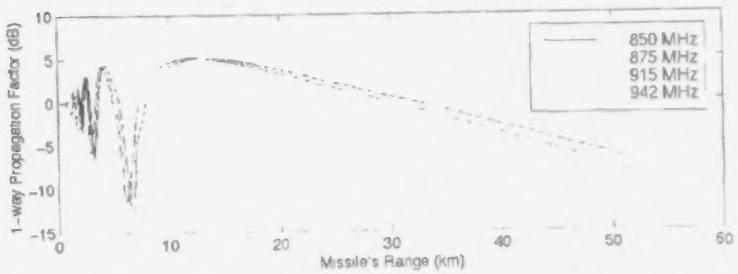

Figure 52. Propagation factor for SPS-49, 30m duct, NOVATOR at 50 m

P517610.PDF [Page: 71 of 123]

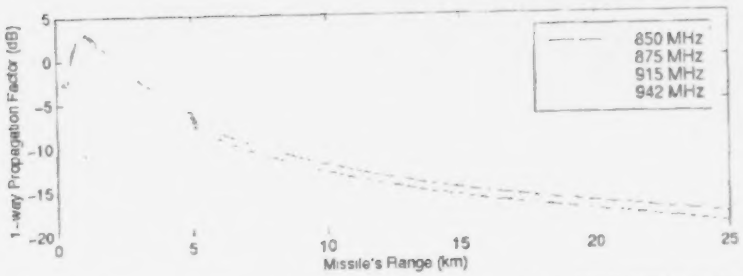

Figure 53. Propagation factor for SPS-49, 30m duct, NOVATOR at 3 m

P517610.PDF [Page: 72 of 123]

Annex B: SEA GIRAFFE Performance

This annex gives the value of propagation factors calculated by TERPEM for the Sea Giraffe radar. The probability of detecting the missiles as a function of range is also shown when there is a discontuity in the 0.9 P_d detection coverage. This has been done using using equation (14) and (16).

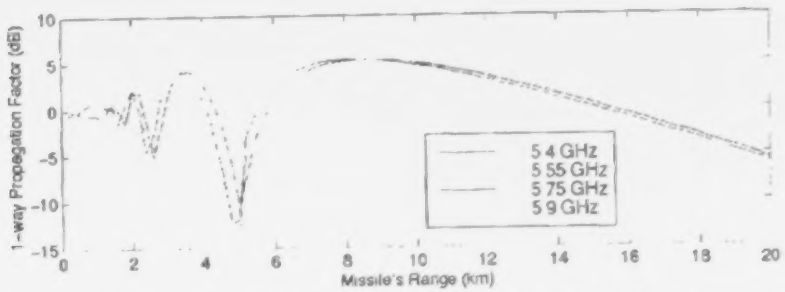

Figure 54. Propagation factor for Sea Giraffe, standard atmosphere, Exocet at 9 m

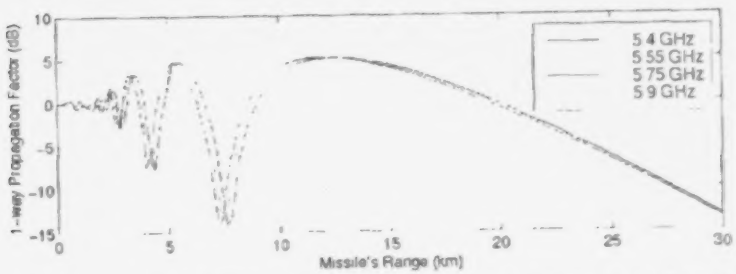

Figure 55. Propagation factor for Sea Giraffe, standard atmosphere, Exocet at 15 m

Figure 56. Probability of Detection for Sea Giraffe, standard atmosphere, Exocet at 15 m

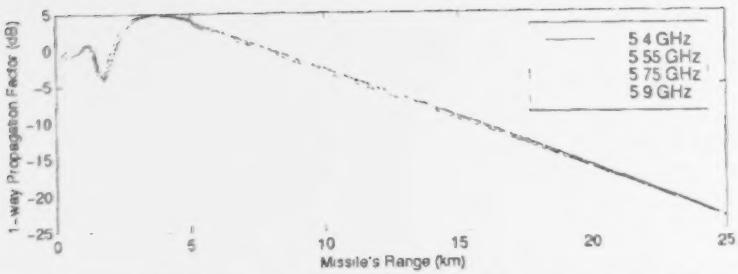

Figure 57. Propagation factor for Sea Giraffe, standard atmosphere, Exocet at 3 m

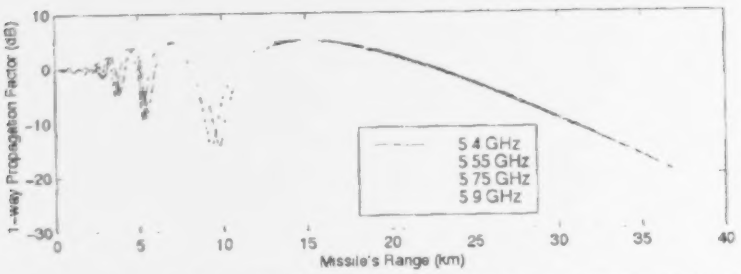

Figure 58. Propagation factor for Sea Giraffe, standard atmosphere, SS-N-22 at 20 m

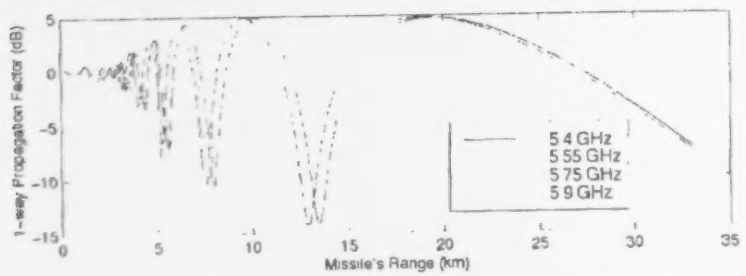

Figure 59. Propagation factor for Sea Giraffe, standard atmosphere, SS-N-22 at 30 m

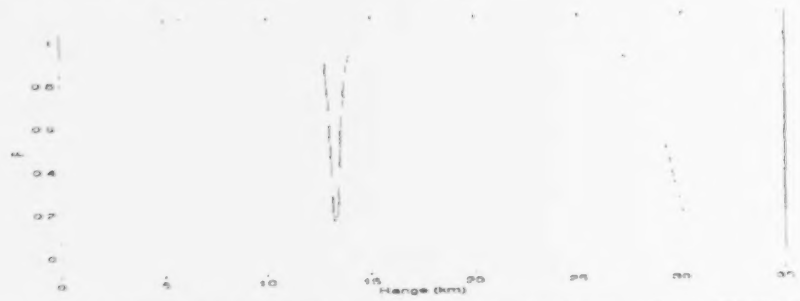

Figure 60. Probability of Detection for Sea Giraffe, standard atmosphere, SS-N-22 at 30 m

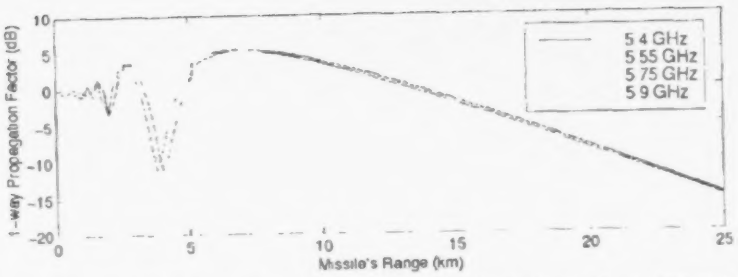

Figure 61. Propagation factor for Sea Giraffe, standard atmosphere, SS-N-22 at 7 m

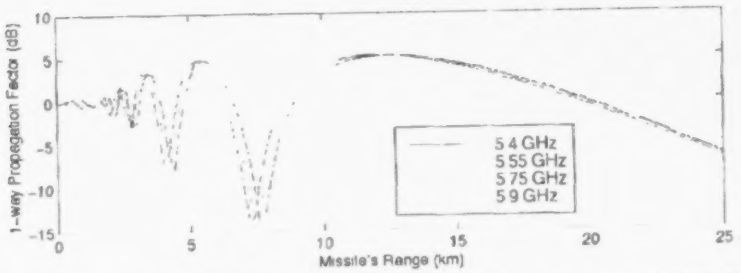

Figure 62. Propagation factor for Sea Giraffe, standard atmosphere, NOVATOR at 15 m

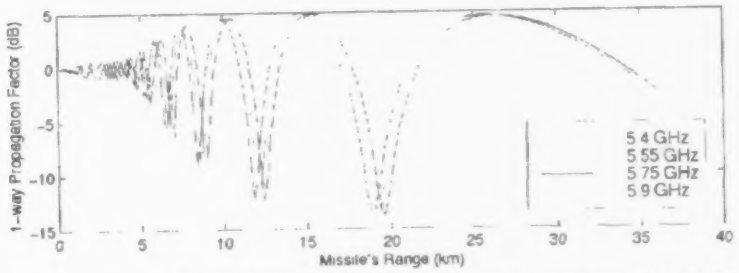

Figure 63. Propagation factor for Sea Giraffe, standard atmosphere, NOVATOR at 50 m

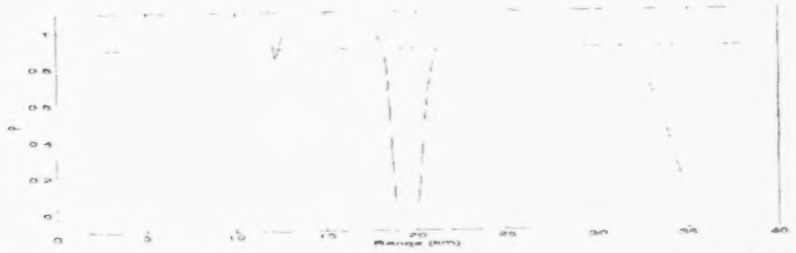

Figure 64. Probability of Detection for Sea Giraffe, standard atmosphere, NOVATOR at 50 m

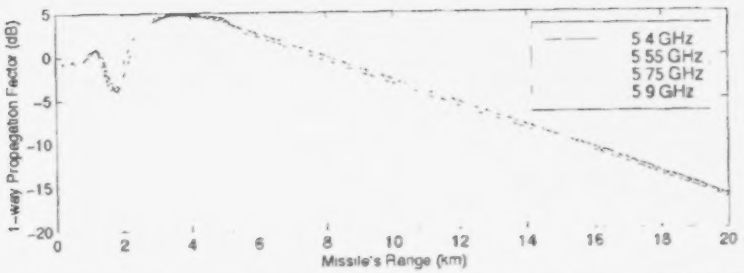

Figure 65. Propagation factor for Sea Giraffe, standard atmosphere, NOVATOR at 3 m

Figure 66. Propagation factor for Sea Giraffe, 10 duct, Exocet at 9 m

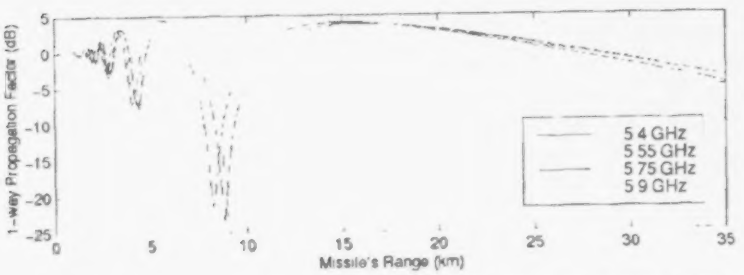

Figure 67. Propagation factor for Sea Giraffe, 10 duct, Exocet at 15 m

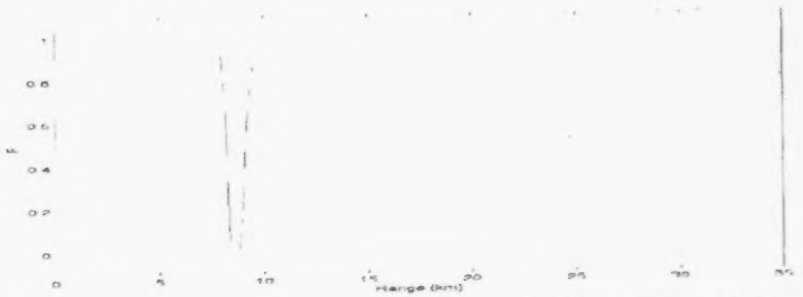

Figure 68. Probability of Detection for Sea Giraffe, 10 duct, Exocet at 15 m

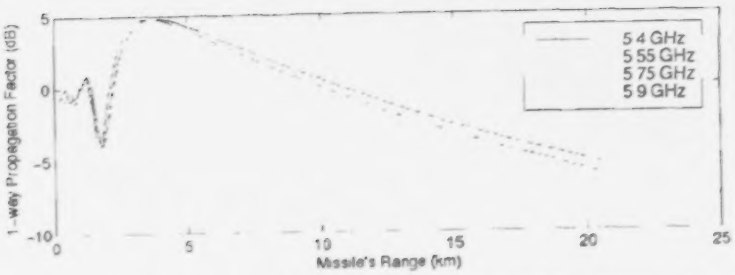

Figure 69. Propagation factor for Sea Giraffe, 10 duct, Exocet at 3 m

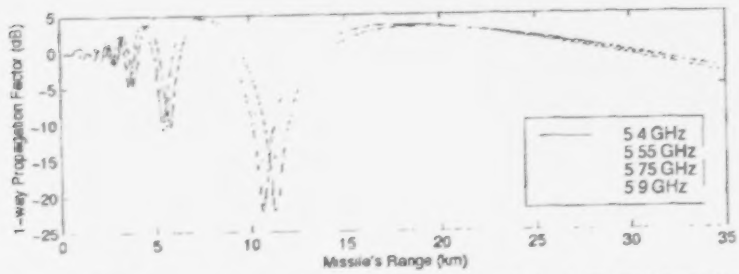

Figure 70. Propagation factor for Sea Giraffe, 10 duct, SS-N-22 at 20 m

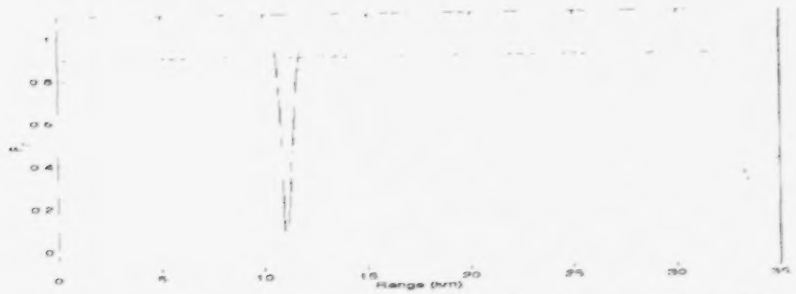

Figure 71. Probability of Detection for Sea Giraffe, 10 duct, SS-N-22 at 20 m

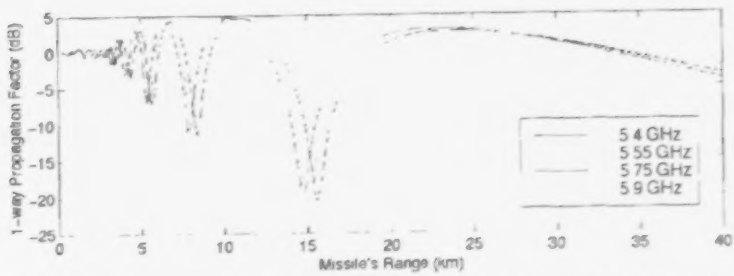

Figure 72. Propagation factor for Sea Giraffe, 10 duct, SS-N-22 at 30 m

Figure 73. Probability of Detection for Sea Giraffe, 10 duct, SS-N-22 at 30 m

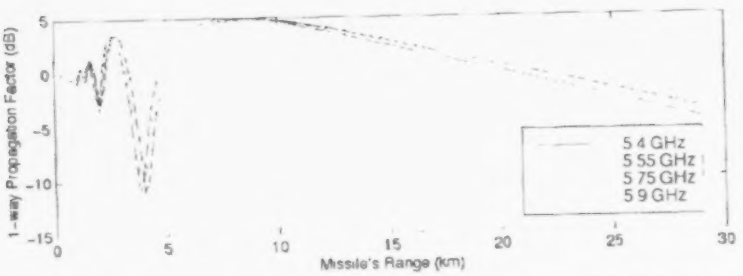

Figure 74. Propagation factor for Sea Giraffe, 10 duct, SS-N-22 at 7 m

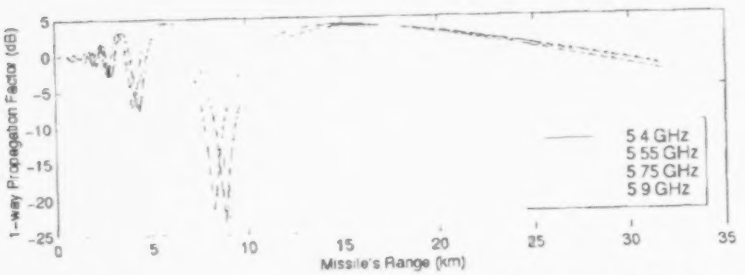

Figure 75. Propagation factor for Sea Giraffe, 10 duct, NOVATOR at 15 m

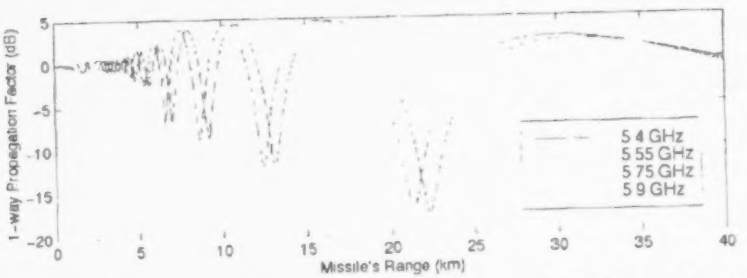

Figure 76. Propagation factor for Sea Giraffe, 10 duct, NOVATOR at 50 m

P517610.PDF [Page: 78 of 123]

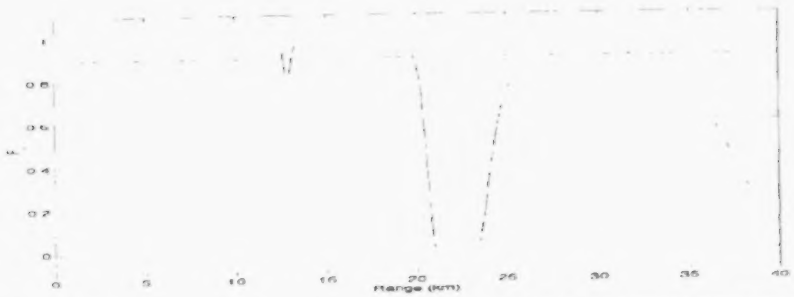

Figure 77. Probability of Detection for Sea Giraffe, 10 duct, NOVATOR at 50 m

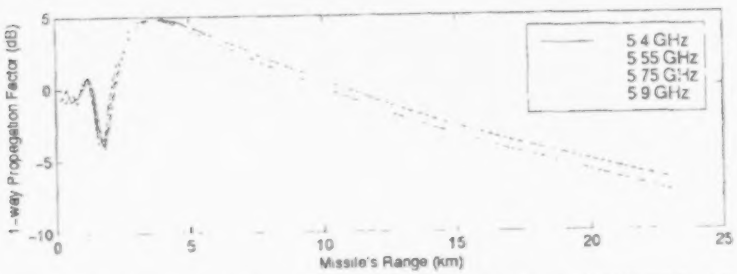

Figure 78. Propagation factor for Sea Giraffe, 10 duct, NOVATOR at 3 m

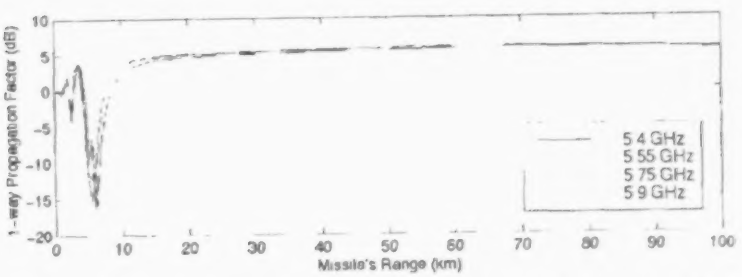

Figure 79. Propagation factor for Sea Giraffe, 20 duct, Exocet at 9 m

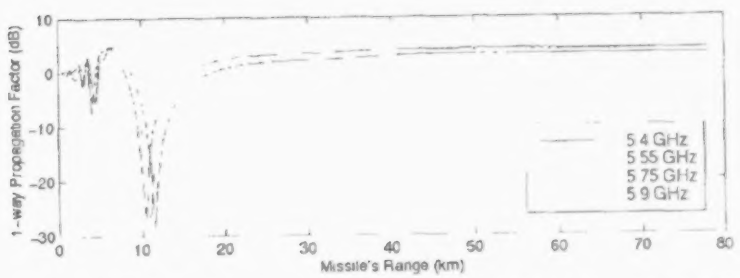

Figure 80. Propagation factor for Sea Giraffe, 20 duct, Exocet at 15 m

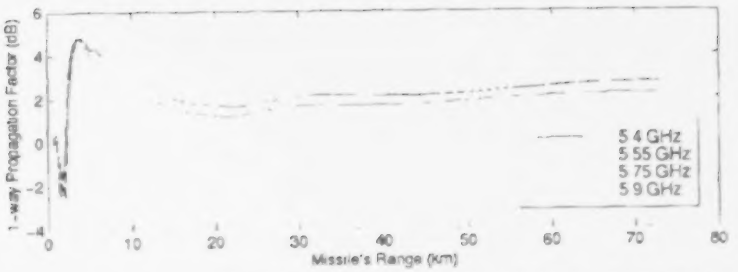

Figure 81. Propagation factor for Sea Giraffe, 20 duct, Exocet at 3 m

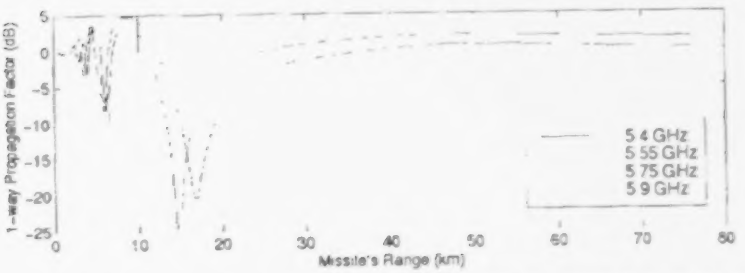

Figure 82. Propagation factor for Sea Giraffe, 20 duct, SS-N-22 at 20 m

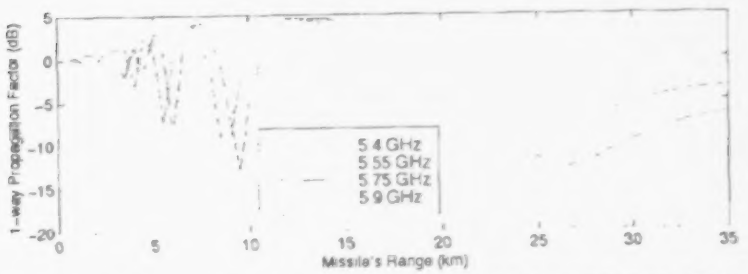

Figure 83. Propagation factor for Sea Giraffe, 20 duct, SS-N-22 at 30 m

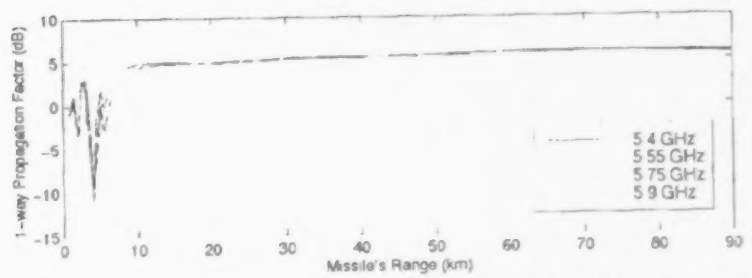

Figure 84. Propagation factor for Sea Giraffe, 20 duct, SS-N-22 at 7 m

P517610.PDF [Page: 80 of 123]

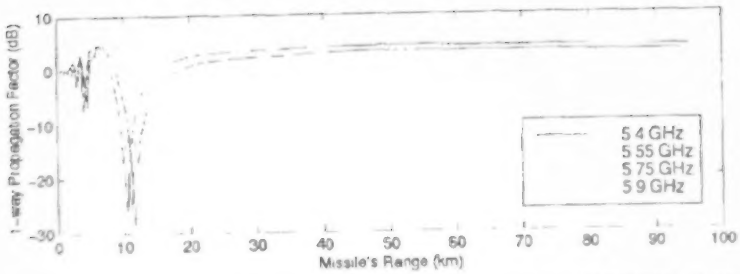

Figure 85. Propagation factor for Sea Giraffe, 20 duct, NOVATOR at 15 m

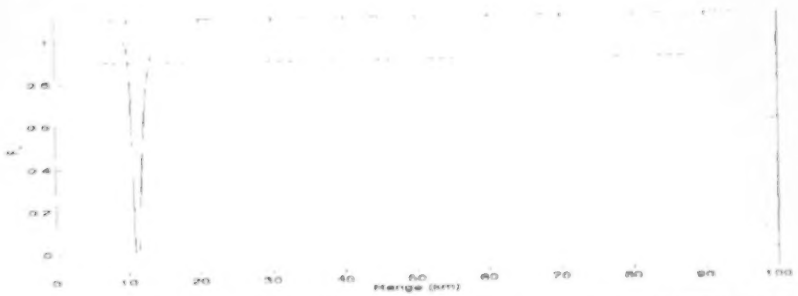

Figure 86. Probability of Detection for Sea Giraffe, 20 duct, NOVATOR at 15 m

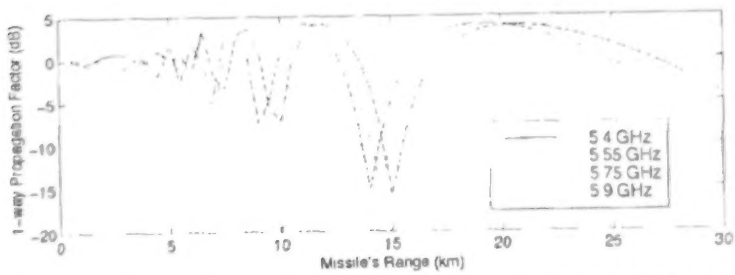

Figure 87. Propagation factor for Sea Giraffe, 20 duct, NOVATOR at 50 m

Figure 88. Probability of Detection for Sea Giraffe, 20 duct, NOVATOR at 50 m

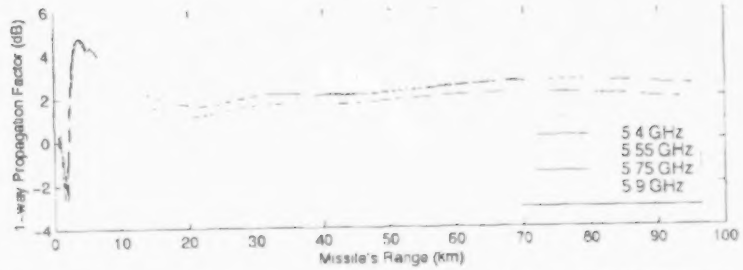

Figure 89. Propagation factor for Sea Giraffe, 20 duct, NOVATOR at 3 m

Figure 90. Propagation factor for Sea Giraffe, 30 duct, Exocet at 9 m

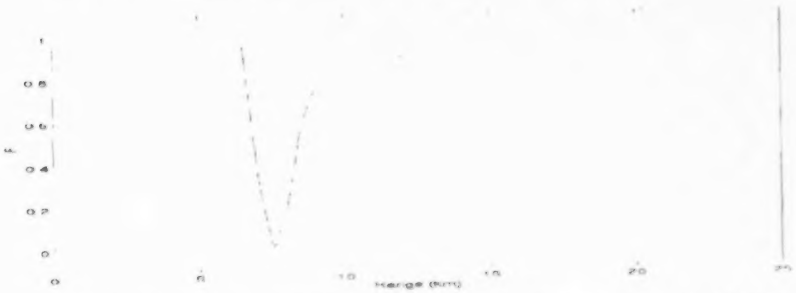

Figure 91. Probability of Detection for Sea Giraffe, 30 duct, Exocet at 9 m

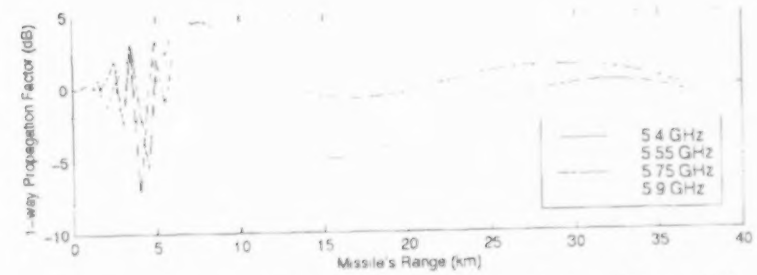

Figure 92. Propagation factor for Sea Giraffe, 30 duct, Exocet at 15 m

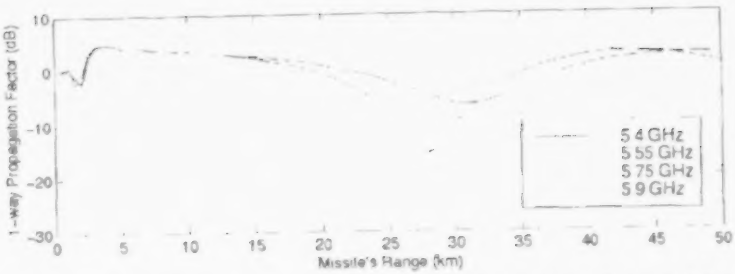

Figure 93. Propagation factor for Sea Giraffe, 30 duct, Exocet at 3 m

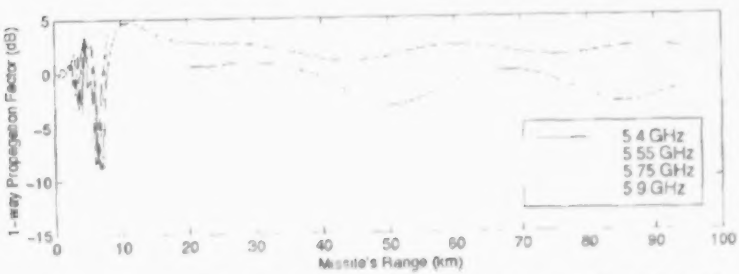

Figure 94. Propagation factor for Sea Giraffe, 30 duct, SS-N-22 at 20 m

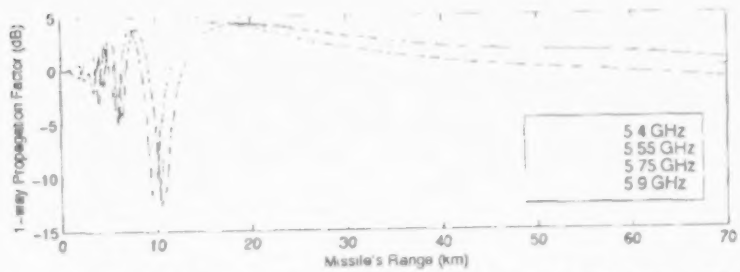

Figure 95. Propagation factor for Sea Giraffe, 30 duct, SS-N-22 at 30 m

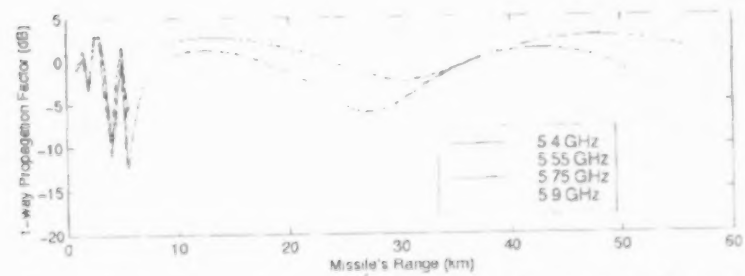

Figure 96. Propagation factor for Sea Giraffe, 30 duct, SS-N-22 at 7 m

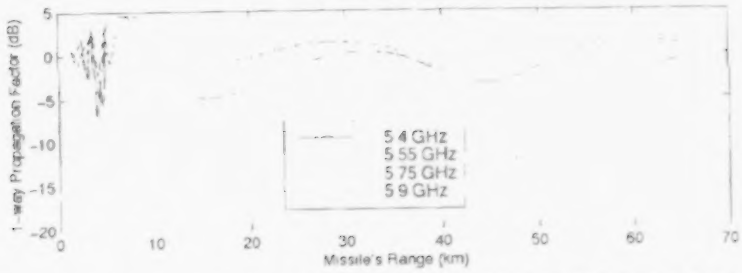

Figure 97. Propagation factor for Sea Giraffe, 30 duct, NOVATOR at 15 m

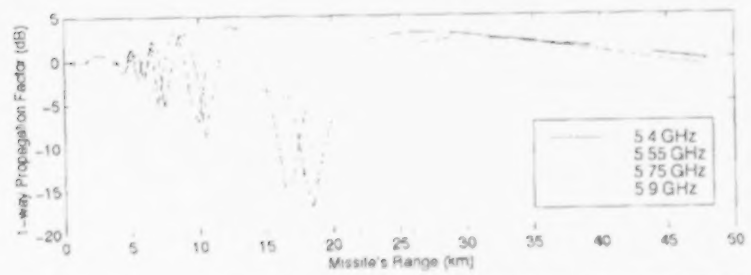

Figure 98. Propagation factor for Sea Giraffe, 30 duct, NOVATOR at 50 m

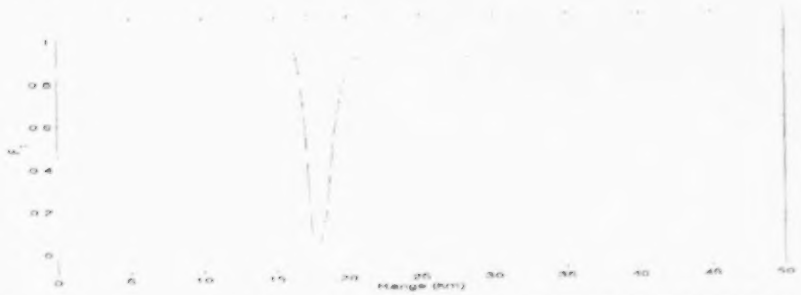

Figure 99. Probability of Detection for Sea Giraffe, 30 duct, NOVATOR at 50 m

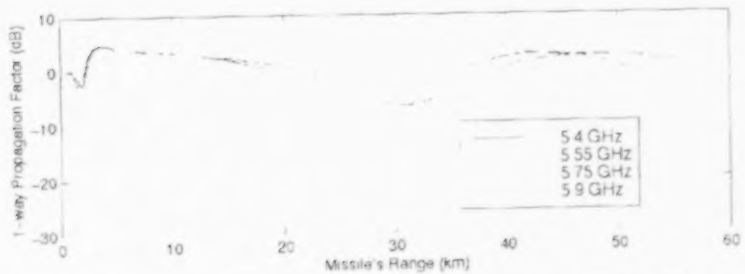

Figure 100. Propagation factor for Sea Giraffe, 30 duct, NOVATOR at 3 m

P517610.PDF [Page: 84 of 123]

Annex C: MFR Performance

This annex gives the value of propagation factors calculated by TERPEM, the probability of detection per burst, and the probability of detection per dwell for binary integration (3 out of 4) as well as for incoherent integration.

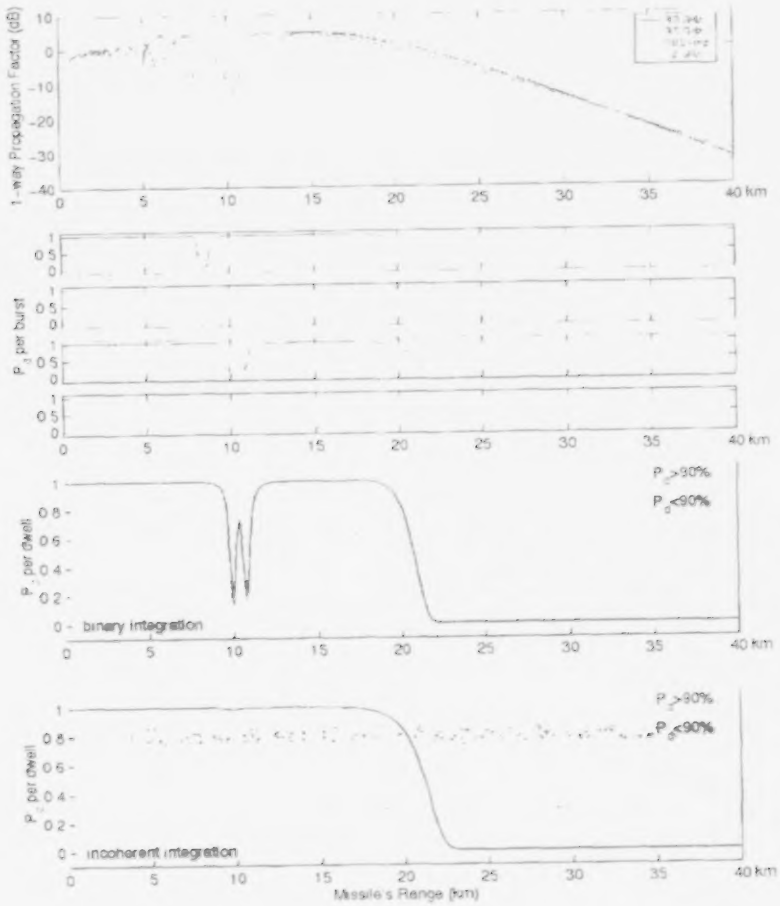

Figure 101. MFR results, Standard atmosphere, Exocet at 9 m

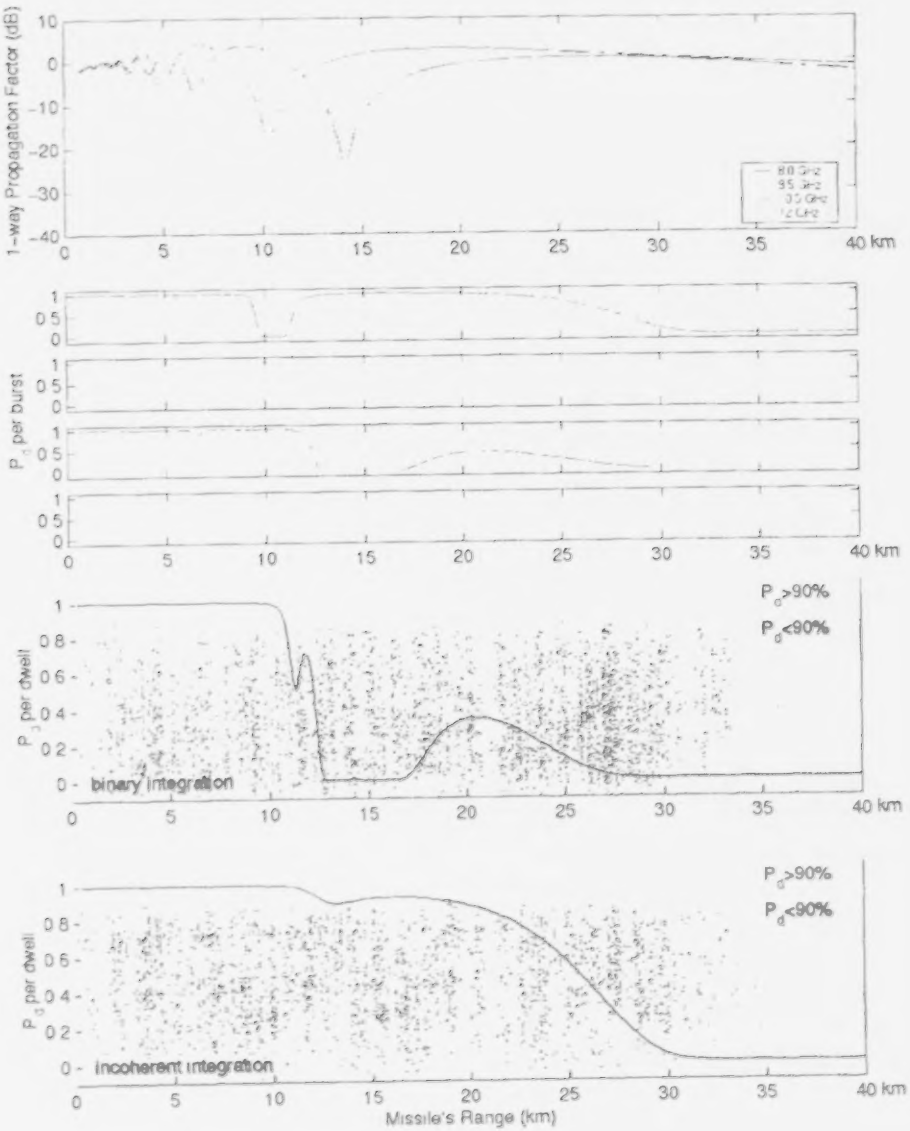

Figure 102. MFR results, duct 10m, Exocet at 9 m

P517610.PDF [Page: 86 of 123]

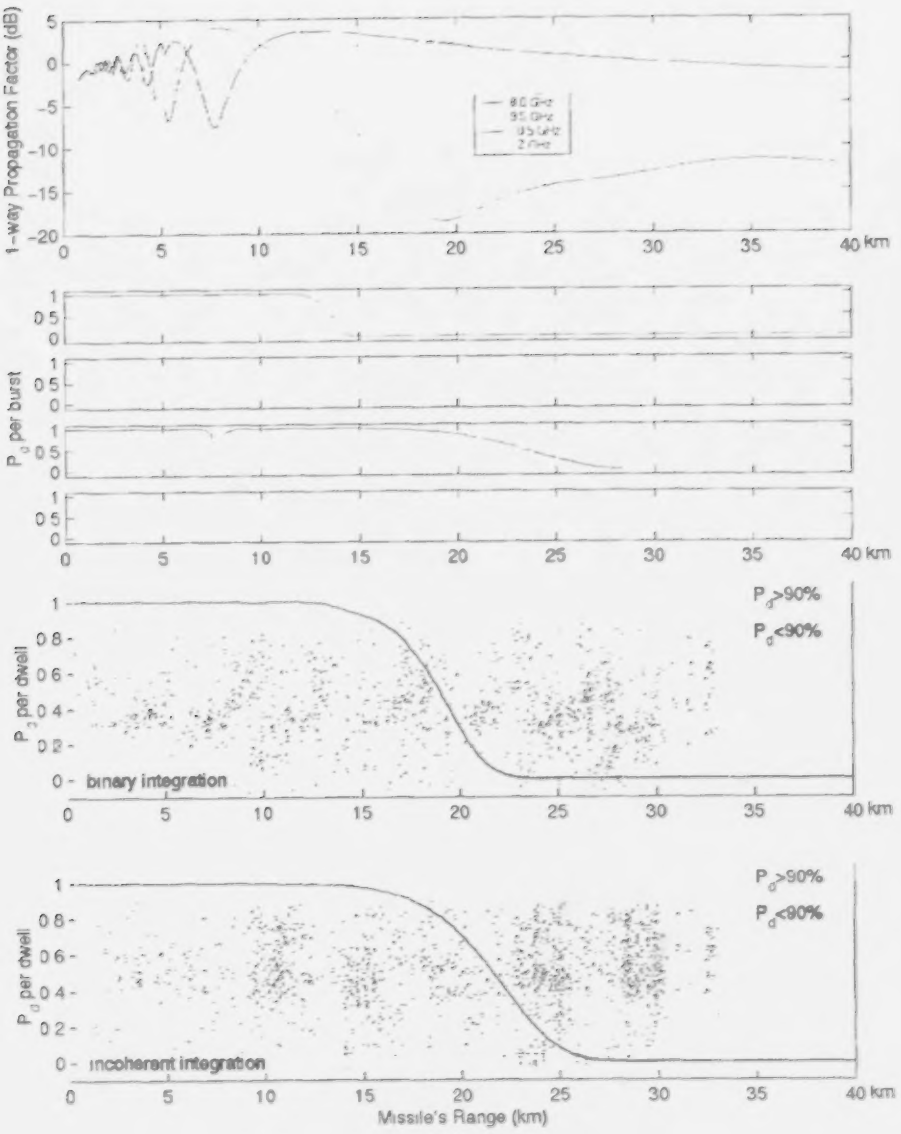

Figure 103. MFR results, duct 20m, Exocet at 9 m

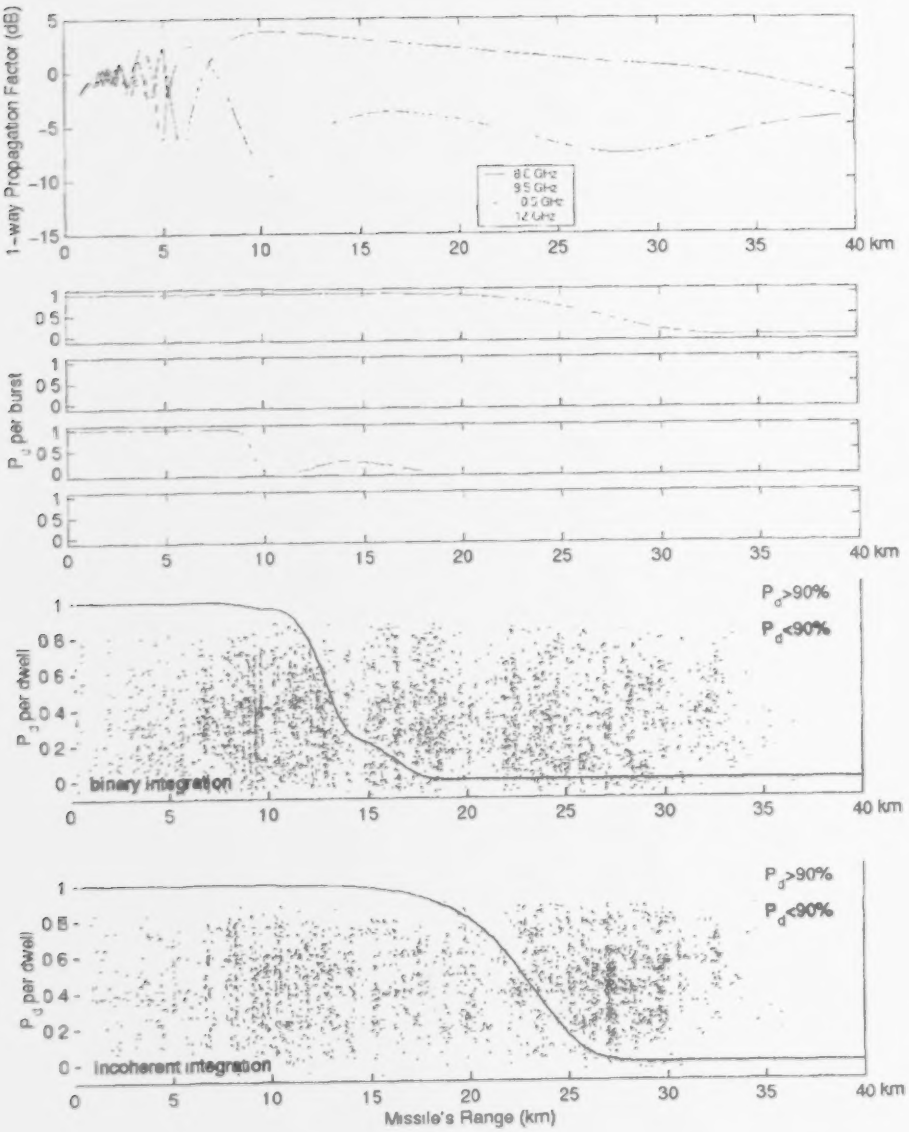

Figure 104. MFR results, duct 30m, Exocet at 9 m

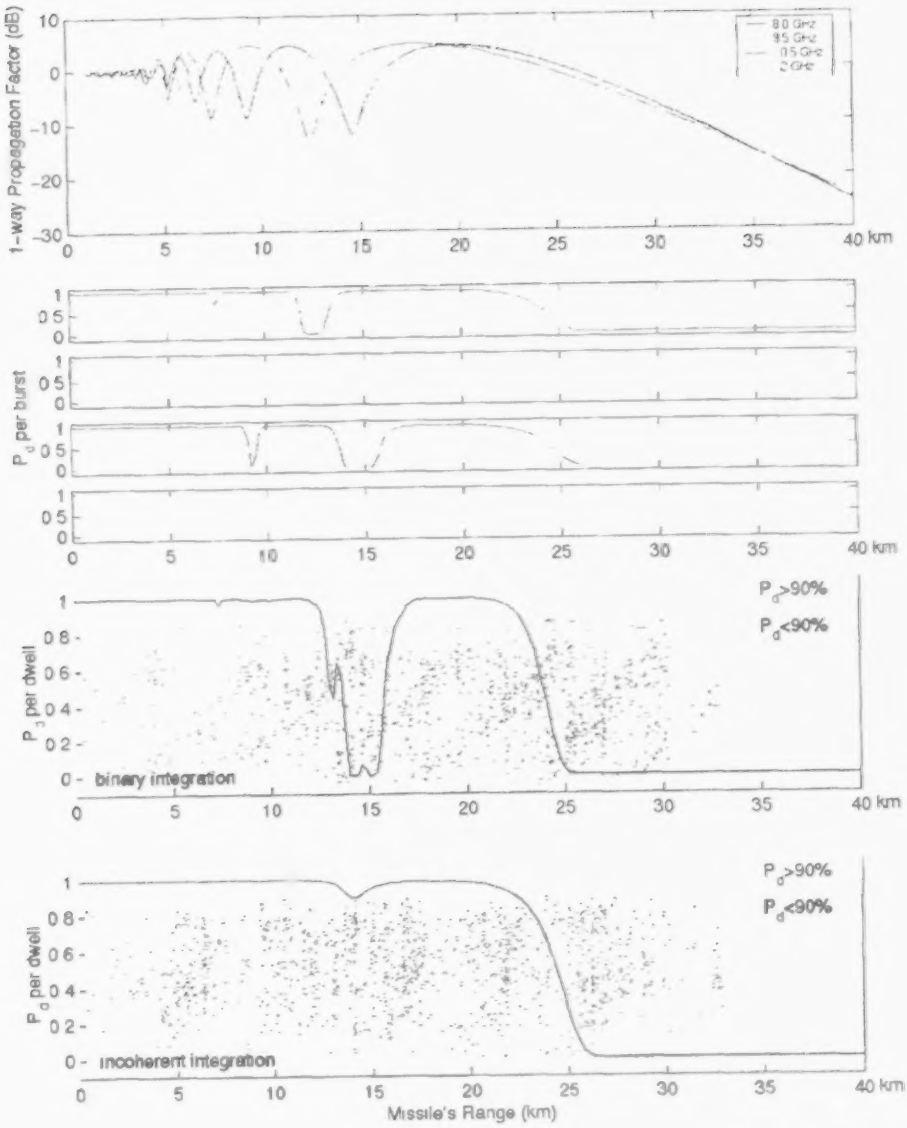

Figure 105. MFR results, Standard atmosphere, Exocet at 15 m

P517610.PDF [Page: 89 of 123]

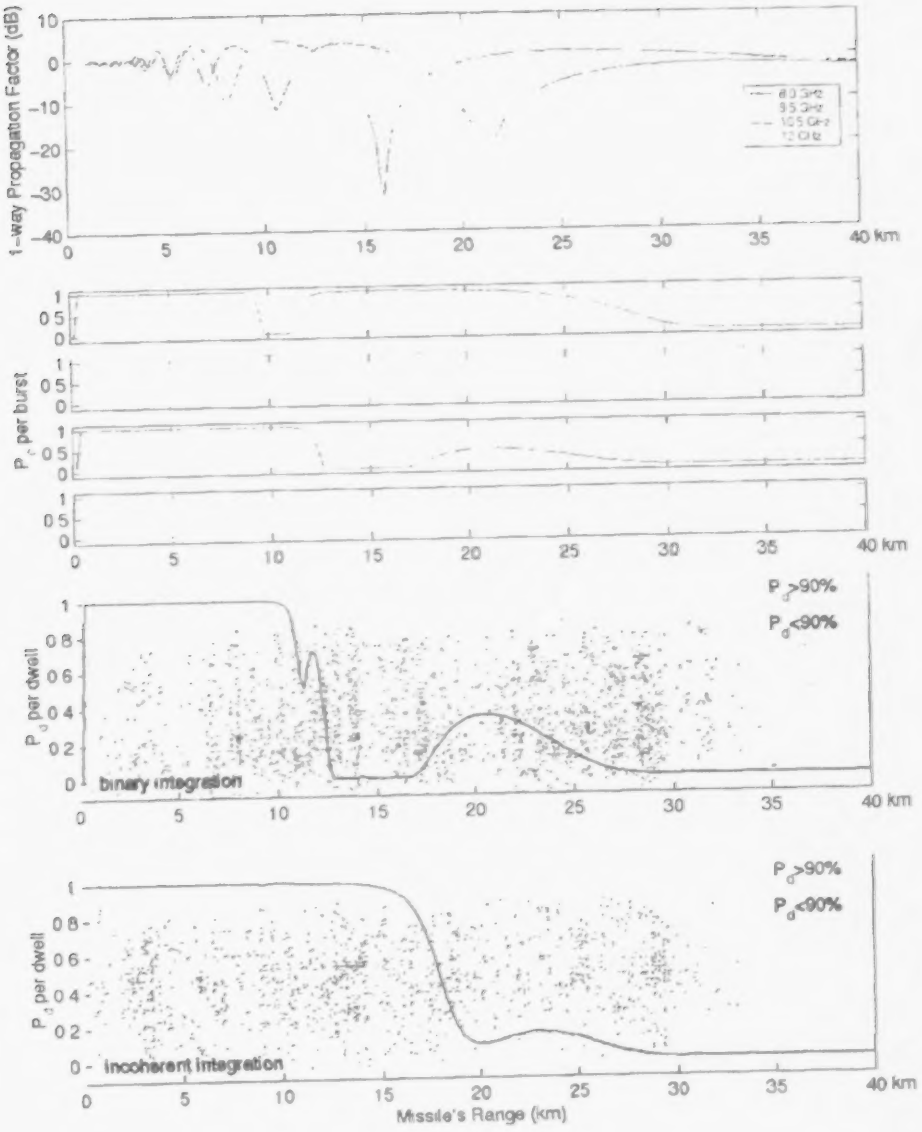

Figure 106. MFR results, 10m duct, Exocet at 15 m

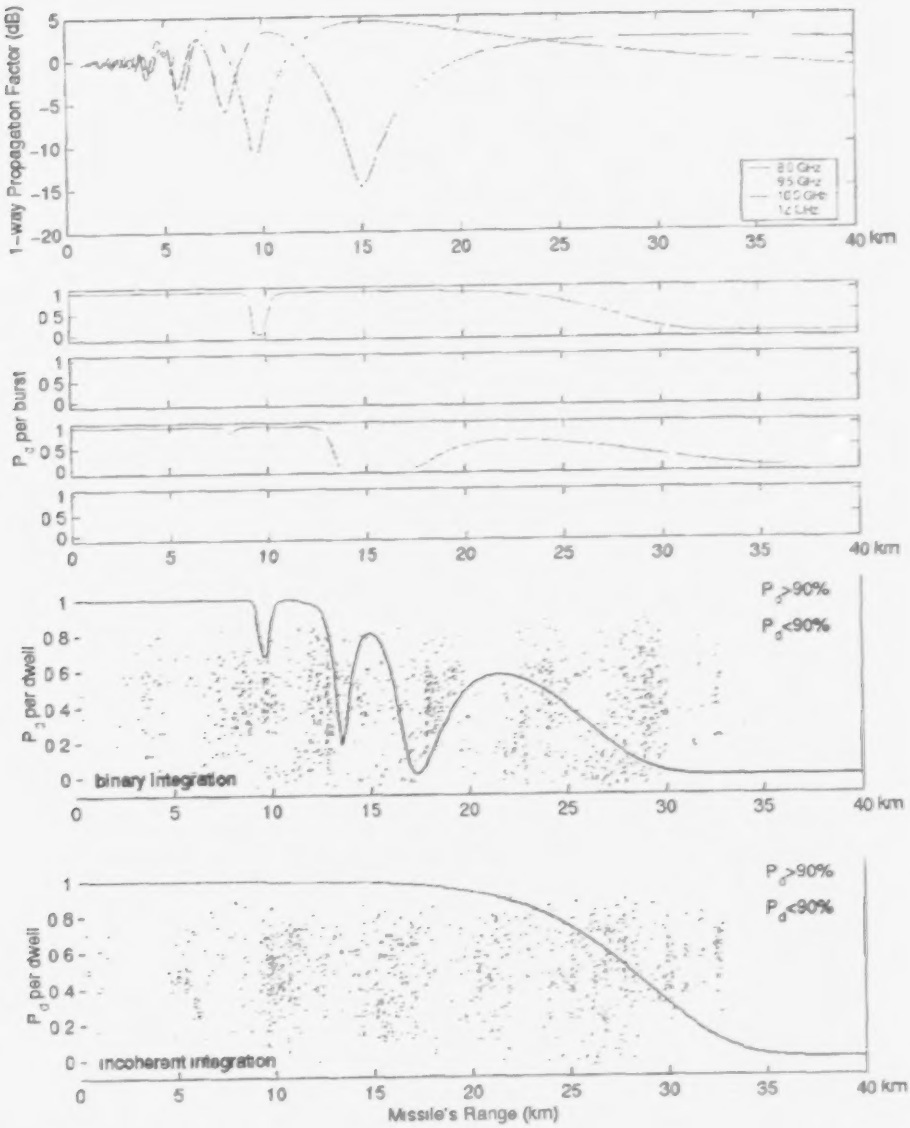

Figure 107. MFR results, 20m duct, Exocet at 15 m

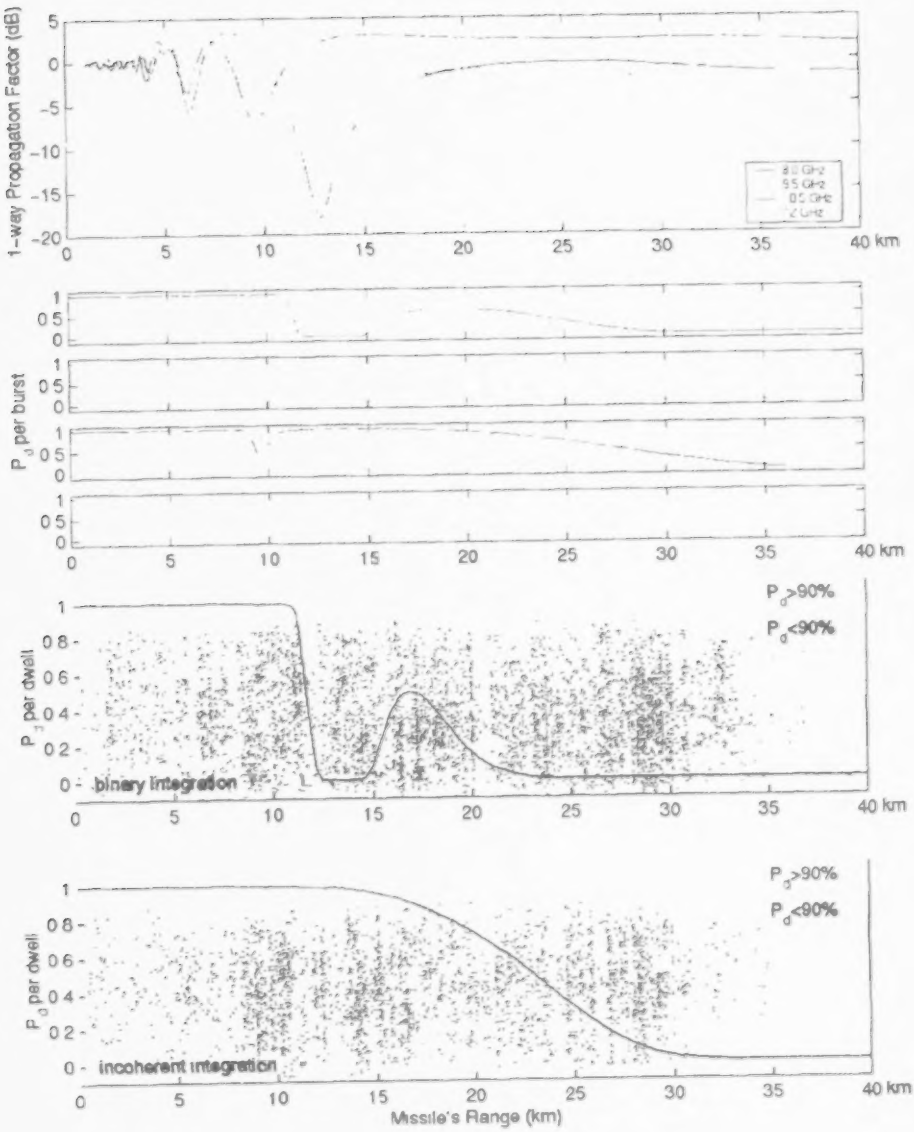

Figure 108. MFR results, 30m duct, Exocet at 15 m

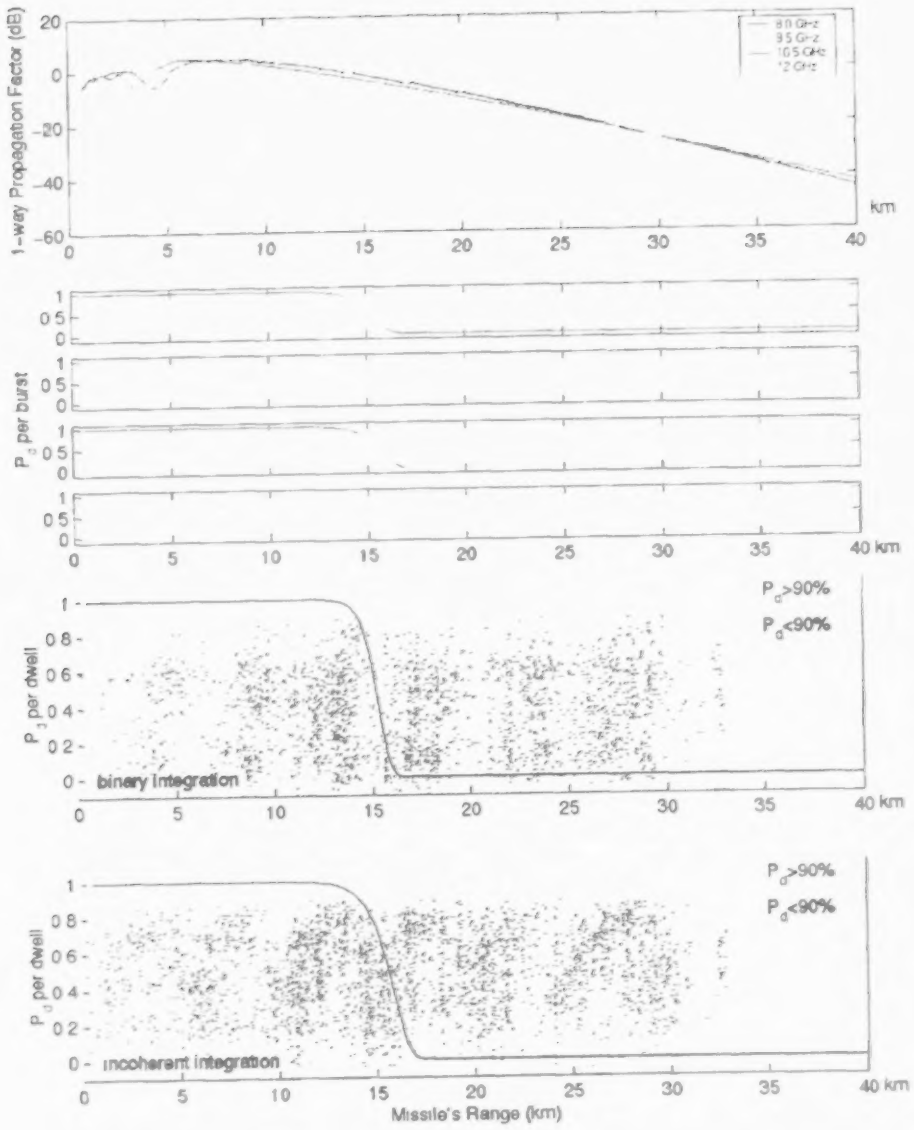

Figure 109. MFR results, Standard atmosphere, Exocet at 3 m

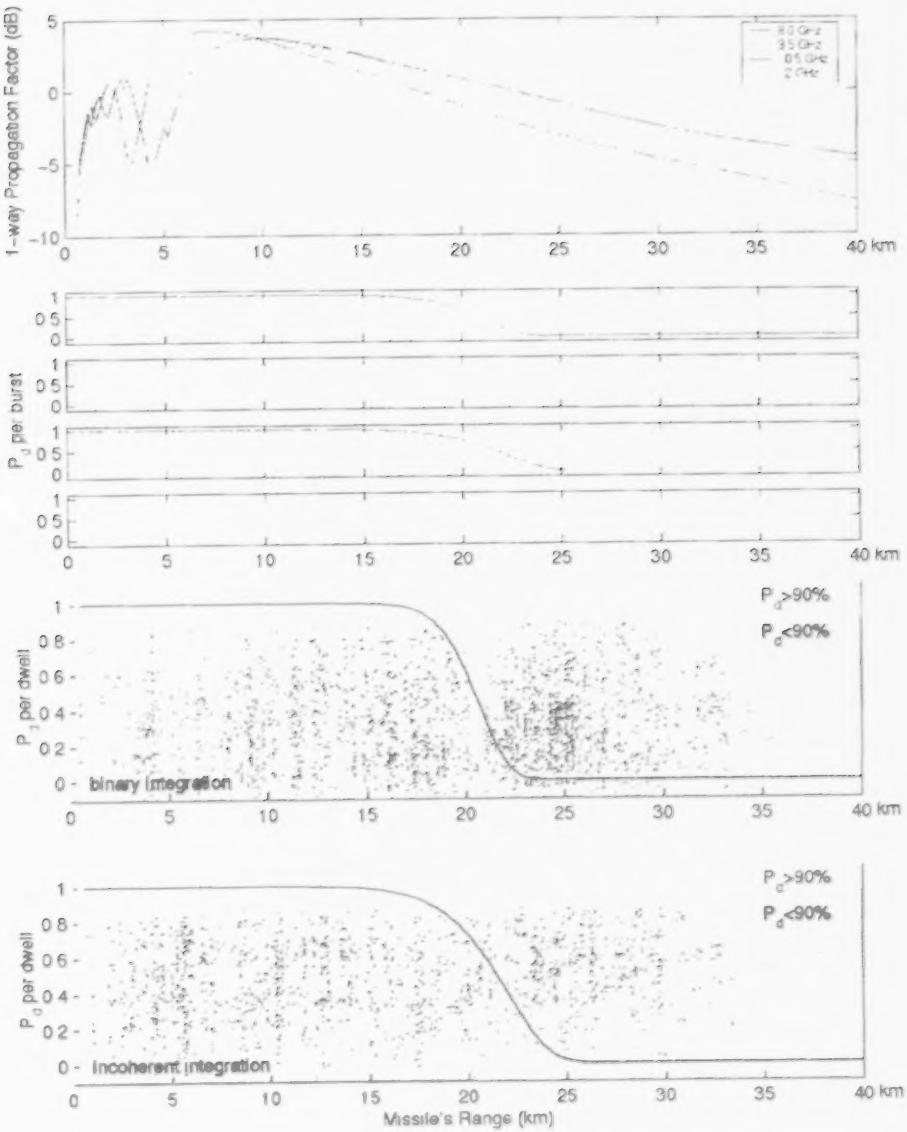

Figure 110. MFR results, 10m duct, Exocet at 3 m

P517610.PDF [Page: 94 of 123]

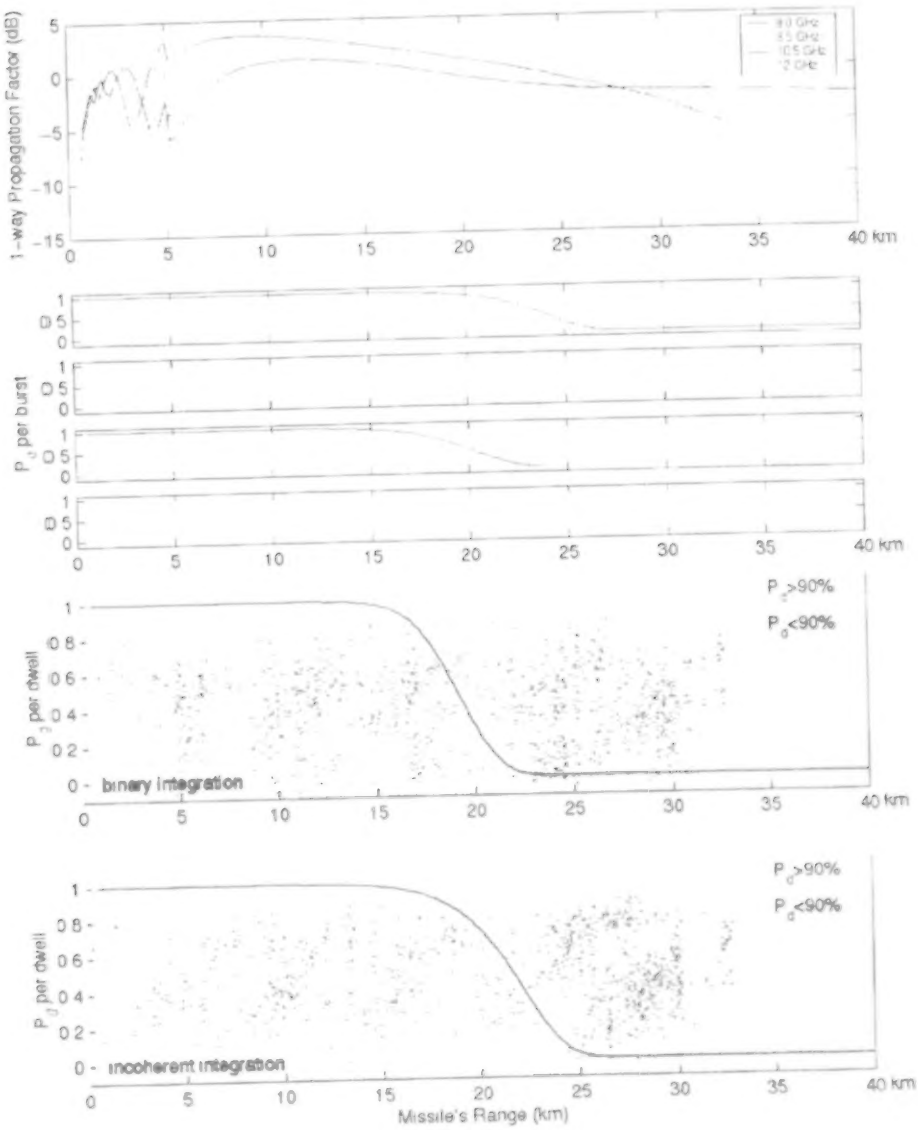

Figure 111. MFR results, 20m duct, Exocet at 3 m

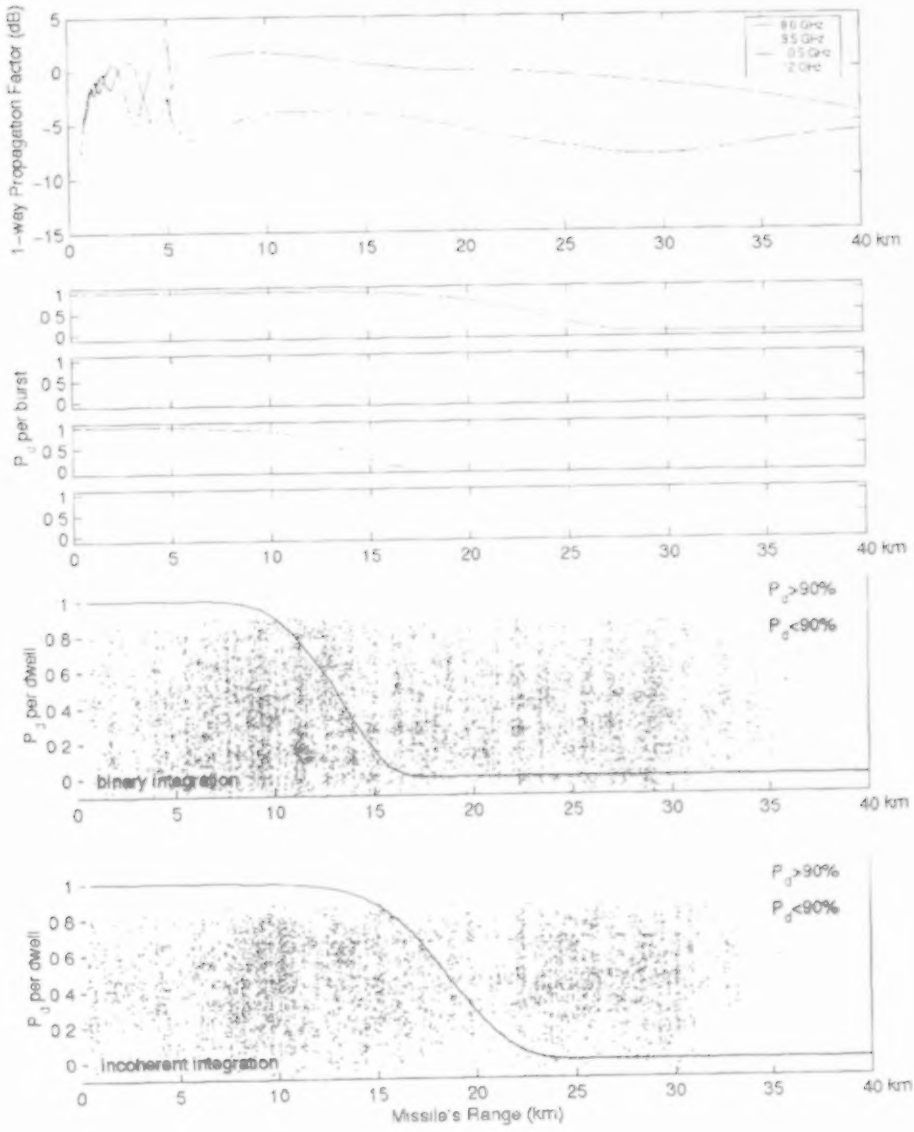

Figure 112. MFR results, 30m duct, Exocet at 3 m

P517610.PDF [Page: 96 of 123]

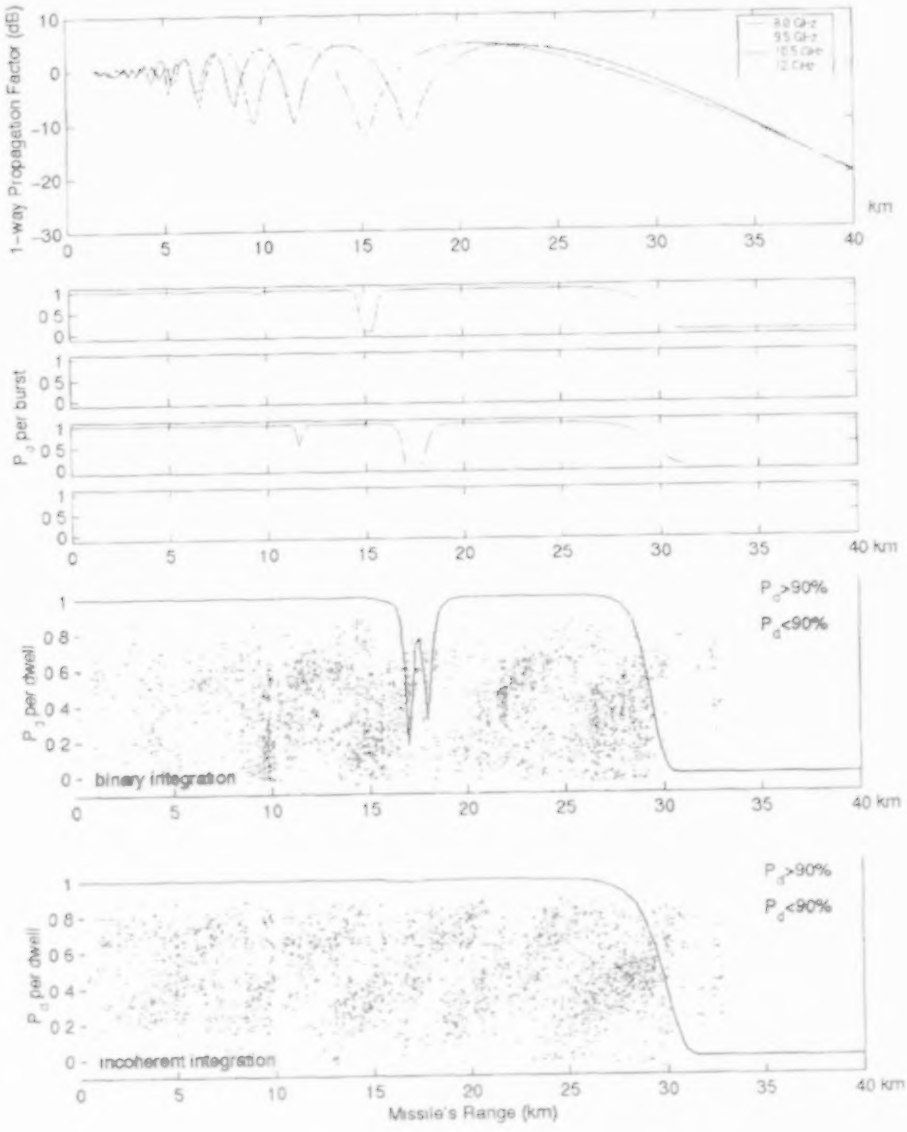

Figure 113. MFR results, Standard atmosphere, SS-N-22 at 20 m

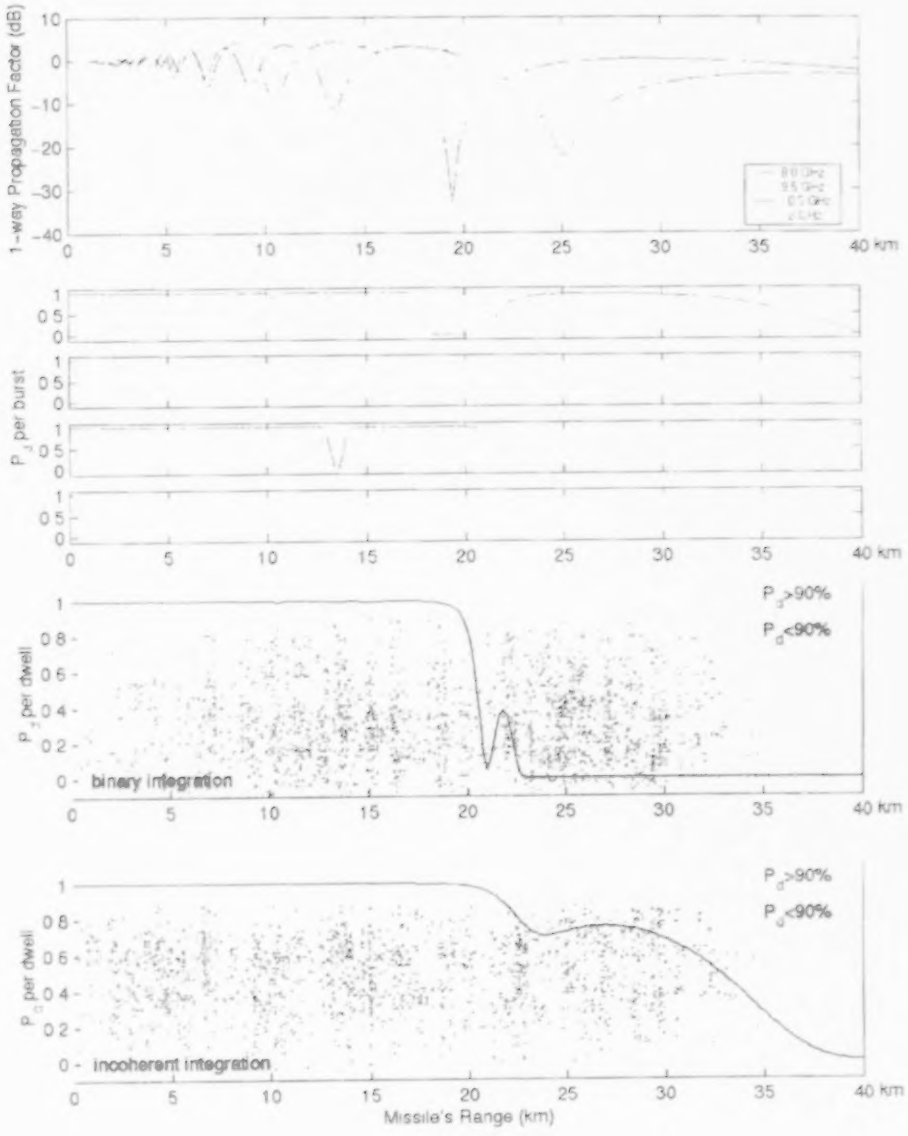

Figure 114. MFR results, 10m duct, SS-N-22 at 20 m

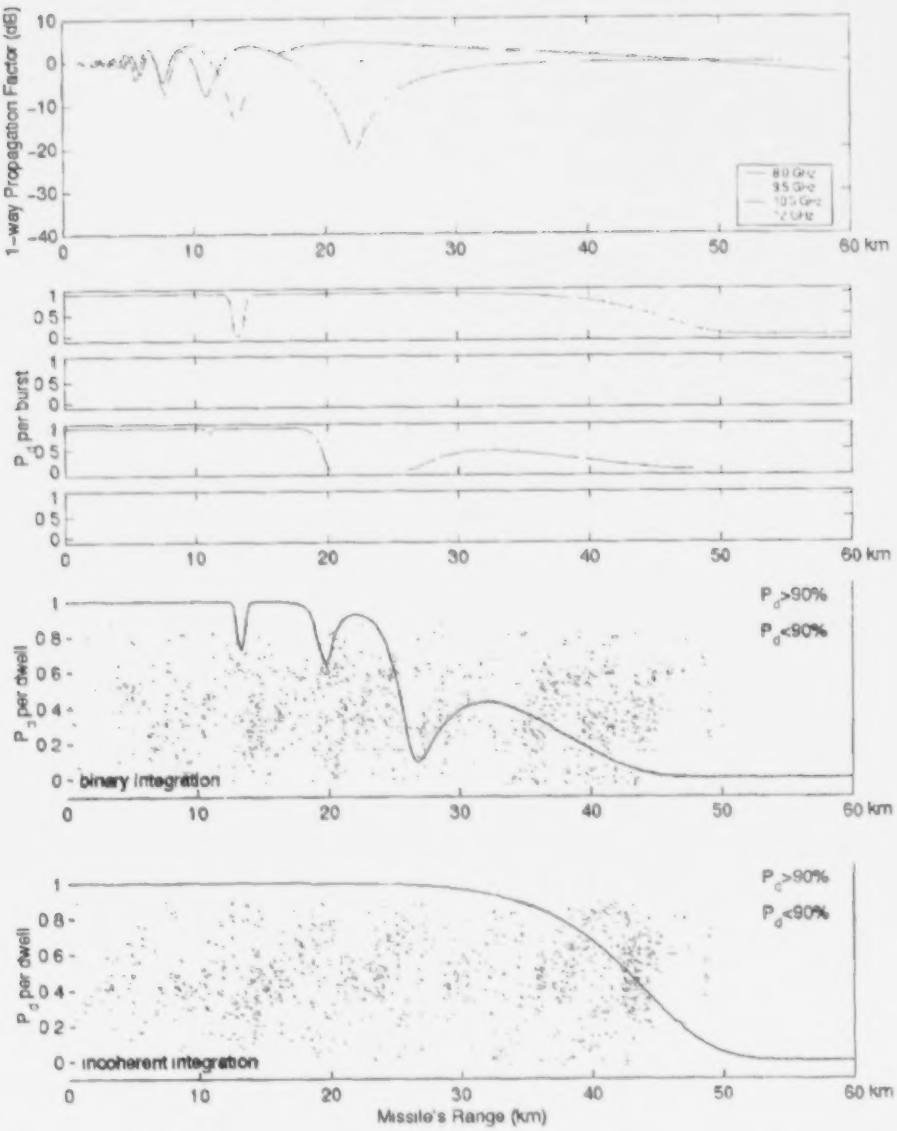

Figure 115. MFR results, 20m duct, SS-N-22 at 20 m

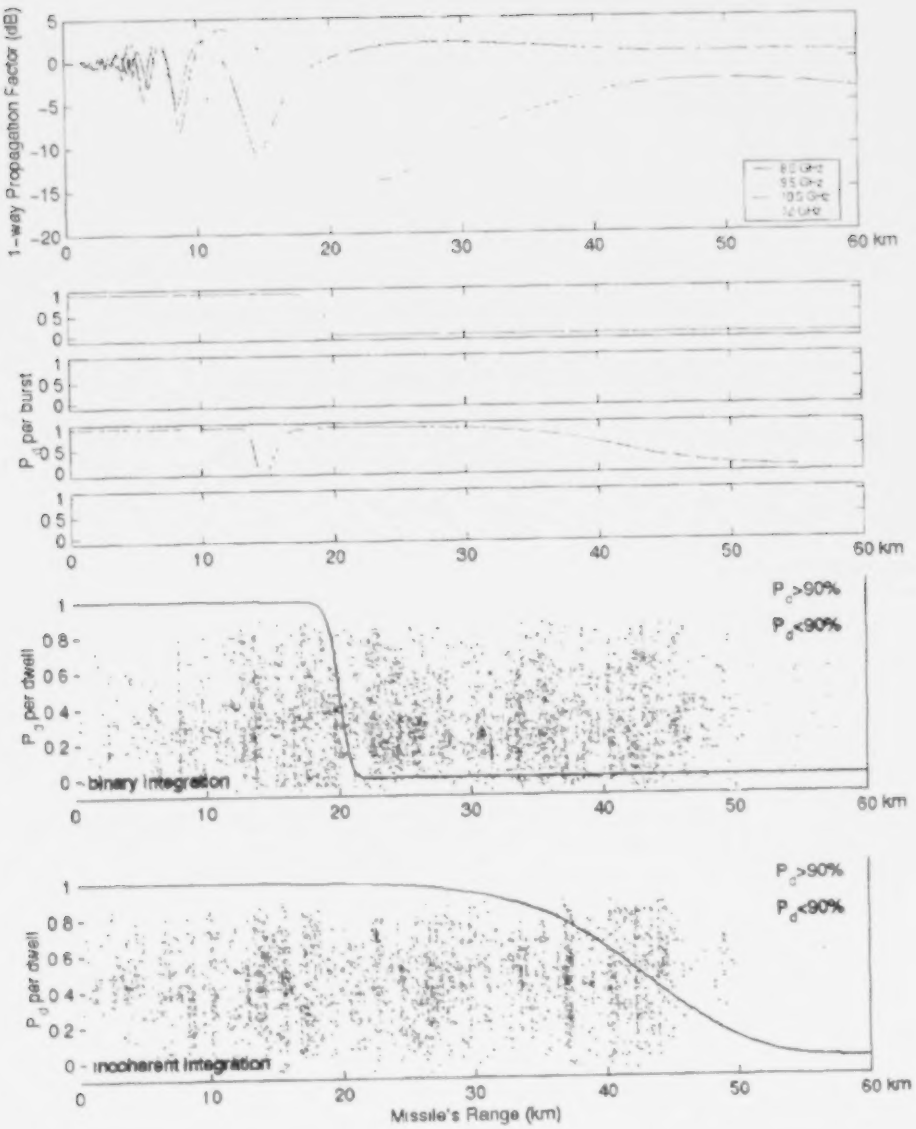

Figure 116. MFR results, 30m duct, SS-N-22 at 20 m

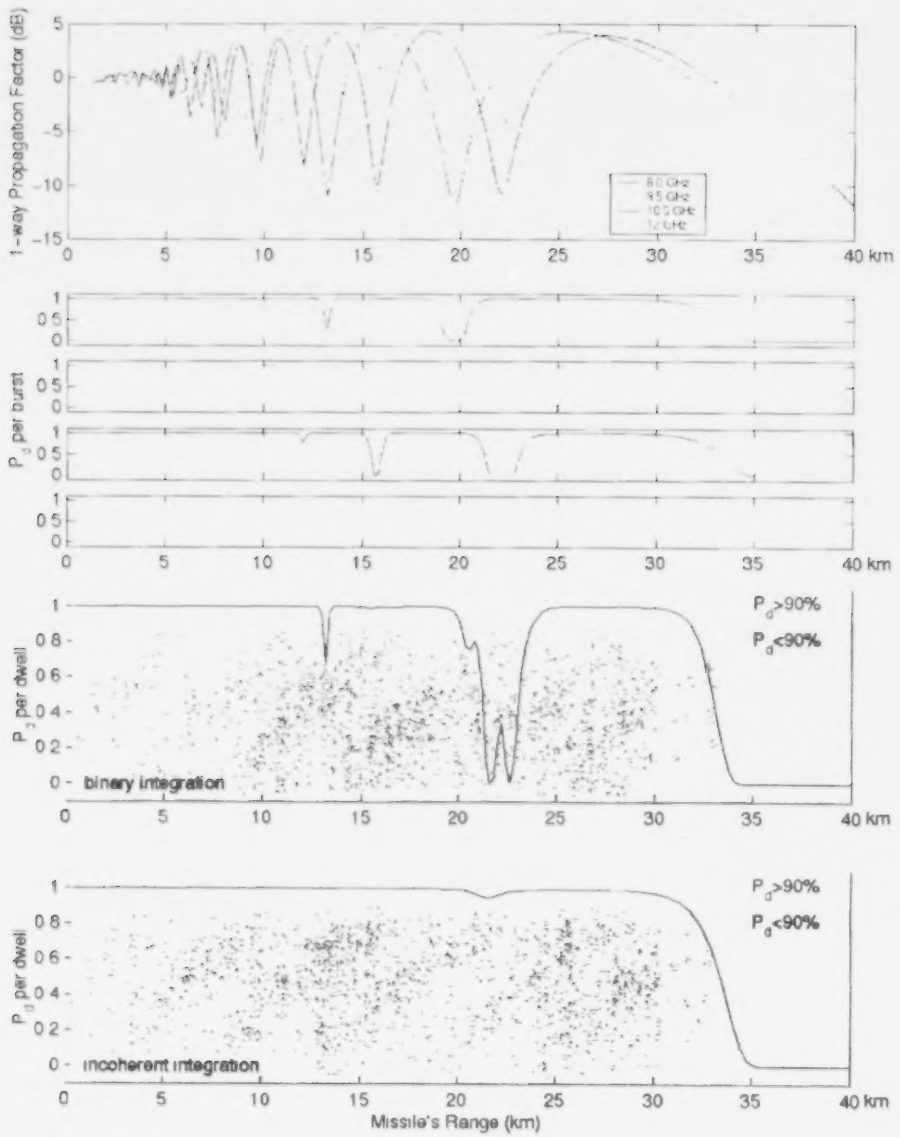

Figure 117. MFR results, Standard atmosphere, SS-N-22 at 30 m

P517610.PDF [Page: 101 of 123]

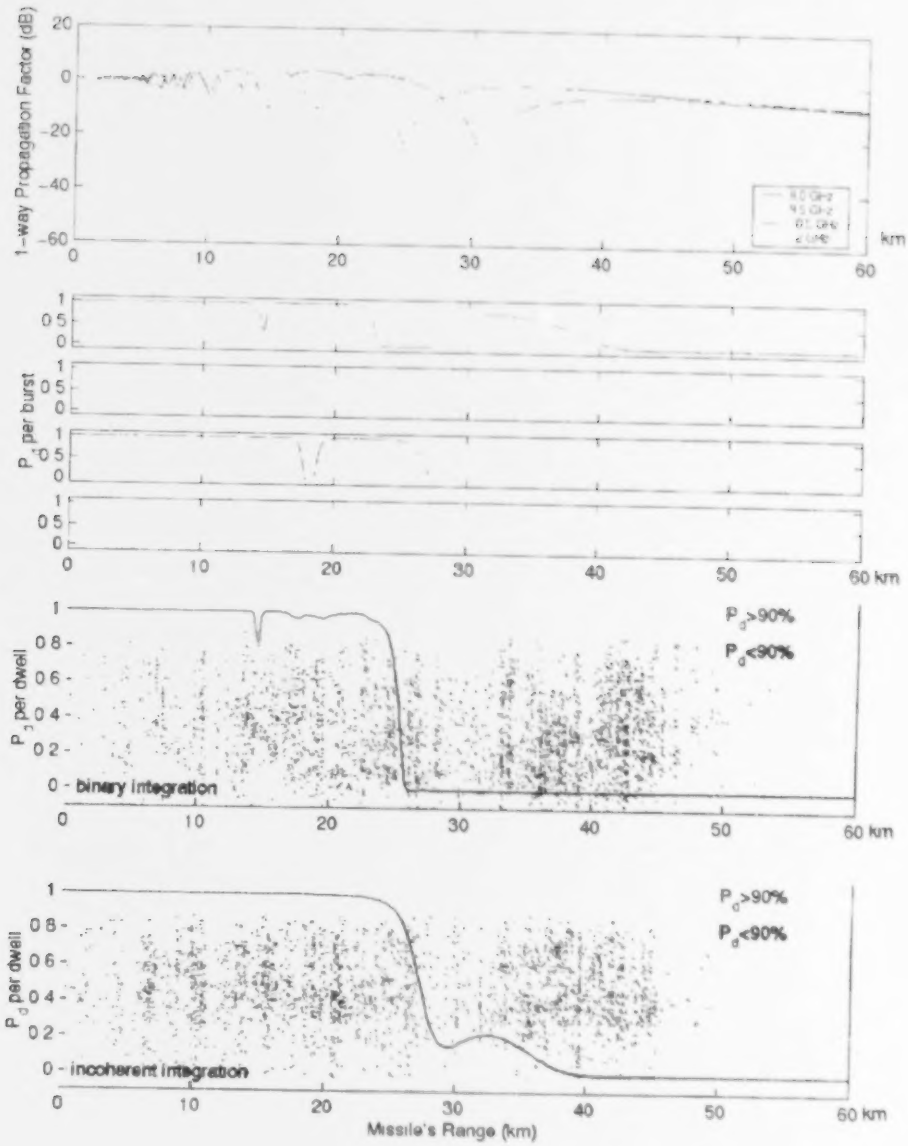

Figure 118. MFR results, 10m duct, SS-N-22 at 30 m

P517610.PDF [Page: 102 of 123]

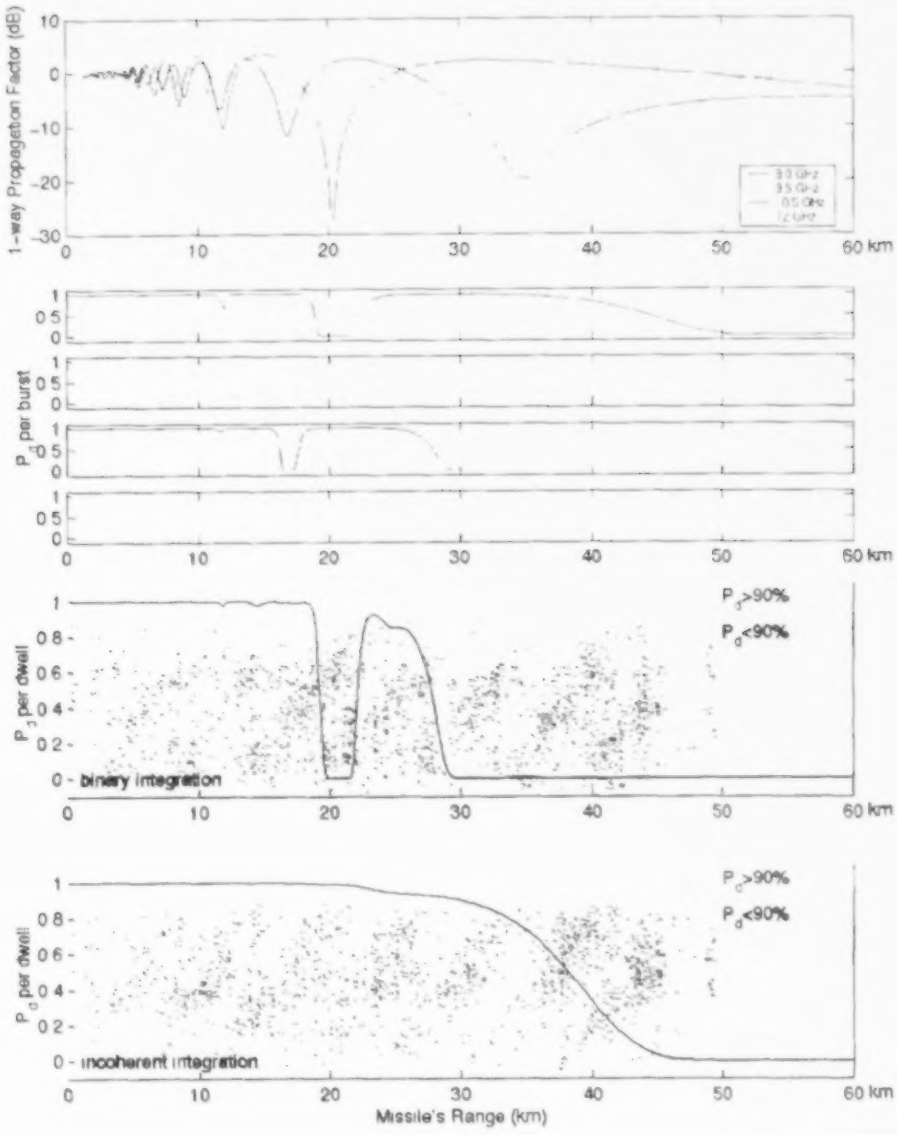

Figure 119. MFR results, 20m duct, SS-N-22 at 30 m

P517610.PDF [Page: 103 of 123]

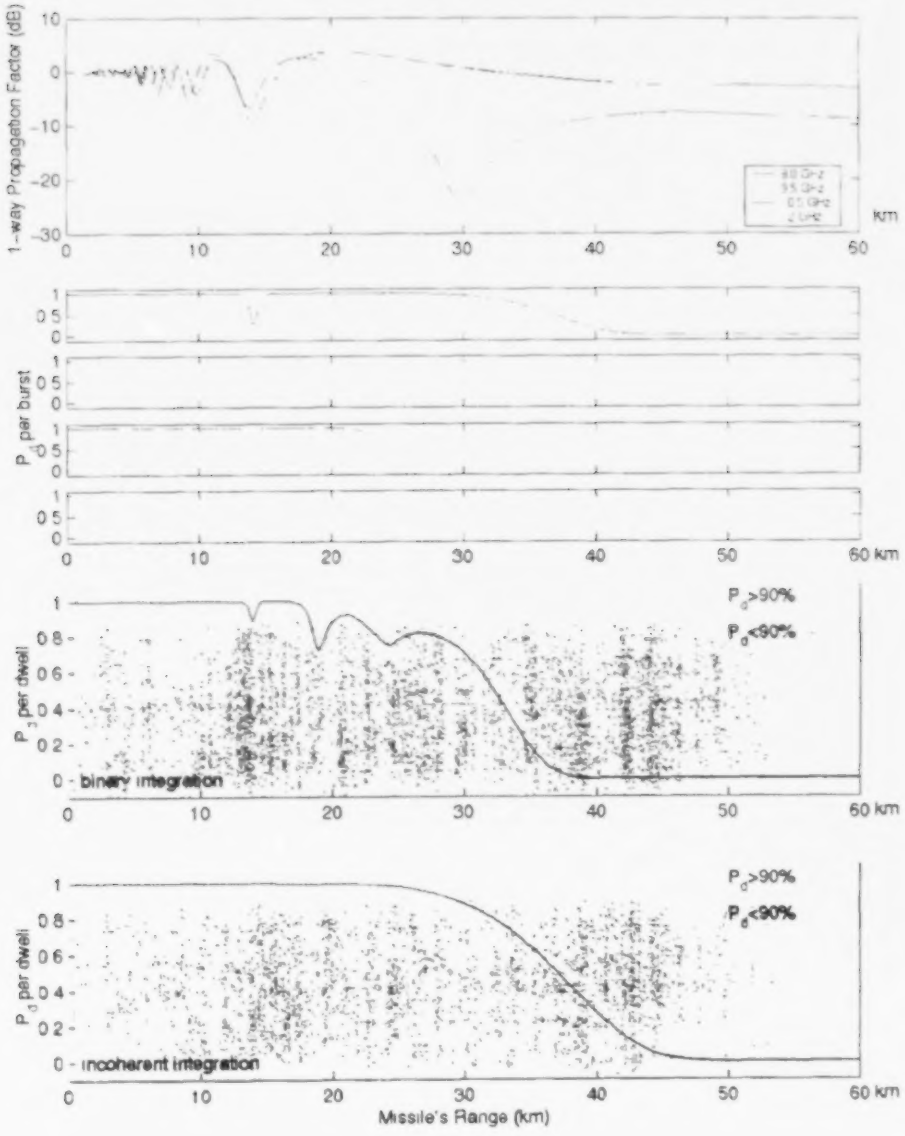

Figure 120. MFR results, 30m duct, SS-N-22 at 30 m

P517610.PDF [Page: 104 of 123]

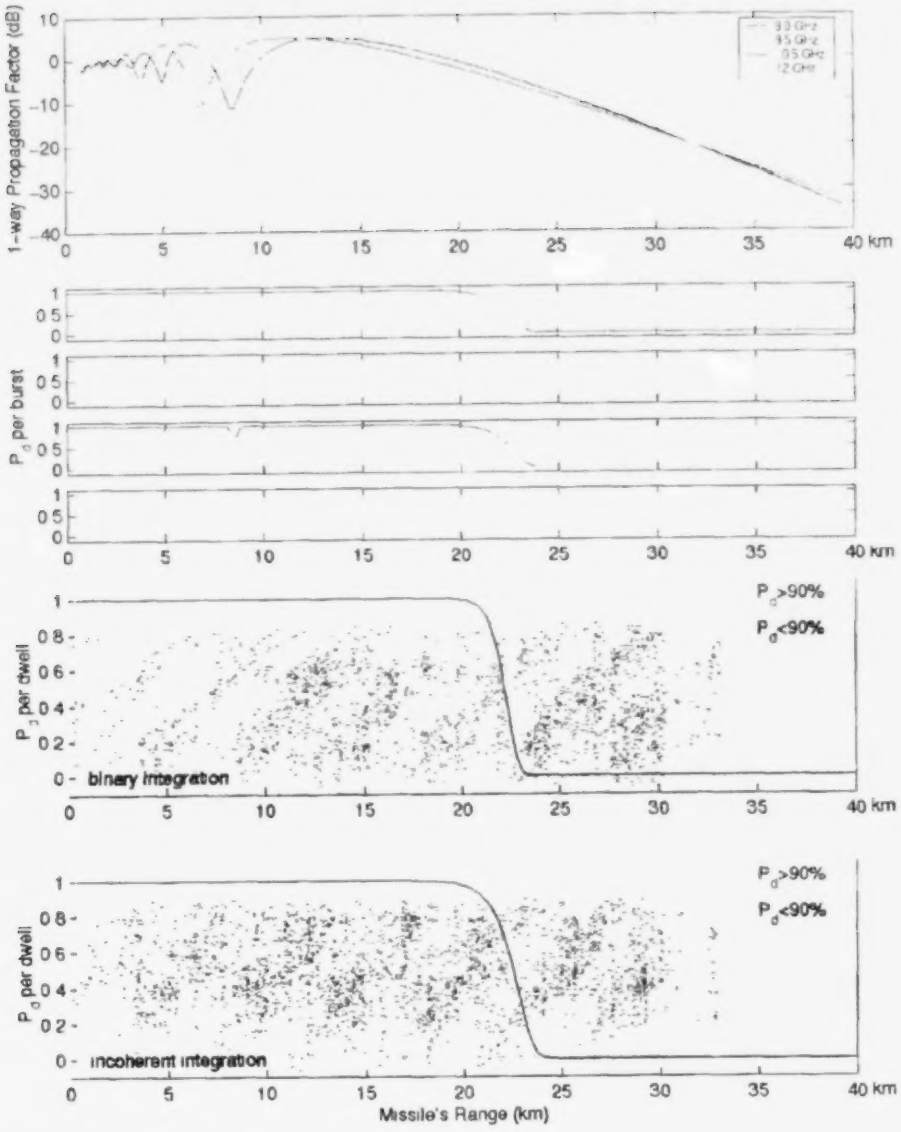

Figure 121. MFR results, Standard atmosphere, SS-N-22 at 7 m

P517610.PDF [Page: 105 of 123]

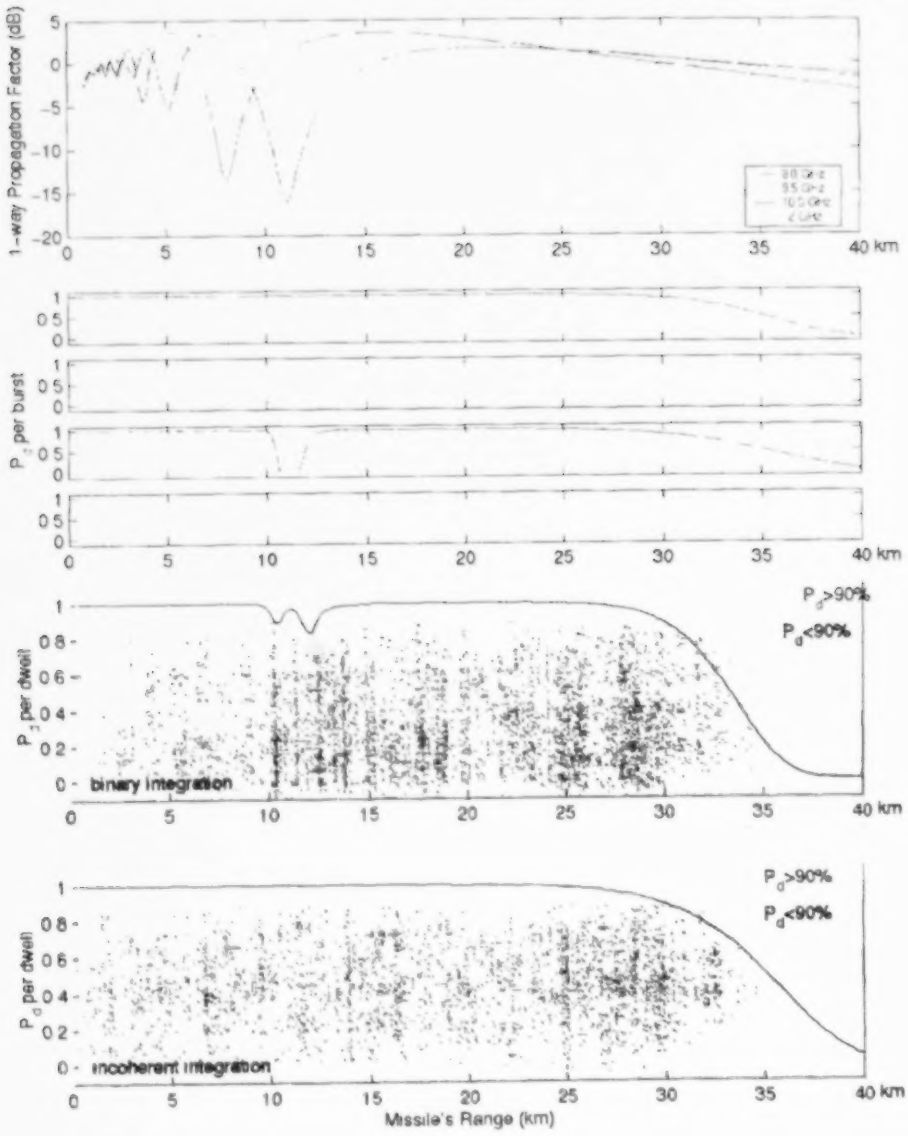

Figure 122. MFR results, 10m duct, SS-N-22 at 7 m

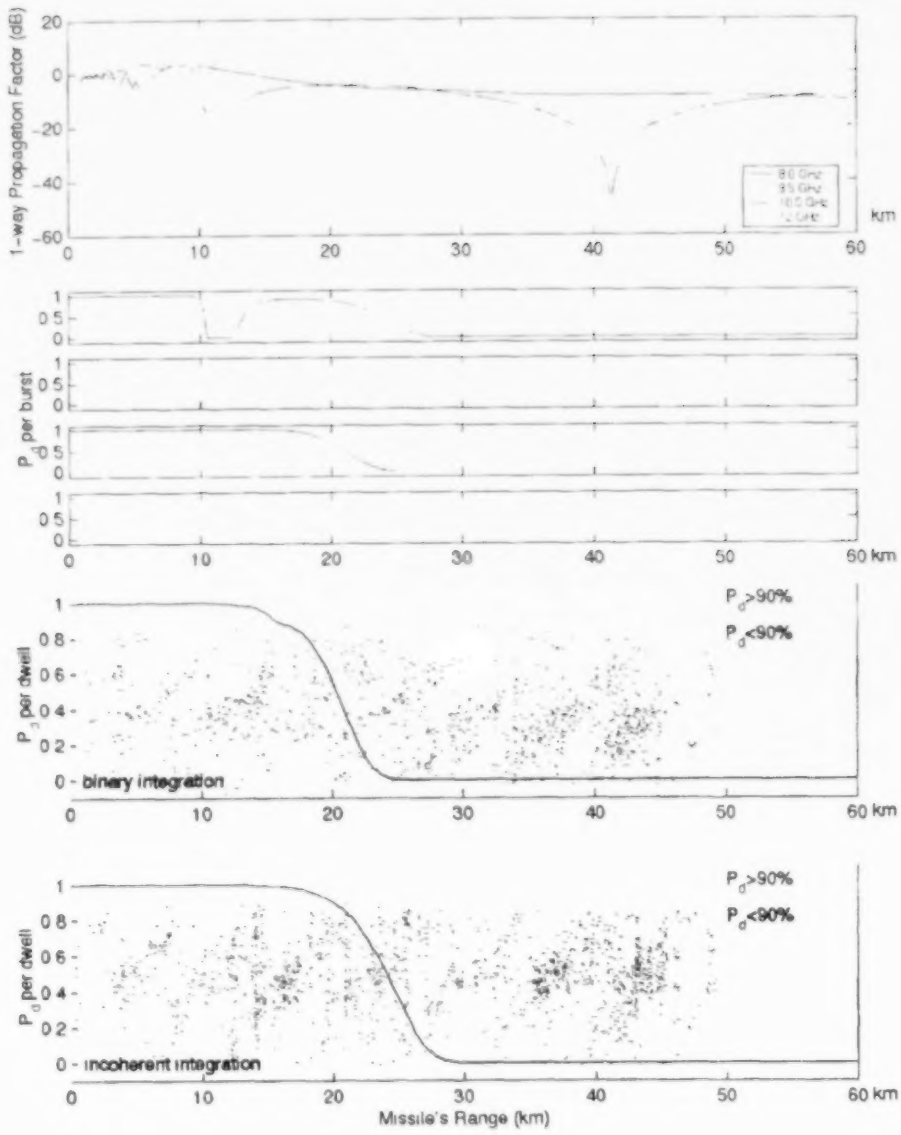

Figure 123. MFR results, 20m duct, SS-N-22 at 7 m

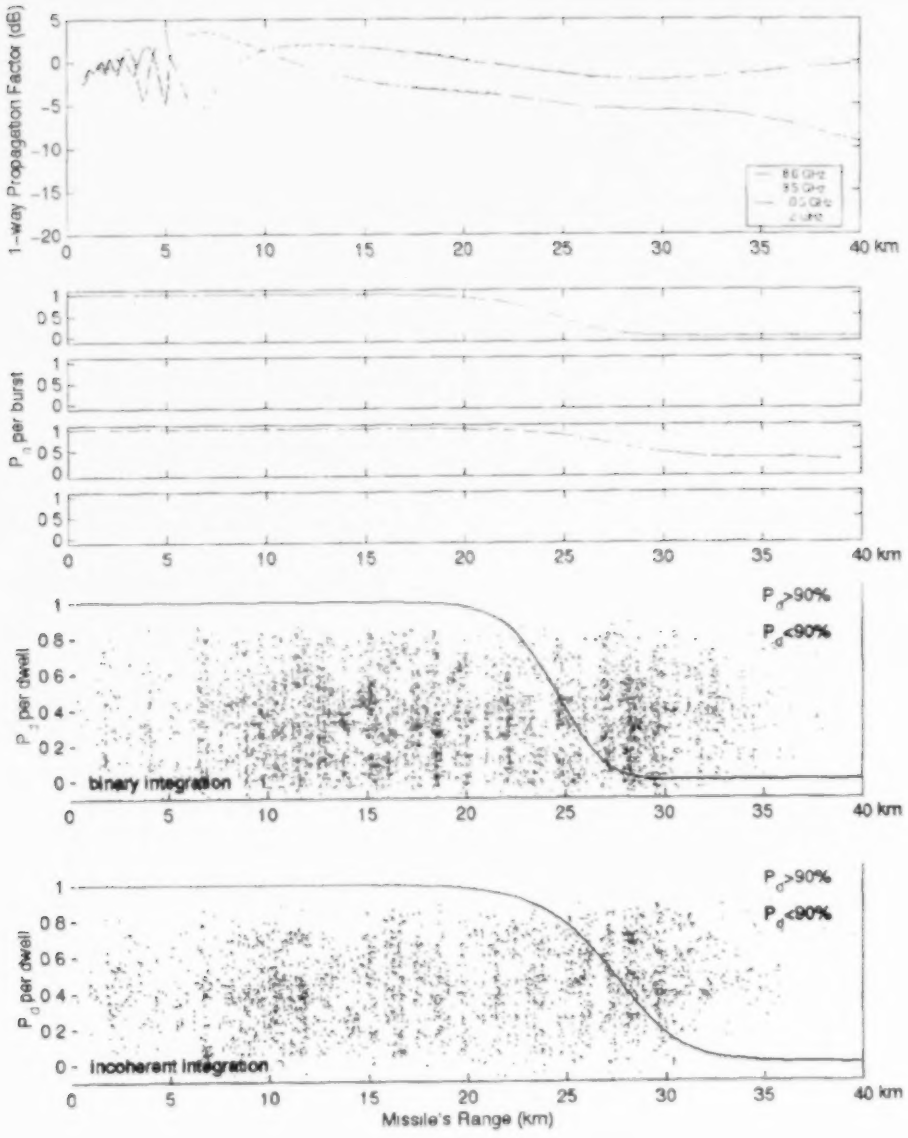

Figure 124. MFR results, 30m duct, SS-N-22 at 7 m

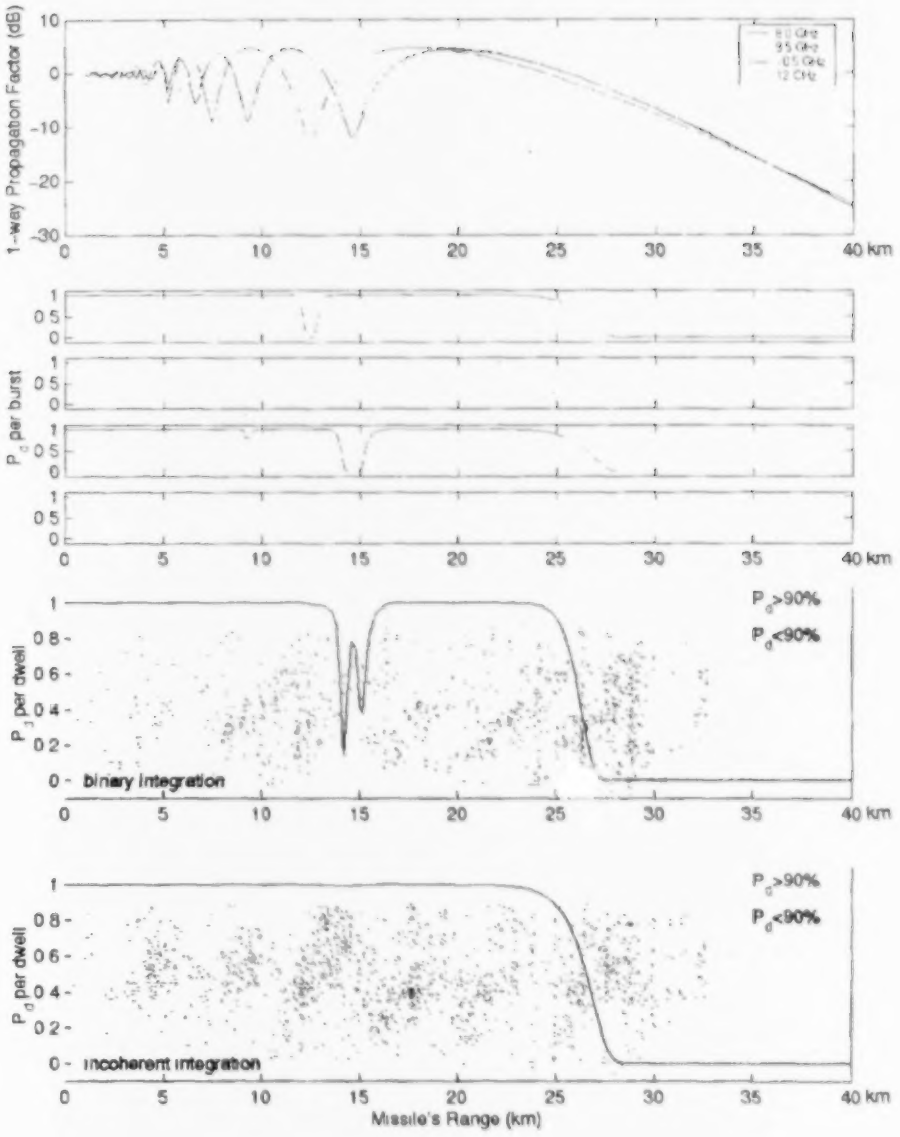

Figure 125. MFR results, standard atmosphere, NOVATOR at 15 m

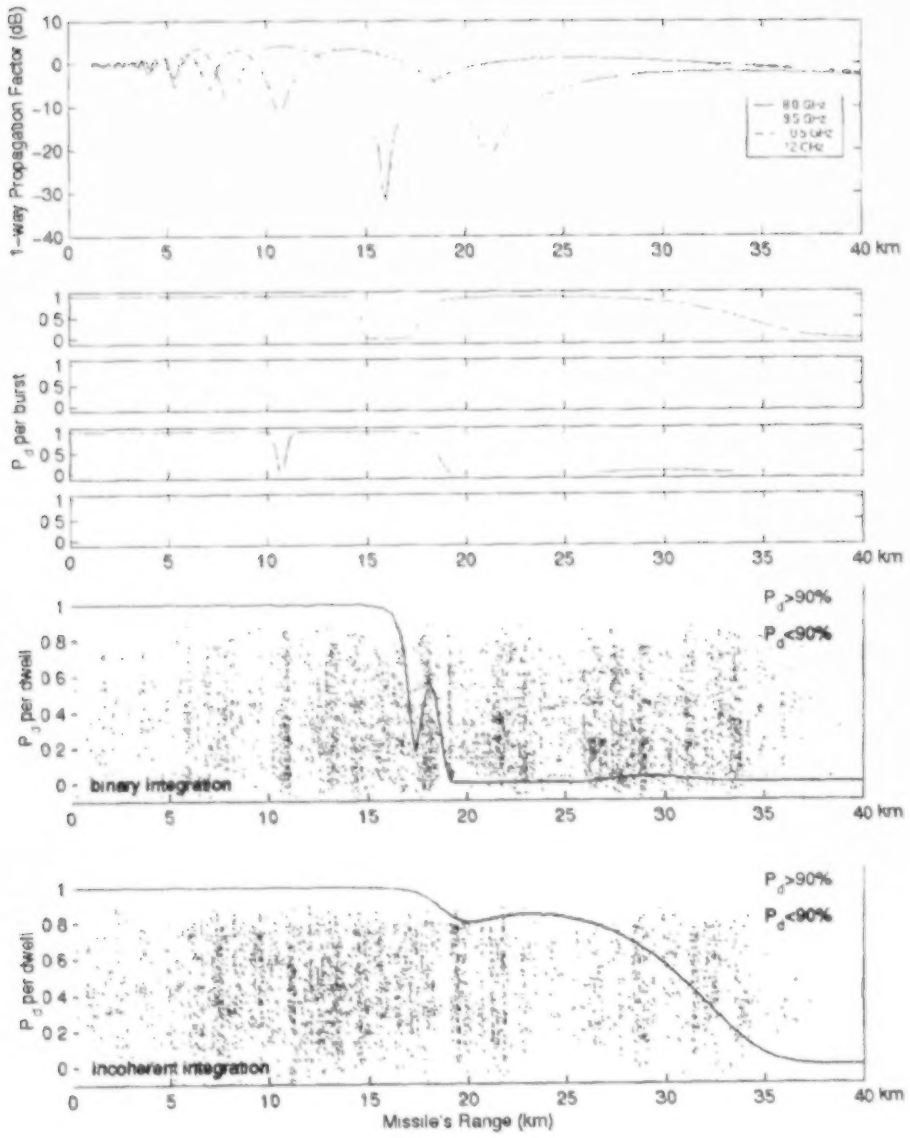

Figure 126. MFR results, 10m duct, NOVATOR at 15 m

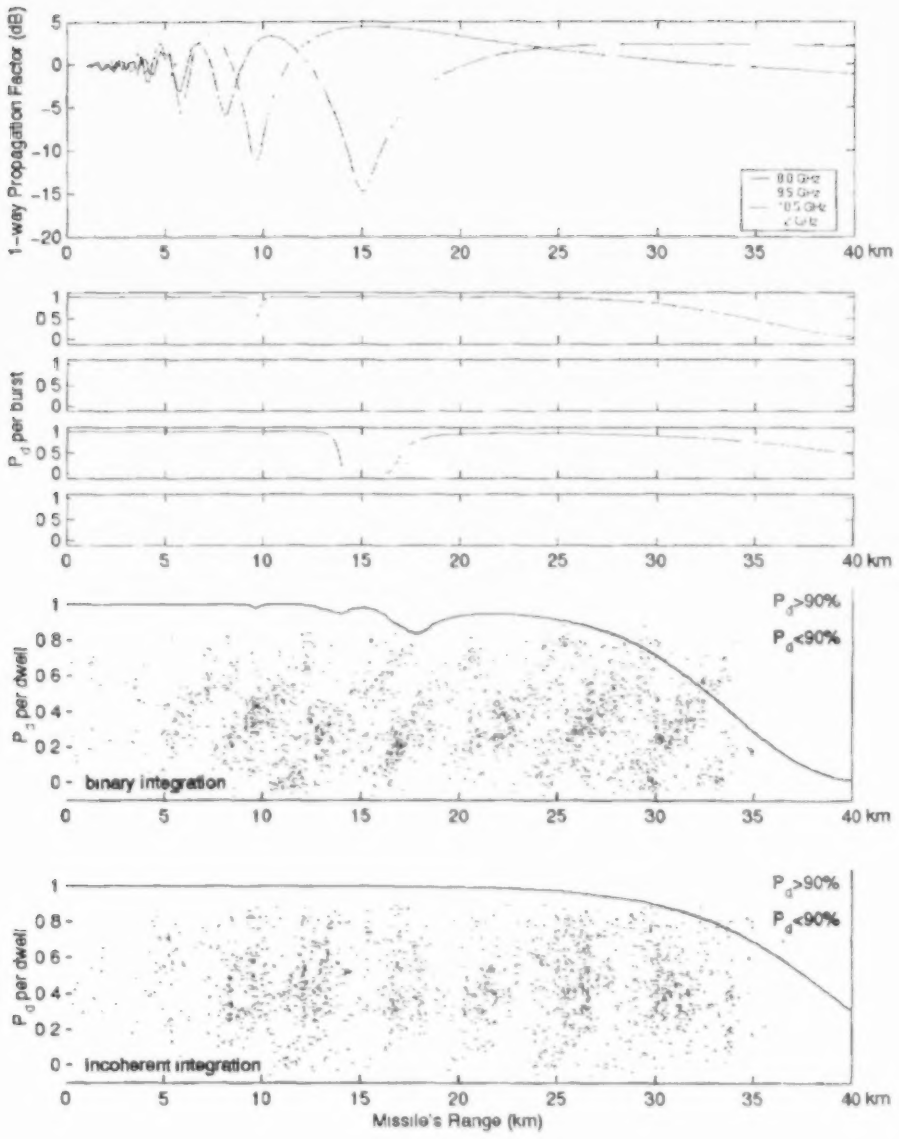

Figure 127. MFR results, 20m duct, NOVATOR at 15 m

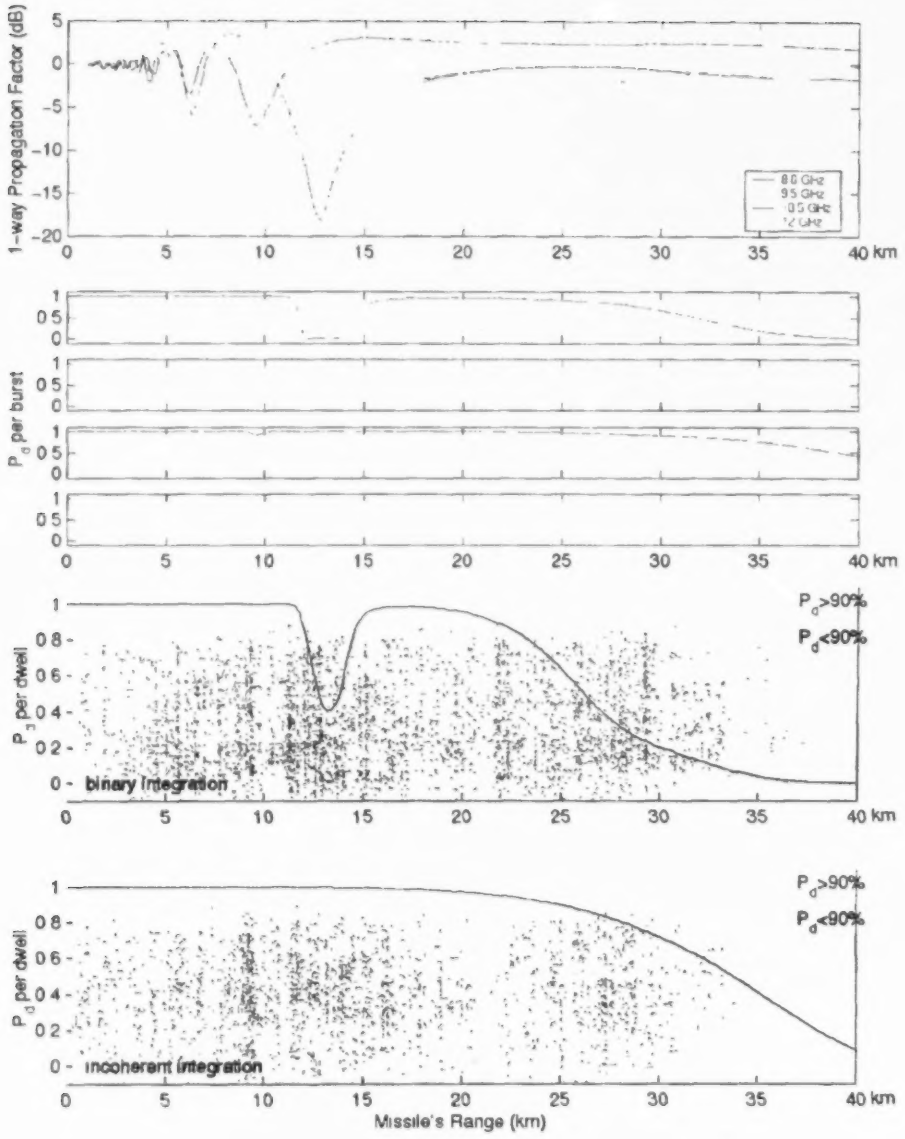

Figure 128. MFR results, 30m duct, NOVATOR at 15 m

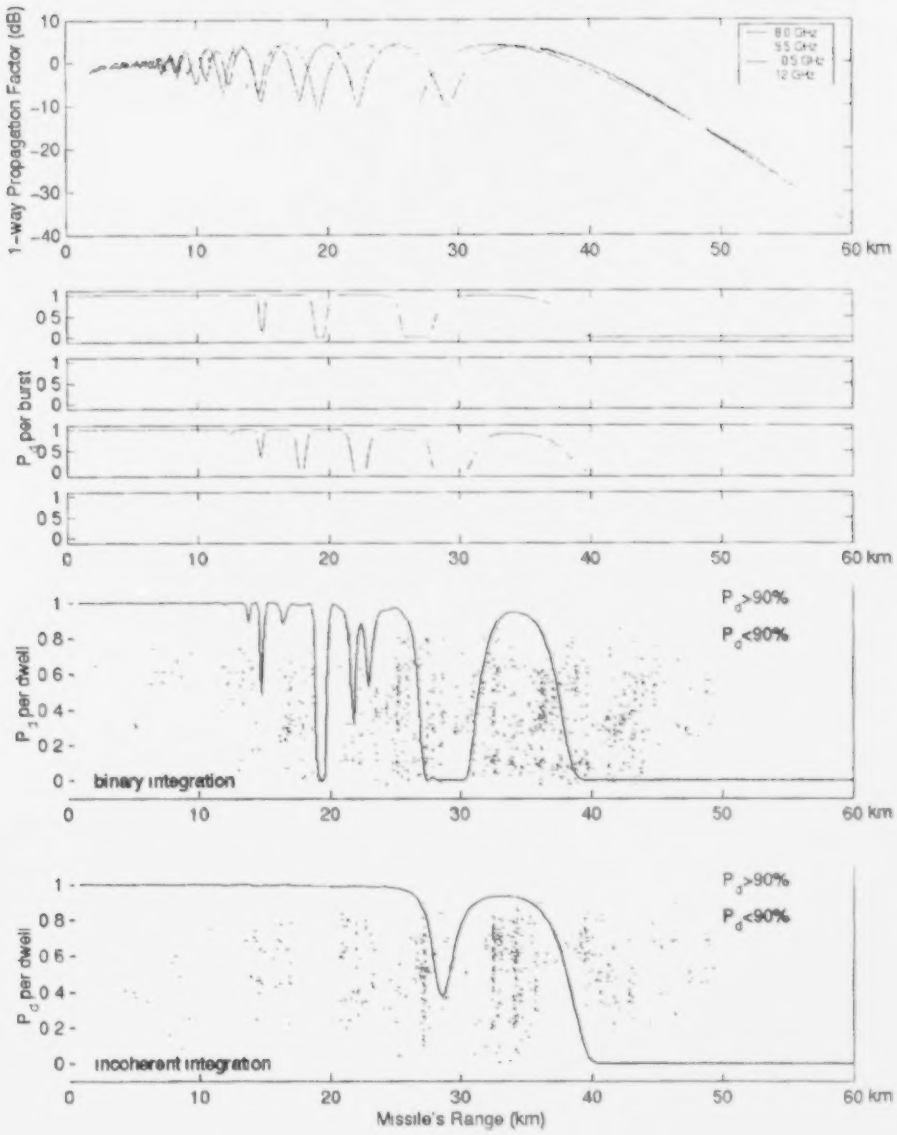

Figure 129. MFR results, Standard atmosphere, NOVATOR at 50 m

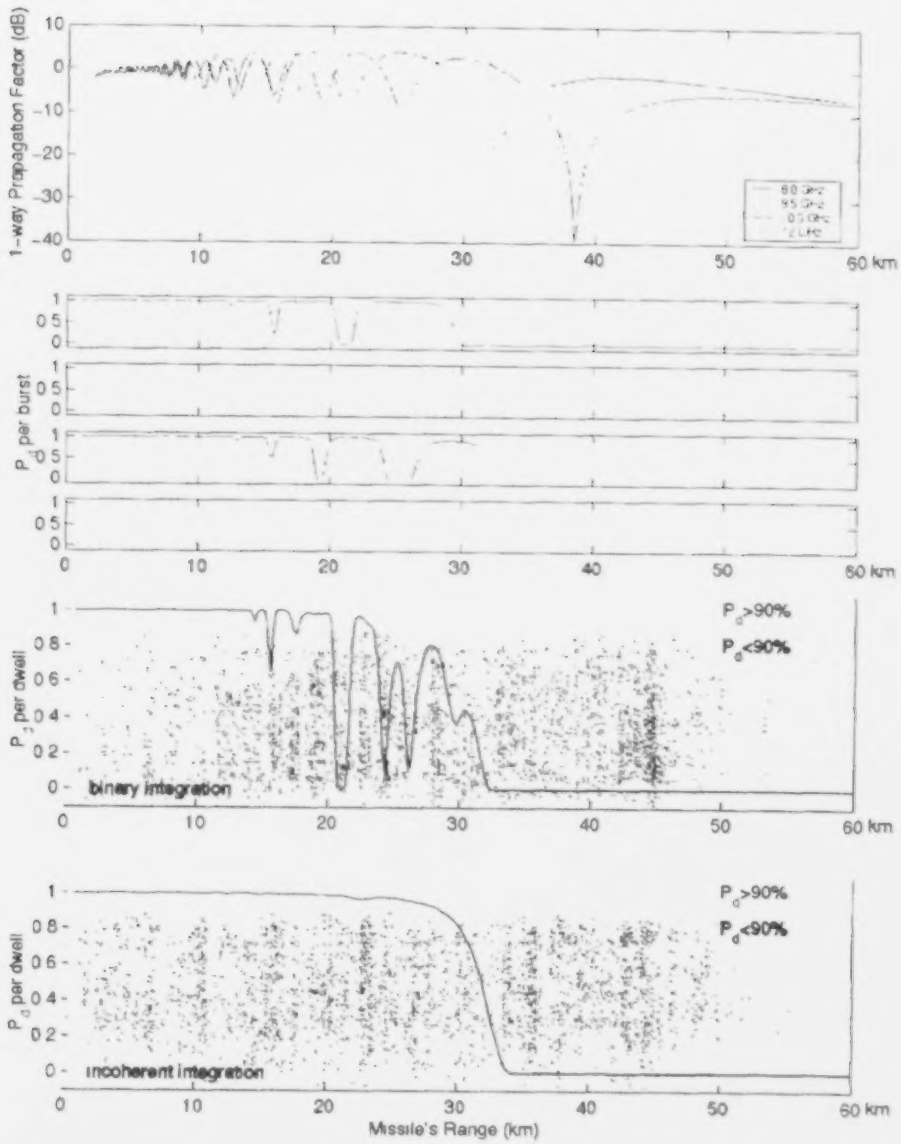

Figure 130. MFR results, 10m duct, NOVATOR at 50 m

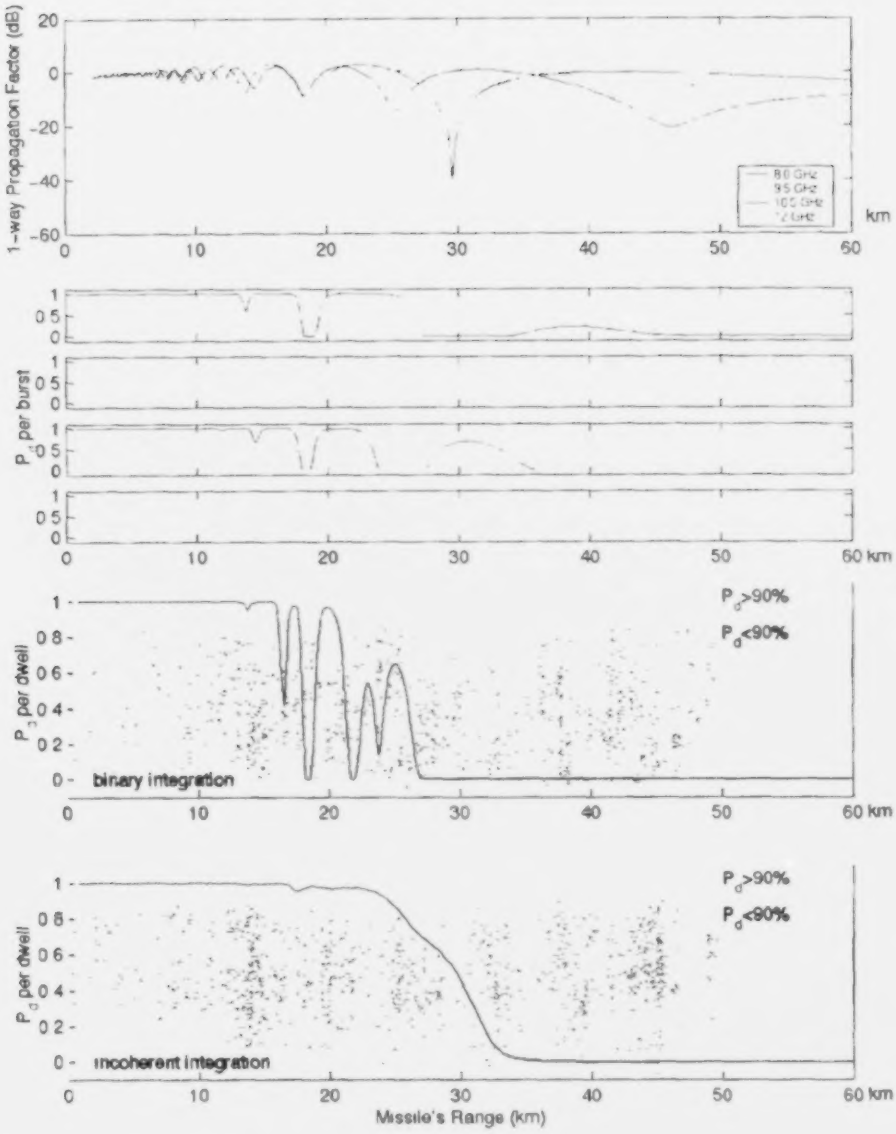

Figure 131. MFR results, 20m duct, NOVATOR at 50 m

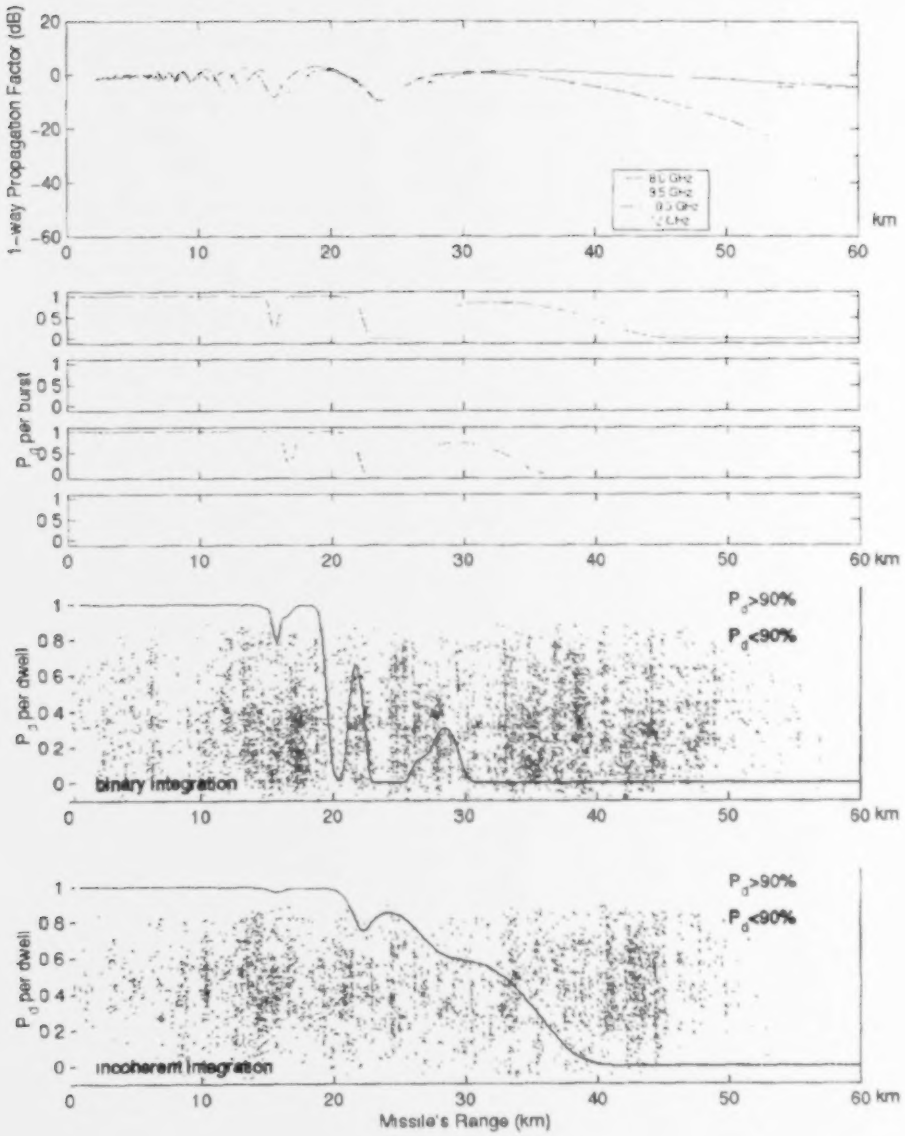

Figure 132. MFR results, 30m duct, NOVATOR at 50 m

P517610.PDF [Page: 116 of 123]

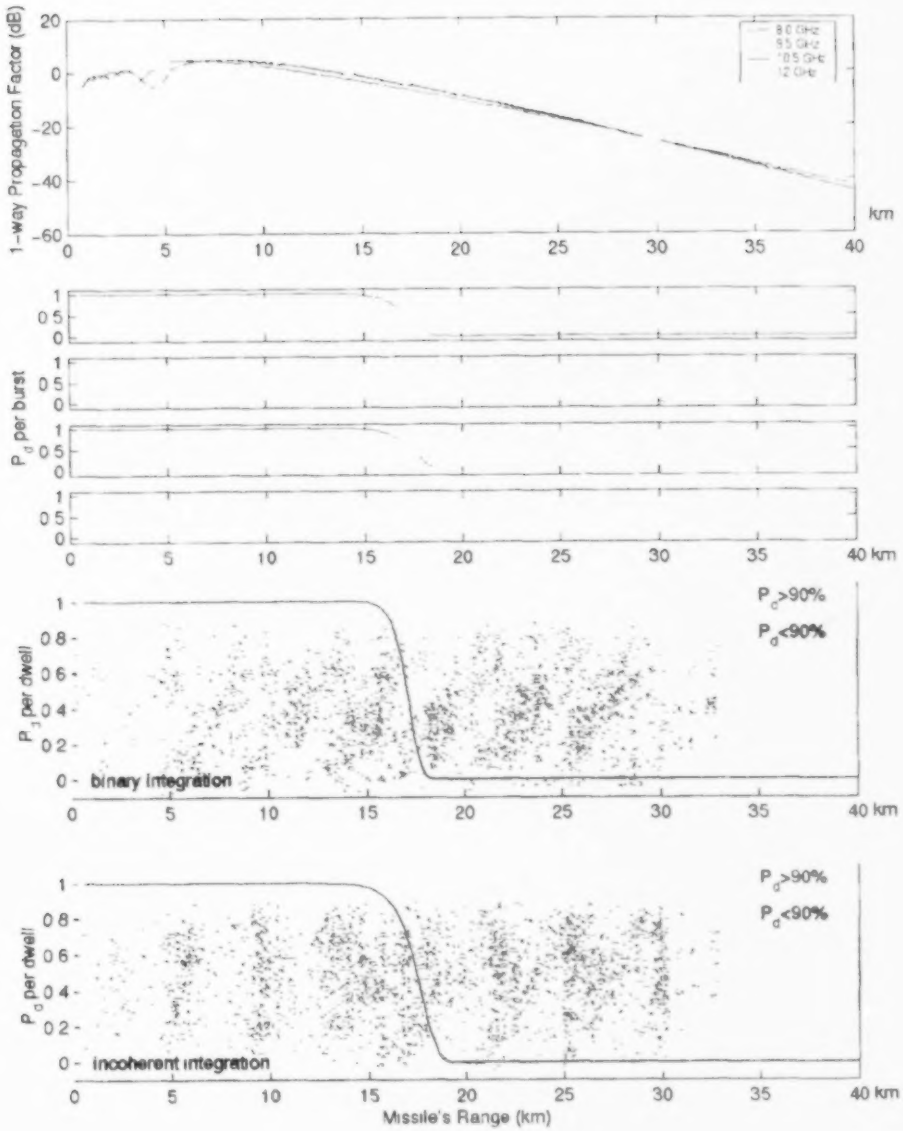

Figure 133. MFR results, standard atmosphere, NOVATOR at 3 m

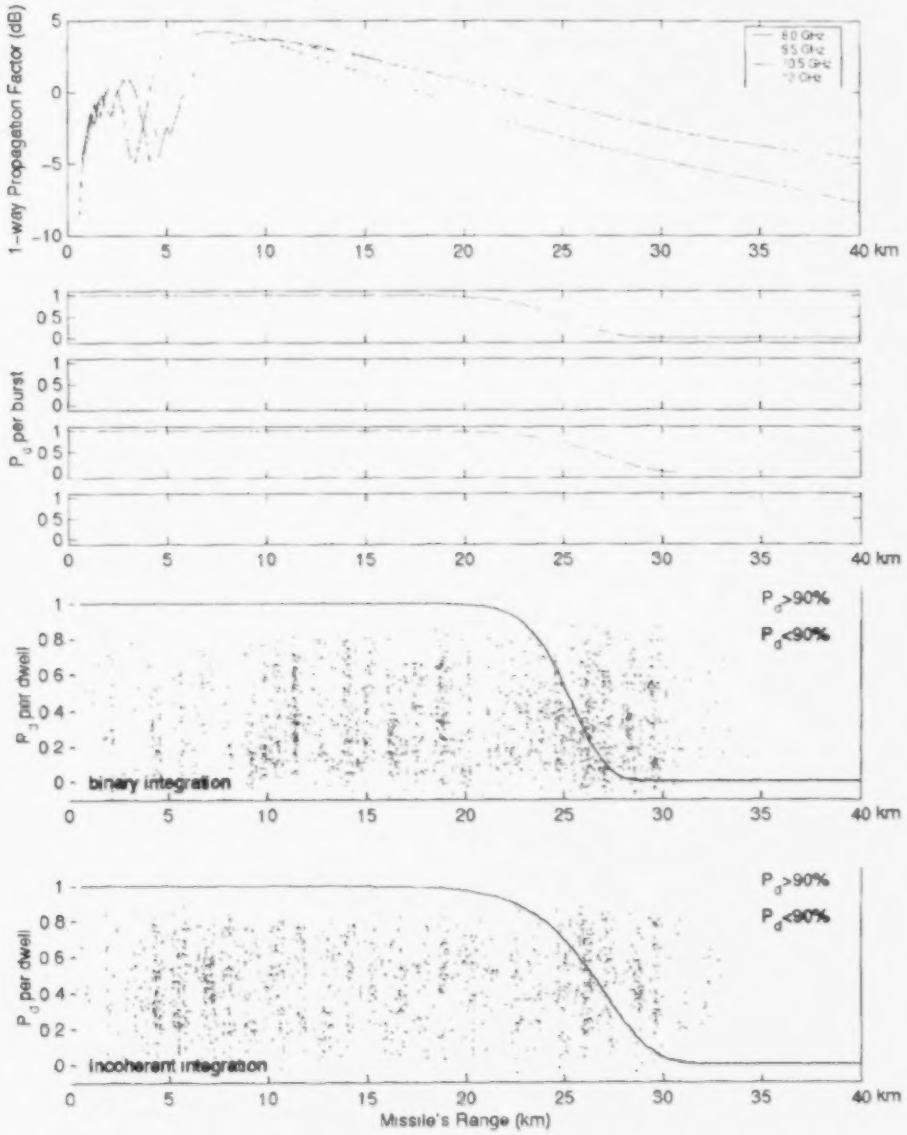

Figure 134. MFR results, 10m duct, NOVATOR at 3 m

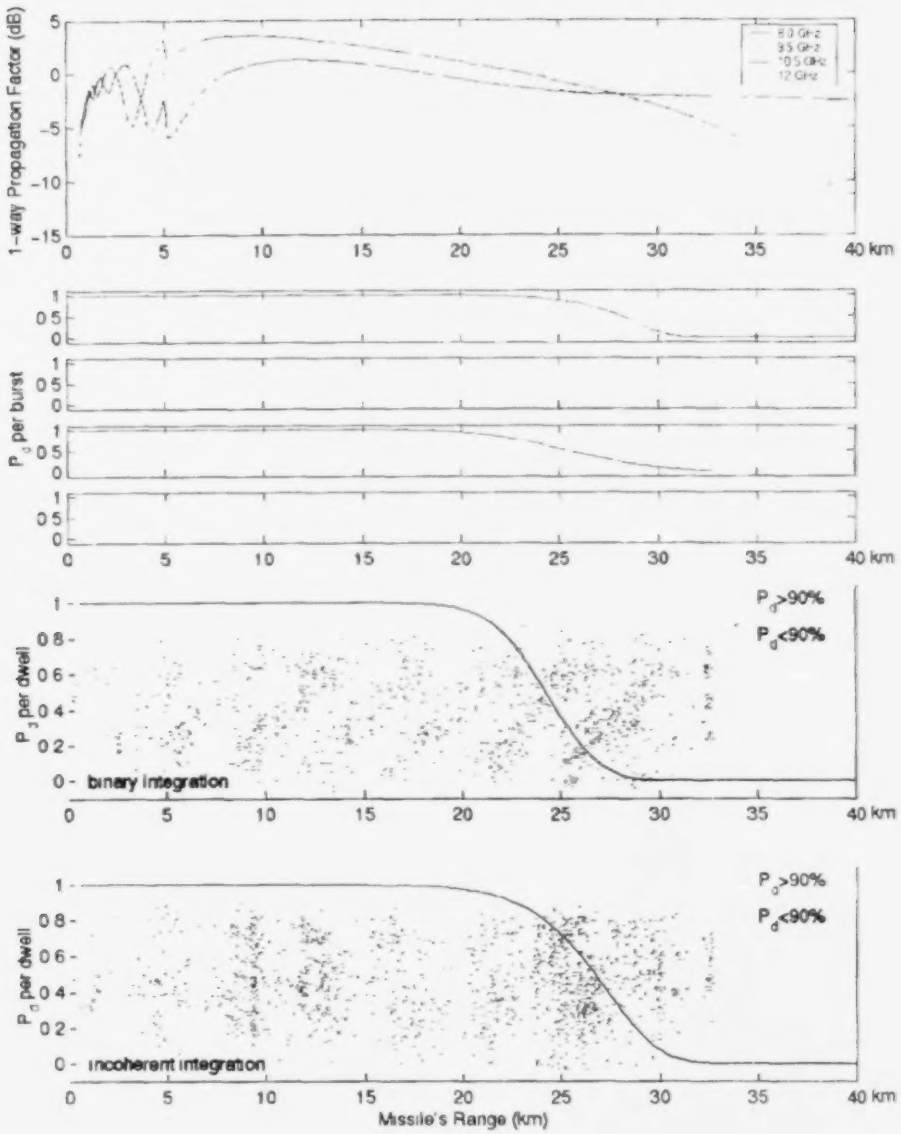

Figure 135. MFR results, 20m duct, NOVATOR at 3 m

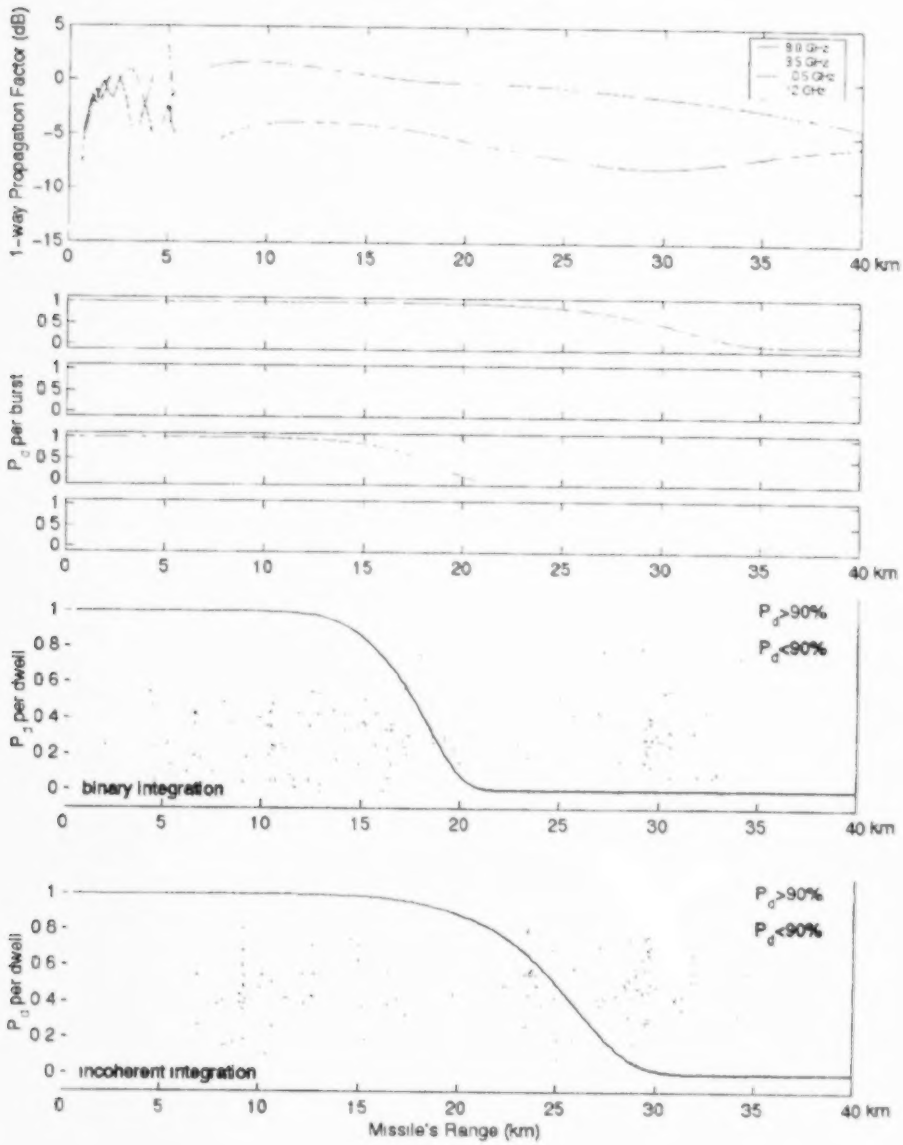

Figure 136. MFR results, 30m duct, NOVATOR at 3 m

P517610.PDF [Page: 120 of 123]

List of symbols/abbreviations/acronyms/initialisms

dB_i	Decibel relative to an isotropic antenna
DND	Department of National Defence
ASM	Antiship missile
RCS	Radar cross-section
RF	Radio-Frequency
LOS	Line-of-sight
SNR	Signal-to-noise ratio
CPF	Canadian Patrol Frigate

UNCLASSIFIED

SECURITY CLASSIFICATION OF FORM
(highest classification of Title, Abstract, Keywords)

DOCUMENT CONTROL DATA

(Security classification of title, body of abstract and indexing annotation must be entered when the overall document is classified)

1 ORIGINATOR (the name and address of the organization preparing the document Organizations for whom the document was prepared, e g Establishment sponsoring a contractor's report, or tasking agency, are entered in section 8)

DEFENCE RESEARCH ESTABLISHMENT OTTAWA

2 SECURITY CLASSIFICATION (overall security classification of the document, including special warning terms if applicable)

UNCLASSIFIED

3 TITLE (the complete document title as indicated on the title page Its classification should be indicated by the appropriate abbreviation (S,C or U) in parentheses after the title)

NAVAL RADAR PERFORMANCE Under Ducting Conditions (U)

4 AUTHORS (Last name, first name, middle initial)

GAUTHIER S M., RISEBOROUGH E.S., THOMSON, A.D.

5 DATE OF PUBLICATION (month and year of publication of document)	6a NO OF PAGES (total containing information Include Annexes, Appendices, etc)	6b NO OF REFS (total cited i document)
December 2001	117	25

7 DESCRIPTIVE NOTES (the category of the document, e g technical report, technical note or memorandum If appropriate, enter the type of report, e g interim, progress, summary, annual or final Give the inclusive dates when a specific reporting period is covered)

DREO TECHNICAL REPORT

8 SPONSORING ACTIVITY (the name of the department project office or laboratory sponsoring the research and development Include the address)

DREO

9a PROJECT OR GRANT NO (if appropriate, the applicable research and development project or grant number under which the document was written Please specify whether project or grant)	9b CONTRACT NO (if appropriate, the applicable number under which the document was written)
PROJECT 1AA11	

10a ORIGINATOR'S DOCUMENT NUMBER (the official document number by which the document is identified by the originating activity This number must be unique to this document)	10b OTHER DOCUMENT NOS (Any other numbers which may be assigned this document either by the originator or by the sponsor)
DREO TR 2001-148	

11 DOCUMENT AVAILABILITY (any limitations on further dissemination of the document, other than those imposed by security classification)

(X) Unlimited distribution
( ) Distribution limited to defence departments and defence contractors, further distribution only as approved
( ) Distribution limited to defence departments and Canadian defence contractors, further distribution only as approved
( ) Distribution limited to government departments and agencies, further distribution only as approved
( ) Distribution limited to defence departments, further distribution only as approved
( ) Other (please specify)

12 DOCUMENT ANNOUNCEMENT (any limitation to the bibliographic announcement of this document This will normally correspond to the Document Availability (11) However, where further distribution (beyond the audience specified in 11) is possible, a wider announcement audience may be selected)

13 ABSTRACT (a brief and factual summary of the document It may also appear elsewhere in the body of the document itself It is highly desirable that the abstract of classified documents be unclassified Each paragraph of the abstract shall begin with an indication of the security classification of the information in the paragraph (unless the document itself is unclassified) represented as (S), (C), or (U) It is not necessary to include here abstracts in both official languages unless the text is bilingual)

This report evaluates the detection capabilities of three naval radars against current antiship missile (ASM) threats under various ducting conditions The parameters of three naval radars and ASMs are first defined for this study The subject radars are the SPS-49, the Sea Giraffe and an active multifunction radar (MFR) The ASMs of concerns in this study are the Exocet, the SS-N-22, and the Novator sea skimming missiles. The defined radars are then evaluated against the ASMs under four atmospheric conditions. standard atmosphere, and with evaporation ducts at heights of 10m, 20m and 30m

This report shows that ducting conditions can have a strong impact on the detection capability of naval radar The maximum detection range is often increased by the presence of ducts but can also be significantly decreased which puts the survivability of the ship at a higher risk The volume search radar has the best detection capability against the missiles flying 15m and higher for any atmospheric conditions. The MFR of this report using a 3-out-of-4 binary detector has its performance seriously degraded in the presence of evaporation ducts as shown by this report.

14 KEYWORDS, DESCRIPTORS or IDENTIFIERS (technically meaningful terms or short phrases that characterize a document and could be h in cataloguing the document They should be selected so that no security classification is required Identifiers such as equipment model designation, trade name, military project code name, geographic location may also be included If possible keywords should be selected fr published thesaurus e g Thesaurus of Engineering and Scientific Terms (TEST) and that thesaurus-identified If it is not possible to select indexing terms which are Unclassified, the classification of each should be indicated as with the title)

RADAR
EVAPORATION DUCTS
ASM

Defence R&D Canada
is the national authority for providing
Science and Technology (S&T) leadership
in the advancement and maintenance
of Canada's defence capabilities.

R et D pour la défense Canada
est responsable, au niveau national, pour
les sciences et la technologie (S et T)
au service de l'avancement et du maintien des
capacités de défense du Canada.

#517610
CA020869

DEFENCE R&D DÉFENSE

www.drdc-rddc.dnd.ca